Università degli Studi di
Modena e Reggio Emilia

International Doctorate School in
Industrial Innovation Engineering
XXVIII Cycle

From Vibrations Mechanics to a Sensorless approach for Machine Diagnostics

Doctoral Dissertation of
Michele Cotogno

Advisor
Prof. Riccardo Rubini

I.I.I. Doctorate School Dean and Coordinator
Prof. Mauro Dell'Amico

Table of contents

Table of contents **3**
List of Figures **5**
Abstract **9**
Sommario in lingua Italiana **11**
1 – Introduction **13**

1.1 – Maintenance Activity and Sensorless Diagnostics 13
1.2 – Signal Processing 17

1.2.1 – Signal Classification 17
1.2.2 – Basic Signal Processing Techniques 20

1.2.2.1 – Fourier Analysis *20*
1.2.2.2 – Convolution Theorem *23*
1.2.2.3 – Hilbert Transform and Demodulation *24*
1.2.2.4 – Time Synchronous Averaging *25*
1.2.2.5 – Order Tracking *25*
1.2.2.6 – Moving Average *26*
1.2.2.7 – Spatial Acceleration Modulus *27*

1.3 - Companies Involved in this Thesis 29

2 – Diagnostics of Hydraulic Valves **31**

2.1 – Introduction 31
2.2 – Experimental Set-Up 34
2.3 – Data Analysis 38
2.4 – Conclusions 44

3 – Diagnostics of Blades for Steel Tubes Cutting **45**

3.1 – Introduction 45
3.2 – Experimental Set-Up 47
3.3 – Data analysis 50

3.3.1 – OTO Headquarters' Data Analysis 50
3.3.2 – Customer's site data analysis 51

3.4 – Conclusions 68

4 – Diagnostics of an Epicyclic Gearbox **71**

4.1 – Introduction 71
4.2 – Experimental Set-Up 72
4.3 – Data analysis 76

4.3.1 – General Theory of Gearbox Condition Monitoring 76
4.3.2 – Indicators and Calculations Details 77
4.3.3 – Analysis Results 80
4.4 – Conclusions 87

5 – Final Comments 89
6 – References 91
Acknowledgements 93

List of Figures

Figure 1.1: signals classification. 17

Figure 1.2: examples of signal types. 18

Figure 1.3: Autocorrelation function of a triangle wave @ 5Hz 19

Figure 1.4: Autocorrelation function of white noise. 19

Figure 1.5: obtaining of the Spatial Acceleration Modulus. Acceleration vector at and its projections on the reference system $x(t)$, $y(t)$ and $z(t)$. SAM is the norm (i.e.: the length) of $a(t)$ 27

Figure 2.1: general outline of the monitored valve's sealing 32

Figure 2.2: extract of the test bench hydraulic scheme. 33

Figure 2.3: detail of the test bench hydraulic scheme. Valves Block and sensors hydraulic placement 34

Figure 2.4: the valves block of the test bench. 35

Figure 2.5: detail of the accelerometer positioning and the orientation of its axes. 35

Figure 2.6: the acquisition hardware used for the acquisition campaign 36

Figure 2.7: signals coming from the blow-by test of a 3 cursors distributor acquired on the test bench. 36

Figure 2.8: the hydraulic scheme of the test rig. 37

Figure 2.9: particular of the test rig. Pressure sensor and the hydraulic piping directed to the tested valve intake port. 37

Figure 2.10: particular of the test-rig; the steel block which hosts the valve under testing and the accelerometer with the indication of the orientation of its axes. The y axis is parallel to the valve's cursor axis, and its positive direction is concordant with the movement of the cursor when the latter is closing. 38

Figure 2.11: raw data acquired on the test rig with a healthy (brand-new) valve in test when closing. The upper graph reports the 3 acceleration axes and the SAM, the lower graph reports the pressure. 39

Figure 2.12: raw data acquired on the test rig with a faulty valve in test when closing. The upper graph reports the 3 acceleration axes and the SAM; the lower graph reports the pressure. 39

Figure 2.13: time synchronous average of the openings of the brand-new valve. 40

Figure 2.14: time synchronous average of the openings of a faulty valve. 40

Figure 2.15: difference of vibration between the average of a faulty valve and a brand-new valve when opening. 41

Figure 2.16: time synchronous average of the closings of the brand-new valve. 42

Figure 2.17: time synchronous average of the closing of the faulty valve. 42

Figure 2.18: difference of vibrations between the average of a faulty valve and a brand-new valve when closing. 43

Figure 3.1: the Cut-off unit. The yellow part is the carriage which hosts the blade under study. 46

Figure 3.2: difference between HSS and TCT blades teeth..... 46

Figure 3.3: accelerometer placement. 48

Figure 3.4: detail of the accelerometer placement and its axes. The blade lies parallel to the YZ plane. 48

Figure 3.5: placement of the compactRio. 49

Figure 3.6: spectrum of vibration along the Z direction (lying on the blade plane) in case of a healthy blade. The teeth frequency (amplitude: 0.88) and its harmonics dominate the spectrum..... 51

Figure 3.7: spectrum of vibration along the Z direction (lying on the blade plane) in case of the same blade of Fig. 3.6 without a tooth. The teeth frequency amplitude rises to 1.04, and some of its harmonics amplitudes rise too. 51

Figure 3.8: example 1 of the result of the pre-processing of the torque signal. The theoretical torque $T(t)$ is the red curve, the raw acquired torque $A(t)$ is the green curve, which after processing (MA filters) and synchronization becomes the blue curve $Acut(t)$..... 53

Figure 3.9: example 2 of the result of the pre-processing of the torque signal. The theoretical torque $T(t)$ is the red curve, the raw acquired torque $A(t)$ is the green curve, which after processing (MA filters) and synchronization becomes the blue curve $Acut(t)$..... 54

Figure 3.10: maximum, variance and RMS of the Y vibration signal during blade A life. 56

Figure 3.11: entropy of the Y vibration signal during blade A life..... 56

Figure 3.12: maximum, mean, variance and RMS of the $Acut(t)$ signal during blade A life. 57

Figure 3.13: entropy of the $Acut(t)$ signal during blade A life..... 57

Figure 3.14: maximum, mean, variance and RMS of the $D(t)$ signal during blade A life. 58

Figure 3.15: entropy of the $D(t)$ signal during blade A life..... 58

Figure 3.16: maximum, variance and RMS of the Y vibration signal during blade B life. 59

Figure 3.17: entropy of the Y vibration signal during blade B life. 59

Figure 3.18: maximum, mean, variance, RMS and a zoom of the variance of the $Acut(t)$ signal during blade B life. 60

Figure 3.19: entropy of the $Acut(t)$ signal during blade B life..... 60

Figure 3.20: maximum, mean, variance, RMS and a zoom of the variance of the Dt signal during blade B life. 61
Figure 3.21: entropy of the $D(t)$ signal during blade B life. 61
Figure 3.22: maximum, variance and RMS of the Y vibration signal during blade C life. 62
Figure 3.23: entropy of the Y vibration signal during blade C life. 62
Figure 3.24: maximum, mean, variance, RMS and a zoom of the variance of the $Acut(t)$ signal during blade C life. 63
Figure 3.25: entropy of the $Acut(t)$ signal during blade C life. 63
Figure 3.26: maximum, mean, variance, RMS and a zoom of the variance of the Dt signal during blade C life. 64
Figure 3.27: entropy of the $D(t)$ signal during blade C life. 64
Figure 3.28: maximum, variance and RMS of the Y vibration signal during blade D life. 65
Figure 3.29: entropy of the Y vibration signal during blade D life. 65
Figure 3.30: maximum, mean, variance and RMS of the $Acut(t)$ signal during blade D life. 66
Figure 3.31: entropy of the $Acut(t)$ signal during blade D life. 66
Figure 3.32: maximum, mean, variance and RMS of the $D(t)$ signal during blade D life. 67
Figure 3.33: entropy of the $D(t)$ signal during blade D life. 67
Figure 4.1: the gearbox test bench. 73
Figure 4.2: the damaged ring gear of the E50 stage. 74
Figure 4.3: the first incision on the sun gear of the E50 stage. 74
Figure 4.4: the second incision on the sun gear of the E50 stage. 75
Figure 4.5: the third incision on the sun gear of the E50 stage. 75
Figure 4.6: RMS and Kurtosis of the vibration signal. 80
Figure 4.7: Crest Factor (CF) and Energy Operator (EO) of the vibration signal. 81
Figure 4.8: FM4 evaluated for the E50 sun gear from the vibration signal. 81
Figure 4.9: NB4 of the E50 stage vibrations during the first 517 records of the endurance test. 82
Figure 4.10: NB4 of the E50 stage torque during the first 517 records of the endurance test. 82
Figure 4.11: NB4 of the E50 stage vibrations from record 517 to record 1694. 83
Figure 4.12: NB4 of the E50 stage torque from record 517 to record 1694. 83
Figure 4.13: NB4 of the E50 stage vibrations from record 1694 to record 2190. 84

Figure 4.14: NB4 of the E50 stage torque from record 1694 to record 2190. 84

Figure 4.15: NB4 of the E50 stage vibrations from record 2189 to the end of the endurance test..... 85

Figure 4.16: NB4 of the E50 stage torque from record 2189 to the end of the endurance test..... 85

Figure 4.16: NB4 of the E50 stage vibrations during the test with incised sun gear. 86

Figure 4.17: NB4 of the E50 stage torque during the test with incised sun gear. 86

Abstract

The Maintenance activity – i.e.: the set of operations which preserve or restore a particular operative state of a good – is one of the most critical in industry, because of its repercussions on the productive activity mainly in terms of time (e.g.: production time losses due to machinery maintenance) and money cost. Several Maintenance Strategies exist: this thesis is in the "Predictive Maintenance" framework, i.e.: that Maintenance strategy that (more or less) continuously monitors the process (or the part) which had been identified as "critical" in order to estimate its functional status. Thus, the maintenance activities are optimized on the basis of this crucial information. As mentioned, the main point of this maintenance strategy is the correct estimation of the state of the monitored process/part: this importance comes from the necessity of dedicated sensors, the corresponding acquisition chain and an algorithm able to interpret the sensors' data and to provide an accurate diagnosis. From the point of view of a producer that aims to implement a diagnosis system on its products, all these requirements cause a rise of the product costs, which comes from the aforementioned extra hardware and the system developing time (the latter embodies also the experimental campaign necessary to develop and test the diagnostic algorithm). These "initial costs" are more easily evaluable than the gain that a condition monitoring system provides: indeed, this gain is spread in the future time because it comes from an optimized maintenance phase. This is briefly the main motivation that explains why the Predictive Maintenance started to grow in the industrial environment only in recent years, despite the availability of hardware and theoretical knowledge at least from the first nineties. The aim of this thesis is therefore to reduce the aforementioned initial costs by means of the so-called "Sensorless Diagnostics", i.e.: "Diagnostics without extra (dedicated) sensors": indeed, given the ever-growing automation of industrial machines, an equally growing presence of sensors is observed – sensors that are necessary for the automation itself. The basic idea of this thesis is to use those "automation" sensors (e.g.: a current sensor used to close the control loop of an electric motor) for condition monitoring purposes also (e.g.: estimate the state of the motor shaft bearing via the motor current analysis). By doing this, the condition monitoring hardware cost is strongly reduced while the other aforementioned costs remains: this allow the producer to be more competitive on the market, because he can offer a product with condition monitoring on board which have (ideally) the same monitoring performances of a "classic" diagnostic system but it is less costly. In this thesis work, three different industrial cases have been studied in order to develop a Sensorless condition monitoring system, these being: condition monitoring of

hydraulic valves used in a hydraulic distributors test bench, condition monitoring of a blade of a steel tubes cutter, condition monitoring of a gearing on a test bench.

Sommario in lingua Italiana

La fase di manutenzione – insieme delle operazioni che preservano o ristabiliscono uno specifico stato operativo di un bene – è una delle più critiche in ambito industriale a causa delle sue ripercussioni sull'attività produttiva principalmente in termini di tempo e costi. Esistono diverse strategie di manutenzione in ambito industriale: in questa tesi si è nell'ambito della "Manutenzione predittiva", ovvero quella strategia di manutenzione che prevede un monitoraggio (più o meno) continuo del processo o del particolare identificato come critico al fine di stimarne lo stato funzionale. Sulla base di questa informazione cruciale, si attueranno poi operazioni di manutenzione che saranno così ottimizzate rispetto alla particolare condizione in cui ci si trova. Come accennato, il punto cruciale di questa strategia manutentiva è la corretta stima dello stato del processo/oggetto monitorato: questa importanza deriva anche dal fatto che per effettuare il monitoraggio, vi è solitamente necessità di aggiungere sensori dedicati, una catena di acquisizione dei dati provenienti dal sensore e un algoritmo capace di interpretare questi dati fornendo una diagnosi affidabile. Dal punto di vista di una realtà industriale che intende implementare sui suoi prodotti un sistema di diagnostica, tutte queste necessità provocano un aumento dei costi del prodotto, costi provenienti dall'hardware e dal tempo e dalle prove sperimentali necessari per sviluppare l'algoritmo di diagnostica. Questi costi iniziali sono molto meglio definibili rispetto invece ai ricavi che il sistema diagnostico offre: infatti, questi sono dilazionati nel tempo poiché saranno percepiti al momento di fare la manutenzione, che sarà però ottimizzata. In breve, è questa la motivazione principale per la quale solamente negli ultimi anni la manutenzione predittiva sta iniziando a entrare in scala apprezzabile nel settore produttivo, nonostante vi sia disponibilità di hardware e conoscenze teoriche sufficienti perlomeno dai primi anni '90. Questa tesi è volta alla riduzione dei citati costi iniziali di un sistema di diagnostica tramite alcuni studi di fattibilità della cosiddetta "Diagnostica Sensorless", dove con "Sensorless" si intende "senza sensori aggiuntivi": difatti si constata, data la sempre crescente automazione in ambito industriale, una presenza parimenti crescente di sensori necessari per questa automazione. L'idea di base è di utilizzare questi sensori (ad esempio: un sensore di corrente necessario alla chiusura di un loop di controllo di un motore elettrico) per fini diagnostici (restando nell'esempio: stimare lo stato del cuscinetto supportante l'albero del motore elettrico attraverso l'analisi della corrente che circola all'interno del motore stesso). Sono così eliminate le voci di costo relative a sensori e catena di acquisizione dati, mentre i costi di sviluppo dell'algoritmo restano pressappoco gli

stessi: questo consente una maggior competitività al produttore sul mercato, in quanto offre un prodotto con sistema di diagnostica integrato ad un prezzo inferiore ma a parità di efficienza del monitoraggio. In questa tesi sono state affrontate le problematiche tecniche per ottenere un sistema di monitoraggio “Sensorless” in tre casi in differenti realtà industriali, concernenti: monitoraggio di valvole oleodinamiche utilizzate in un banco di collaudo, monitoraggio dello stato della lama di una troncatrice di tubi, monitoraggio di un riduttore sottoposto a test di durata.

1 – Introduction

1.1 – Maintenance Activity and Sensorless Diagnostics

The Maintenance activity could be defined as the set of operations which preserve or restore a particular operative state of a good. Today this activity is one of the most critical in the industrial setting, because it has severe repercussions on the productive activity mainly in terms of time and money cost. Time costs come from the trivial fact that broken equipment needs time to be repaired; if the breakage happened unexpectedly and there are no spare parts available, additional time is needed to order and ship them to destination. When the equipment is not working, a money loss happens immediately. If one consider that many high-capacity productive plant run continuously, 24 hours a day and seven days a week, one immediately seize the importance of the maintenance activity. Given this importance, different maintenance strategy were developed in last decades, following the progress of technology and the ever new requirements of the industrial environment; a possible classification of the maintenance strategies is given in the following list, accompanied by a brief description for each one of them [1]:

- *Run-to-break maintenance*: it is the most trivial method, and it is performed only when a fault has already manifested, implying the machinery partial or complete stop - with loss of time - in order to restore the desired operational conditions. This gives the longest time between shutdowns but the price to pay is that failures could be catastrophic and could cause consequential damage to the connected equipment. When this occurs the shutdown time will be much longer respect to others maintenance politics. Evidently, this kind of maintenance may be convenient only if there isn't danger of induced faults, when the parts to be replaced are cheap and easily available (e.g.: a fuse) and the loss of time is acceptable.
- *Preventive maintenance*: this strategy is based on a periodic check of the machine state, with time intervals between the inspections shorter than the expected “Mean Time Between Failures” (MTBF). Intervals are commonly chosen to be such that no more than 1-2% of machine will experience failure in that time. This method carry the main advantage of permitting a scheduling of maintenance activities, so far reducing the shutdown time when a fail occurs and also reducing the probability of catastrophic failure. Main disadvantages are that unforeseen failures can still (suddenly) occur, often requiring a re-scheduling of the maintenance operations;

replacing components that are still operational, thus raising maintenance cost with respect to the optimum; production time loss due to scheduled maintenance activity which can be *a posteriori* judged as “non-necessary”. So far, this politic is appropriate when the time-to-failure can be accurately predicted and it isn't statistically wide spread around the mean.

- *Condition-Based Maintenance (CBM)*: it represents the optimum solution to the maintenance problem. It's based on a (more or less) continuous monitoring of machinery conditions and/or machine parameters which are able to communicate its operative/health status. By doing this, one is able to notice the incoming of faults/malfunctions prior to their occurring, without having the necessity of stopping the machinery. Having this crucial information as soon as possible permits: to fully exploit the working life of the part of interest (this happens rarely in preventive maintenance); to schedule the maintenance activity only when it is really needed, and thus to take actions at the optimum time. Consequently, giving these obvious advantages compared to other strategies, the time and money requested for maintenance activities result to be optimized. The condition-based maintenance success depends on the reliability of the monitoring techniques.

This thesis work is embedded in the Condition-Based Maintenance framework. As mentioned, the main point of this maintenance strategy is the correct estimation of the state of the monitored process/part. Usually, this implies the necessity of dedicated sensors, of the corresponding acquisition chain and of an algorithm able to interpret the sensors’ data and to provide an accurate and reliable diagnosis. From the point of view of a machine producer that aims to implement a diagnosis system on its products, all these requirements cause a rise of the product costs, which comes from the aforementioned extra hardware and the system developing time. Indeed, to develop a reliable condition monitoring (CM) system usually is required:

- to perform a data acquisition campaign having the goal of selecting the best machine parameter (or set of parameters) which can supply the information of interest, i.e.: the health status of the machine;
- to develop a condition monitoring algorithm, i.e.: finding the best signal processing techniques to be used on the machine parameter(s) in order to correctly obtain the diagnosis of interest;
- finally, to test the algorithm/condition monitoring system on-field in order to asses (and eventually enhance) its diagnosis’ reliability.

These activities joined with the aforementioned hardware compose the “initial costs” of the CM system. These costs are a lot more easily evaluable than the gains that a CM system provides: in fact, this gain is spread in the future time because it comes from an optimized maintenance activity. If this gain was easily assessable, it would mean that

one could know *a priori* when the machine will break: if this would be the case, then one should use the Preventive Maintenance strategy!

These are the main facts that explain why the Predictive Maintenance started to grow in the industrial environment only in recent years, despite the availability of hardware and theoretical knowledge at least from the first nineties. The aim of this thesis is then to reduce the aforementioned "initial costs" by means of the so-called "Sensorless Diagnostics", i.e.: "Diagnostics without extra (dedicated) sensors". Indeed, given the ever-growing automation of industrial machines, an equally growing presence of sensors is observed – sensors that are necessary for the automation itself. The basic idea of this thesis is to use those "automation" sensors for condition monitoring purposes also: for example, a current sensor used to close the control loop of an electric motor could be used also to estimate the state of the motor shaft bearing via the motor current analysis [9]. By doing this, the condition monitoring hardware cost is strongly reduced or eliminated, while the other costs remains: this allow the producer to be more competitive on the market, because he can offer a product with a CM system on board which has the same monitoring performances of a "classic" diagnostic system but it is less costly.

The aim of this thesis work is twofold: first, it aims to obtain valid diagnostic indicators in the "classical" manner, that is via adding sensors (usually an accelerometer) to the monitored machine and subsequently by analyzing these sensor's signal; second, it aims to perform the Sensorless diagnostic via the analysis of the signals coming from sensors already present on the machinery, sensors which are used for other machine functionalities. This was done in order to demonstrate that the same information of interest (i.e.: the health status of some machine part) can be obtained both from a "classical" approach than from a Sensorless approach; moreover, regarding the Sensorless solutions, these are stronger if their results are concordant with well-established classical methods, and thus they are more reliable. In this thesis work, three different industrial cases have been studied in order to develop Sensorless condition monitoring systems, these being: condition monitoring of hydraulic valves used in a hydraulic distributors test bench, condition monitoring of a blade of a steel tubes cutter, condition monitoring of a gearing on a test bench.

1.2 – Signal Processing

This chapter is a brief introduction to Signal Processing and its methods. A “Signal” could be defined in general as a “temporal variation of a physic quantity or of a physical state of a system”; signals are one way to represent and/or transmit information. Thus, "Signal Processing" could be defined as “the discipline that deals with extracting information from signals by means of some kind of signal manipulation”.

1.2.1 – Signal Classification

In signal processing it is very useful to know which kind of a signal we are dealing with, because this knowledge allows to choose the best set of processing techniques to be used to extract the information of interest. A possible signals classification is in fig. 1.1.

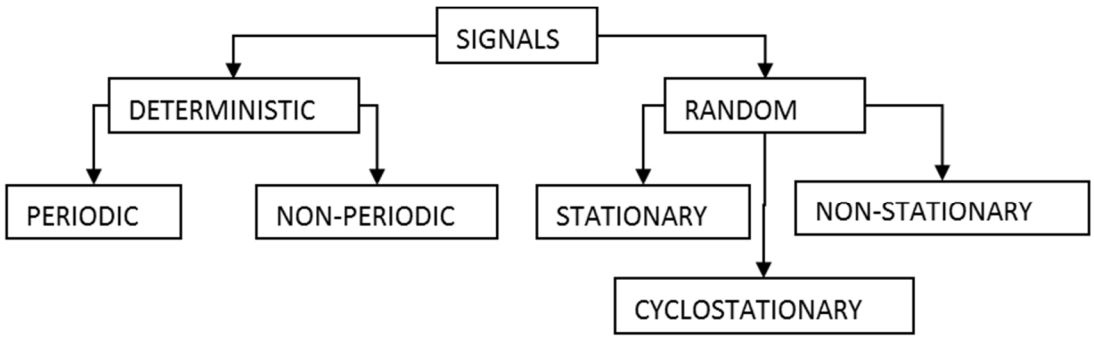

Figure 1.1: signals classification.

Deterministic signals are those signals which can be time-described by explicit mathematical relations. This means that once this relation is known, one can predict future or past signal values. Deterministic signals can further be split in periodic and non-periodic signals: periodic deterministic signals can be represented by a function repeating itself at regular time intervals, such that:

$$x(t) = x(t + nT), \quad n \in \mathbb{N} \tag{1.1}$$

where *T* is named “period” and it represent the aforementioned “regular interval of repetition”. These signals are made up of a sum of discrete sinusoidal components, which frequencies are all integer multiple of the fundamental periodic frequency $\omega_0 = 2\pi/T$. Premium example of this class is the sine/cosine wave, which period is 2π.

Non-periodic signals are the remaining deterministic signals - e.g. transients or a sum of sine waves which periods are non-commensurable – and are still predictable but

non-repetitive. A typical example is given by the vibration signals from a gas turbine engine, which has several independent shafts. Each shaft will normally generate families of harmonics of their fundamental frequency, but the total signal will be quasi-periodic due to incommensurability of their periods – i.e.: the ratio of their fundamental frequencies is an irrational number.

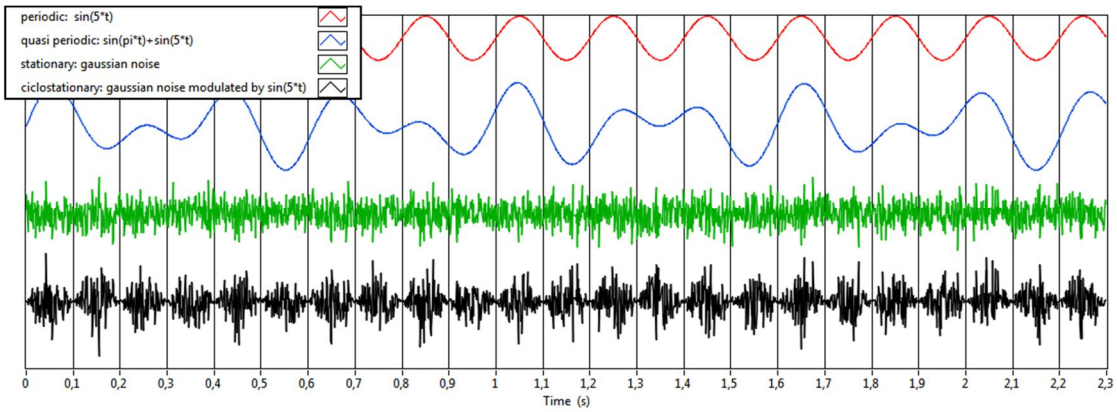

Figure 1.2: examples of signal types.

Random signals - in opposition to deterministic signals - have behaviours that can't be described with explicit mathematical relations, because every occurrence has the unicity property, i.e.: any observation will return only one of the possible outcomings. Therefore, they are usually treated through statistical means which imply the observation of multiple occurrences: the more these occurrences are, the more one knows about the process being studied.
Some of the principal statistical features are reported with their definition:

- Mean value: $\mu = E[x(t)]$ (first order moment).
- Variance or mean square value: $\sigma^2 = E[(x(t) - \mu)^2]$ (second order moment).
- Root Mean Square or RMS value: $x_{rms} = \sigma = \sqrt{E[(x(t) - \mu)^2]}$.
- Skewness: $\frac{E[(x(t)-\mu)^3]}{\sigma^3}$ (third order moment), it gives a measure of the symmetry of the signal's probability distribution.
- Kurtosis: $\frac{E[(x(t)-\mu)^4]}{\sigma^4}$ (fourth order moment), it gives a measure of the peakedness/impulsivity of the signal.
- Autocorrelation function: this function gives a measure of how well a signal correlates (in time) with a displaced version of itself. For periodic signals the autocorrelation function has its maxima when the time lag τ equal the period T (fig. 1.3). The most fundamental definition of the autocorrelation function is given in the following equation 1.2:

$$R_{xx}(t,\tau) = E\left[x\left(t-\frac{\tau}{2}\right)x\left(t+\frac{\tau}{2}\right)\right] \quad (1.2)$$

where t is time and τ is the time lag. The autocorrelation function is usually evaluated at time t over an ensemble of observations of the process. The autocorrelation function has always a maximum at time lag $\tau = 0$ because every signal correlates with itself, even if it is a random signal (fig. 1.4); furthermore, for real valued signals – almost every signal in practice – the autocorrelation is an even function.

- Shannon Entropy: $\sum_{i=1}^{n} p(x_i) \ln p(x_i)$, where $p(x_i)$ is the probability of the event x_i.

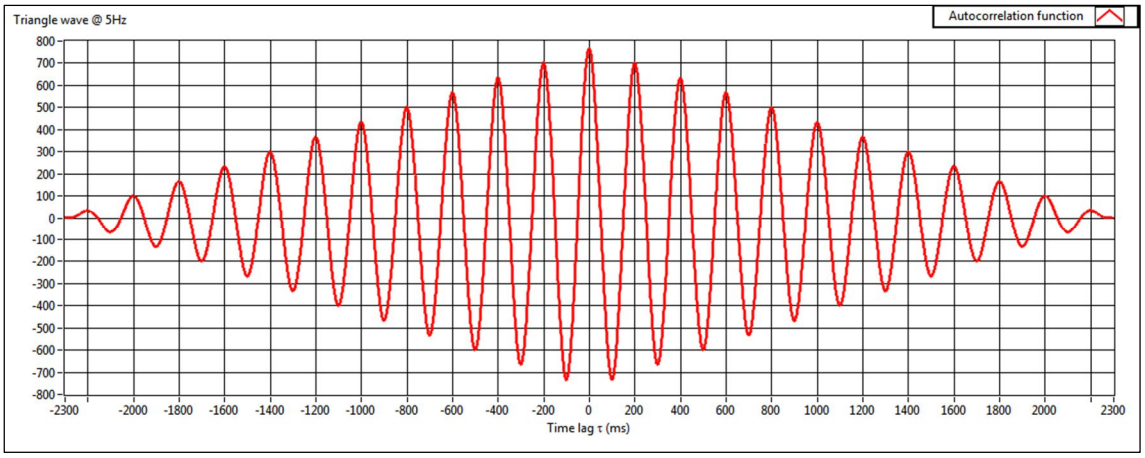

Figure 1.3: Autocorrelation function of a triangle wave @ 5Hz

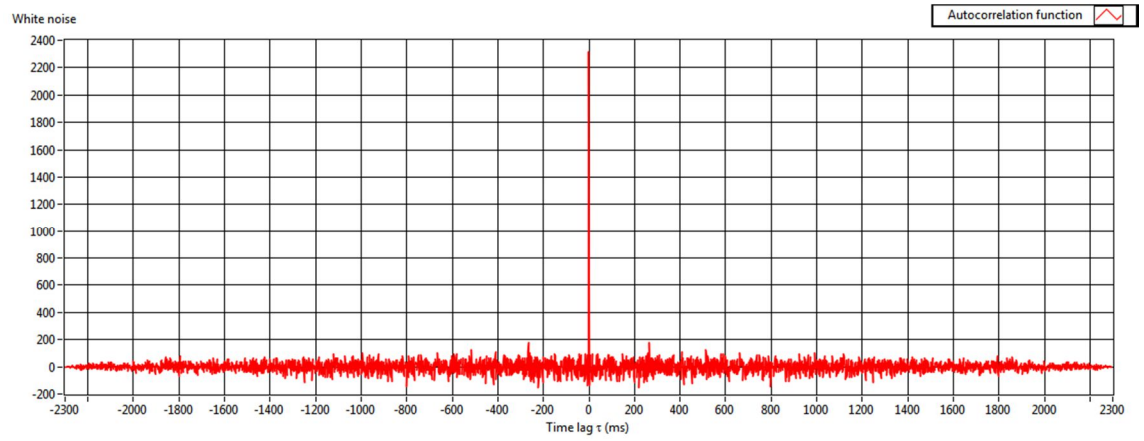

Figure 1.4: Autocorrelation function of white noise.

Within this frame, random signals could further be classified as stationary and non-stationary, the former being those random signal which statistical features do not vary (in statistical sense) from one observation to another (e.g.: white noise) while the latter do. For stationary random signals, the autocorrelation function doesn't depend on time t but it only depends on time lag τ.

In recent years a new class of random signal has been studied, that is cyclostationary random signals, i.e. those signals which - although being random in their nature - are

produced by some hidden periodic mechanisms [2]. A classic example of this kind of signals is white noise modulated by a sine wave (fig. 1.2): despite the modulation, it's still a random signal in its nature. A finer classification of cyclostationary signals is given by the order of cyclostationarity that the signal exhibit: an n^{th} order cyclostationary signal is a signal whose n^{th} order statistics are periodic or, equivalently stated, one which produces a peak in its Fourier Transform after passing through any non-linear transformation involving the n^{th} power . The sine-modulated white noise is an example of second order cyclostationarity, while a periodic signal embedded in additive white noise is an example of first order cyclostationary signal.

1.2.2 – Basic Signal Processing Techniques

1.2.2.1 – Fourier Analysis

Fourier Analysis is a set of mathematical tools that allow viewing a signal in the Frequency-domain rather than in the time-domain. The basic tool in this set is the Fourier Series, which decomposes a periodic signal *f(t)* in a series of sinusoidal waves, as follows:

$$f(t) = f(t \pm nT) = \frac{a_0}{2} + \sum_{n=1}^{\infty}(a_n \cos \mathrm{n}\omega_0 \mathrm{t} + b_n \sin \mathrm{n}\omega_0 \mathrm{t}) \tag{1.3}$$

where

$$\begin{cases} a_0 = \frac{2}{T}\int_{-T/2}^{T/2} f(t)dt \\ a_n = \frac{2}{T}\int_{-T/2}^{T/2} f(t)\cos \mathrm{n}\omega_0 \mathrm{t}\, dt \\ b_n = \frac{2}{T}\int_{-T/2}^{T/2} f(t)\sin \mathrm{n}\omega_0 \mathrm{t}\, dt \end{cases} \tag{1.4}$$

a_n and b_n are called "series coefficients", $\omega_0 = 2\pi/T$ [rad/s] is the "fundamental frequency" and $n\omega_0 = \omega_n, n \in \mathbb{N}$ is called "n^{th} harmonic". The series could be rewritten as

$$f(t) = \frac{\mathrm{a}_0}{2} + \sum_{n=1}^{\infty}(\mathrm{F_n}\cos \omega_n t - \phi_n) \tag{1.5}$$

where $F_n = \sqrt{{a_n}^2 + {b_n}^2}$ and $\phi_n = \tan^{-1}\frac{b_n}{a_n}$.

Using Euler's formula $e^{it} = \cos t - i \sin t$, another shape of the Fourier Series is obtained:

$$f(t) = \sum_{n=-\infty}^{+\infty} \mathrm{c_n e^{i\omega_n t}} \tag{1.6}$$

where complex coefficients c_n are obtained by

$$c_n = \int_{-T/2}^{T/2} f(t)e^{-i\omega_n t}dt \tag{1.7}$$

and are related to real coefficients a_n and b_n by the following relations:

$$c_n = \begin{cases} \frac{a_0}{2} \;\; if \;\; n = 0 \\ \frac{a_n - i b_n}{2} \;\; otherwise \end{cases} \tag{1.8}$$

The complex coefficients c_n have the following property: $c_n^* = c_{-n} = \frac{a_n + i b_n}{2}$ (where x^* denotes the complex conjugate of x). The series of the Fourier coefficients (a_n and b_n , or F_n and φ_n , or c_n) is named "Spectrum" of the time-continuous periodic function *f(t)* and gives a discrete representation of it in the frequency domain.

The Fourier Series exists only if *f(t)* is absolutely integrable over $[-T/2\,, T/2]$ - i.e.: $\int_{-T/2}^{T/2} |f(t)| dt < \infty$ - and only if *f(t)* is periodic, but aperiodic signals can also be expressed as a sum of sinusoids/complex exponentials via the "Fourier Transform". The Fourier Transform could be derived from the Fourier Series by interpreting the function "aperiodicity" as "periodicity of an infinite period $T = 2\pi/\omega$":

$$f(\mathrm{t}) = \sum_{n=-\infty}^{+\infty} \mathrm{c_n} \mathrm{e}^{\mathrm{i}\omega_n \mathrm{t}} = \frac{\omega}{2\pi} \sum_{n=-\infty}^{+\infty} \mathrm{e}^{\mathrm{i}\omega_n \mathrm{t}} \left(\int_{-T/2}^{T/2} f(t) e^{-i\omega_n t} dt \right) =$$
$$= \lim_{\substack{T\to\infty \\ \omega\to 0}} \frac{\omega}{2\pi} \sum_{n=-\infty}^{+\infty} \mathrm{e}^{\mathrm{i}\omega_n \mathrm{t}} \left(\int_{-T/2}^{T/2} f(t) e^{-i\omega_n t} dt \right) \tag{1.9}$$

Applying the limit results in the sum shifts to an integral and $\int_{-T/2}^{T/2} f(t) e^{-i\omega_n t} dt$ to a continuous (rather than discrete) function of ω, $F(\omega) = \int_{-\infty}^{+\infty} f(t) e^{-i\omega t} dt$, thus giving:

$$f(t) = \lim_{\substack{T\to\infty \\ \omega\to 0}} \frac{\omega}{2\pi} \sum_{n=-\infty}^{+\infty} \mathrm{e}^{\mathrm{i}\omega \mathrm{t}} F(\omega) = \frac{1}{2\pi} \int_{-\infty}^{+\infty} F(\omega) e^{i\omega t} d\omega \tag{1.10}$$

F(ω) is named "Fourier Transform" (FT) of *f(t)* and *F(ω)dω* represent the harmonic contribution to *f(t)* of the frequencies in [*ω, ω+dω*]. Like the series, for the Fourier Transform to exist it must be $\int_{-\infty}^{+\infty} |f(t)| dt < \infty$. The forward and inverse Fourier Transform are almost symmetrical, the only differences being the sign of the exponent of *e* in the integral and the division by 2π in the inverse transform, so results that apply to forward transform apply also on the inverse transform (e.g.: the convolution theorem, §1.2.2.2).

All signals which have to be analysed must be digitized by sampling (almost always at a constant sampling frequency $f_S = 1/\Delta \mathrm{t}$) and are in principle of infinite length: this is the inverse case of the Fourier series, where the spectrum is discrete and (generally) infinite and the signal is continuous and periodic, so - via the symmetry of the FT - that means that the spectrum of a sampled time signal is continuous and periodic. Furthermore, in practice recorded signals have finite length, which implies (as in the Fourier series) that their spectrum is discrete, because FT makes them implicitly

periodic (the period is equal to the record duration). In this case, the integrals in the FT become finite sums, expressed as:

$$F(k) = \frac{1}{N}\sum_{n=0}^{N-1} f(n)e^{-\frac{i2\pi kn}{N}}$$
$$f(n) = \sum_{k=0}^{N-1} F(k)e^{\frac{i2\pi kn}{N}} \quad (1.11)$$

Where *k* is the spectral line index, *n* is the time sample index, *N* is the total samples number, *f(n)* is the sample time series and $F(k) \in \mathbb{C}$ is its "Discrete Fourier Transform" or DFT. Since $F(k) = F(k-N)$ the DFT algorithm gives the negative frequencies amplitudes in inverse order for $k > N/2$, so the information recovered with the DFT doesn't extend beyond the spectral line $F(N/2)$, which corresponding to Nyquist Frequency $f_N = f_s/2$. The Sampling frequency and the duration of the record set the frequency resolution Δf, which is the spacing between two consecutive spectral lines in the DFT spectrum, the relation being:

$$\Delta f = \frac{1}{T} = \frac{1}{N\Delta t} = \frac{f_s}{N} \quad (1.12)$$

The three stages in passing from the Fourier transform to the DFT determine some properties of the DFT, these stages being digitization and truncation of the time signal and discrete sampling of the spectrum. Time signal digitization produces a periodic spectrum which period is f_s, but if the original signal contain frequencies above the Nyquist frequency $\pm f_N = f_s/2$ these will overlap with the true component giving rise to aliasing, i.e. higher frequencies are confused with lower ones. Aliasing must be seriously taken in consideration because once it is introduced in the record it can't be removed. Aliasing can be avoided by implementing anti-aliasing filters prior to digitizing the signal: an anti-aliasing filter is a low-pass filter at the Nyquist frequency with a very narrow transition band.

As stated above, a time signal has a finite duration, so its transformation to the frequency domain entails that the signal is (implicitly) replicated in time domain in order to make it periodic, and so transformable. If the replicated (and therefore concatenated) signal has discontinuities, these will result in the frequency domain as the appearing of many fictitious frequencies near the "true" ones: this phenomenon is named "spectral leakage". Leakage can be controlled by eliminating the discontinuities between the beginning and the ending of each segment of the concatenated time series, and a way to achieve this is by "windowing" the signal – that is, multiplying it by a function (the "window" itself) which is zero at the beginning and at the end of the record segment. Some of the most popular data windows in signal processing are:

Hanning window $w_{hn} = 0{,}5\left(1 - \cos 2\pi\frac{t}{T}\right),\ 0 < t < T$ (1.13a)

Hamming window $w_{hm} = 0{,}54 - 0{,}46\cos 2\pi\frac{t}{T},\ 0 < t < T$ (1.13b)

Blackman window $w_{bk} = 0{,}42 - 0{,}5\cos 2\pi\frac{t}{T} + 0{,}08\cos 4\pi\frac{t}{T},\ 0 < t < T.$ (1.13c)

The discrete sampling of the spectrum causes the loss of information about peaks and valley in it because they can't be precisely represented in a discrete frequency axis: this phenomenon is named "picket fence effect", because it is as though the spectrum is viewed through the slits in a picket fence.
The DFT is the most basic signal processing tool, used almost always in the Cooley and Tukey's improved version FFT (fast Fourier transform), which reduce the number of operations involved in DFT's calculation by an algorithm optimization based on N to be a power of 2.

1.2.2.2 – Convolution Theorem

Convolution is the operation by which the output (response) of a linear system is obtained from the input (forcing function) and the transfer properties of the physical system, this being represented in the time domain by the "impulse response function" or IRF – i.e.: the system output when the input is a unit impulse at time zero. The relationship between f(t) (the input), x(t) (the output) and h(t) (the IRF) is expressed by the Duhamel integral:

$$x(t) = \int_{-\infty}^{+\infty} f(\tau)h(t-\tau)d\tau = f(t) * h(t) \quad (1.14)$$

Where $*$ is the convolution operator and τ is a dummy integration variable. The convolution operation is commutative, $f(t) * h(t) = h(t) * f(t)$.
The convolution theorem states that a convolution in the time domain is transformed by the Fourier Transform (FT) in a product in the frequency domain:

$$\mathcal{F}\big(x(t)\big) = \mathcal{F}\big(h(t) * f(t)\big) = X(f) = F(f)H(f) \quad (1.15)$$

The symmetry of the FT also imply that a convolution in the frequency domain equal to a product in the time domain.

1.2.2.3 – Hilbert Transform and Demodulation

If x(t) is a function in time, its Hilbert transform is defined as:

$$\tilde{x}(t) = \frac{1}{\pi}\int_{-\infty}^{+\infty} x(\tau)\frac{1}{t-\tau}d\tau \tag{1.16}$$

This is the convolution of $x(t)$ and the function $1/\pi t$ and for the convolution theorem, it is also:

$$\tilde{X}(f) = X(f)\cdot\mathcal{F}\left(\frac{1}{t}\right) = X(f)\cdot(-i\,\mathrm{sgn}(f)) \tag{1.17}$$

This relation show that the Hilbert transform can be calculated simply by taking the Fourier transform of x(t), shifting the phase of positive frequencies by –π/2 and of the negative frequencies by +π/2 and then transforming back to the time domain [3].
In signal processing the Hilbert transform allow the construction of the *analytic signal*, defined as:

$$\hat{x}(t) = x(t) + i\tilde{x}(t) \tag{1.18}$$

The analytic signal is a complex function of time which real part is the signal itself and imaginary part is the Hilbert transform of the real part. It's useful because the magnitude of the analytic signal $|\hat{x}(t)| = \sqrt{x^2(t)+\tilde{x}^2(t)}$ and its argument $\theta(t) = \tan^{-1}\frac{\tilde{x}(t)}{x(t)}$ are respectively the Envelope and the Instantaneous Phase of the original signal, making the analytic signal a very powerful tool for the signal amplitude and frequency demodulation. A general modulated cosine signal can be represented by:

$$x(t) = A_m(t)\cos\big(2\pi f t + \varphi_m(t)\big) \tag{1.19}$$

where $A_m(t)$ represent the amplitude modulation function and $\varphi_m(t)$ represents the phase modulation function (in radians): the corresponding frequency modulation is $d\varphi_m(t)/dt$. The corresponding analytic signal is given by $\hat{x}(t) = x(t) + i\tilde{x}(t) = A_m(t)e^{2\pi f t+\varphi_m(t)}$, so the modulating functions can be extracted directly from it by the following equations:

$$A_m(t) = |\hat{x}(t)| \tag{1.20a}$$
$$\varphi_m(t) = \arg\big(\hat{x}(t)\big) - 2\pi f t \tag{1.20b}$$

The spectrum of modulated signals exhibits sidebands around the carrier frequency spaced at the modulating frequency.

1.2.2.4 – Time Synchronous Averaging

Time Synchronous Averaging (TSA) [1, 4, 5] is a time-domain technique which separates periodic signals from the background noise. TSA is obtained by averaging together a series of signal segments of equal length *T* (the fundamental period), i.e.:

$$TSA_x(t) = \frac{1}{n}\sum_{k=0}^{n-1} x(t + kT) \tag{1.21}$$

where $TSA_x(t)\,, t \in [0, T]$ is the averaged signal, $x(t)$ the original signal and *n* the number of segments. The extracted segments could be considered as single realizations of a stochastic process in which the random variable is the phase, thus the averaging must be done in terms of signal power (i.e. amplitude squared) rather than signal energy, as it is this which is conserved independent of the phase. This procedure allows to better clarify which parts of the spectrum are random generated or not, because averaging rejects the random contribute to the signal (random signals don't correlate with shifted version of themselves); but TSA could cause a smearing of frequency lines in the spectrum due to slight speed fluctuation recorded in the original signal: this cause that the segments extracted from the signal don't correspond to an even period of rotation *T*, resulting in the aforementioned frequency smearing after the DFT. The number *n* of the required averages is determined by the desired precision, given that the standard deviation of the noise in the averaged signal (for additive Gaussian noise) is $\varepsilon = 1/2\sqrt{n}$ [3].

1.2.2.5 – Order Tracking

Order tracking is a solution to the speed fluctuation issue highlighted in the previous section: it's a technique which result is the signal having the same number of samples (equispaced by $\Delta t = 1/f_s$) in every fundamental period *T* along the record [6]. This is usually performed with the parallel recording of a tachometer signal, which must be synchronous to a reference event in the process cycle (e.g. a revolution of the shaft in an engine) and also to the vibratory signal to be analysed: this is usually achieved by a shaft encoder or (more recently) by the recording of a specific cycle-synchronized control output from the machine control system. Order tracking could be achieved in different manners which depend also from the signal recording equipment, but the simplest and easier way to implement it is by the digital resampling of the signal based on the corresponding "tacho" signal pulses. The "resampling" of a digital signal is the process that deals with changing its sampling frequency. Resampling could be obtained in two ways: in time domain, by inserting the same number of zeros between actual samples (upsampling) and then low-filtering the signal to restore the original signal maximum frequency. In the frequency domain, resampling is obtained by inserting in the (two sided) spectrum the appropriate number of zeros in its centre (i.e. around

Nyquist frequency) and then inverse transforming; since the DFT of a N-point time signal is also constituted by N points, the resulting time signal will have the same (increased) number of samples [1].
Order tracking allow re-mapping the frequency axis to a useful order axis, where order 1 corresponds to the fundamental frequency $f_0 = 1/T$ (i.e.: the inverse of the period used for resampling the signal) and order *n* corresponds to the n^{th} harmonic of the fundamental frequency. Being *T* "driven" by the tachometer signal, the smearing of frequencies due to speed fluctuation is strongly reduced if not eliminated at all.

1.2.2.6 – Moving Average

The Moving Average (MA) is a time-domain technique used in the so-called "historical data analysis" or "time series analysis" in various different fields. There are several types of moving averages, and a definition that describes many versions of it is the following:

$$MA_t = \sum_{i=-n_p}^{n_f} w_i y(t_i) \tag{1.22}$$

where $y(t_i)$ is the (discrete time) signal to be averaged, n_p and n_f are respectively the number of preceding samples and the number of following samples to take into account, and w_i is the weight assigned of the i^{th} sample. If $w_i = \frac{1}{n_p+n_f}$ for all *i*, the moving average is simply the arithmetical average of $y(t_i)$ in the period $\left[t - n_p\ ,\ t + n_f\right]$; other choices of w_i generate different averaging methods (e.g.: exponential moving average) and the choice depends on the particular application required. The MA action can be seen as a filtering action: indeed, one of its possible applications in signal processing is to use it as a "Notch filter", that is: a filter that removes only a particular frequency. This is achieved by setting the temporal length $n_p + n_f$ of the moving average equal to the period of the frequency f to be removed, that is: $n_p + n_f = \frac{1}{f}$, and by choosing the weights as $w_i = \frac{1}{n_p+n_f}$. With these settings, the moving averages take advantage of the fact that sine and cosine functions have a zero mean over their period: thus the signal $y(t_i)$, after being processed with this particular MA filter, will have its oscillation at frequency *f* removed. This is particularly useful if $y(t_i)$ embodies a disturb at a known frequency: the MA in this case can filter out that disturb and restore the original signal.

1.2.2.7 – Spatial Acceleration Modulus

Despite not being an analysis technique, or a signal manipulation technique *stricto sensu*, the definition of the Spatial Acceleration Modulus (SAM) is included in this introductory chapter for convenience because it will be used in the rest of this thesis. Indeed, the SAM is a physical quantity that can be obtained from a triaxial accelerometer, that is an accelerometer able to sense the acceleration along three orthogonal axes x, y and z [7, 8]. The SAM is a scalar value and is defined as:

$$SAM(t) = \sqrt{(x(t) - \mu_x)^2 + (y(t) - \mu_y)^2 + (z(t) - \mu_z)^2} \tag{1.23}$$

where $x(t)$, $y(t)$ and $z(t)$ are the acceleration values at time t along the three axes and μ_x , μ_y and μ_z are the temporal averages of the respective axis (fig. 1.5).

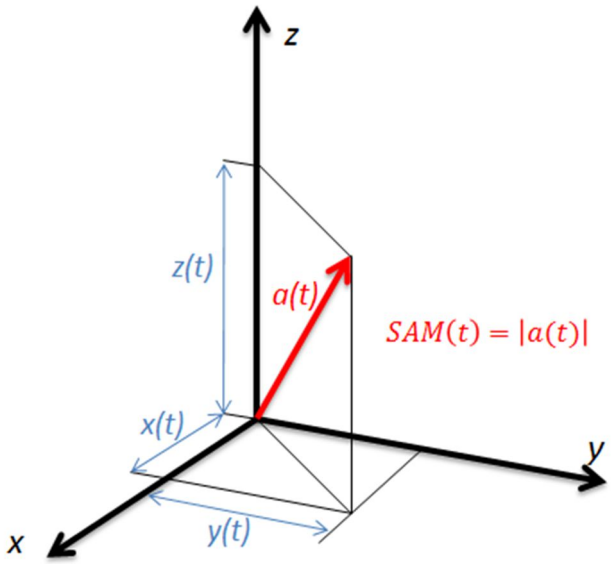

Figure 1.5: obtaining of the Spatial Acceleration Modulus. Acceleration vector $a(t)$ and its projections on the reference system $x(t)$, $y(t)$ and $z(t)$. SAM is the norm (i.e.: the length) of $a(t)$.

The SAM is simply the length of the acceleration vector with component $x(t)$, $y(t)$ and $z(t)$: in eq. 1.23 the averages of each axis are subtracted to their relative axis values in order to have each axis values with zero mean, that is: to compensate for the inevitable non-idealities that every real acceleration signal have because they are quantized both in time and amplitude. Thus, the SAM is basically a "derived" signal: it represent the total amount of acceleration experienced by the accelerometer, and can be treated and analysed just as the other signals (note: the SAM has always positive values). To the best of the author's knowledge, it was first proposed in [7] where it was used for rolling element bearings (REB) diagnostics with very good results: it was there

shown that its behaviour and performances are similar to the reference technique in REB diagnostics, that is the “High Frequency Resonance technique” or “Envelope analysis”.

1.3 - Companies Involved in this Thesis

Bucher Hydraulics, part of the Bucher Industries group, is a leading international manufacturer in the field of mobile and industrial hydraulics. Bucher Hydraulics designs and produces customized hydraulic drive and control equipment for specific applications. The wide range includes hydraulic components and system solutions for agricultural machinery, construction machines, municipal equipment, lift/elevator engineering, industrial hydraulics and high-voltage switchgear. Bucher has production facilities and sales subsidiaries in Europe, India, China, Brazil and the USA. The activities of this thesis work were performed at the Bucher Hydraulics branch in Reggio Emilia.

Fives OTO has been designing, manufacturing and installing complete units for the production of welded tubes and/or profiles for 30 years. Fives OTO is the production and engineering core of the Marcegaglia Group; its experience background as well as typical skills of a company paying the due attention to the sector technological innovations, allowed Fives OTO to enjoy good credits among its customers. A pioneer in the high speed line production techniques, Fives OTO is based in Boretto (Reggio Emilia) and employs 300 people among technicians and engineers divided among the four companies and the three production sites.

Brevini Power Transmission was founded in 1960 by Renato, Luciano e Corrado Brevini. Today it is one of the world's first companies in the epicyclic gearing and mechanic transmissions sector, having a global presence in industrial applications (steel industry, mining and logistics of raw materials, shipyards) and in innovative systems like wind turbines, plant for waste recycling and power plants. Brevini Power Transmission is based in Reggio Emilia; it has 5 production units (one in Germany, one in China and three in Italy) with 1,700 employees, of which about 1,000 are permanently employed abroad.

2 – Diagnostics of Hydraulic Valves

2.1 – Introduction

This chapter deals with the condition monitoring of hydraulic valves used on a hydraulic distributors test bench by Bucher Hydraulics. On this test bench, the freshly-produced hydraulic distributor is tested to check its conformity to the required specifications prior to its shipping to the customer. A sequence of tests is carried on the test bench in a semi-automatic manner, and the following list reports the main test steps:

1. Oil flow and flow resistance test
2. Calibration of max pressure relief
3. Calibration of anti-impact valves
4. Cursors' Internal blow-by test
5. Check valves' sealing test
6. Distributor's Functionality and smoothness test

During the various steps of the test, the oil is routed alternatively from the distributor to the test bench's valves block and vice versa (fig. 2.2 and 2.3): this block hosts the valves studied in this thesis and the pressure and flow rate sensors that are necessary to measure the desired quantities. The valves (fig. 2.1) are poppet valves 2-way normally open (and solenoid-operated), and they have the function of routing the oil appropriately in the test bench during the various testing steps. The block hosts 5 pairs of valves, thus permitting to test distributors with a maximum of 5 cursors: each pair is dedicated to one distributor's cursor, so only a pair of valves is used at a time. Given that the distributor is brand-new, i.e.: it has just finished to be lapped (the last machining performed), it may contains metallic debris in its ducts despite the washing that follows the lapping. When present, these particles are carried away by the oil flux during testing, and they are spread in some zones of the test bench's hydraulic circuit, in particular in the valves block under study. Occasionally (and completely unpredictably), a particle is trapped between the valve's cursor and its seat while the valve is closing: the result is that the sealing is compromised, and consequently the valve will have a blow-by oil flow.

The problem studied in this chapter arises in step 4, the cursors' internal blow-by test, where the maximum blow-by flow rate of each cursor of the distributor is evaluated and checked to be less than a specific value. Given the position of the flow rate sensor in the hydraulic circuit of the test bench, when a valve's sealing is spoiled it will read the sum of the blow-by flow rate of the distributor's cursor and the valve's cursor. If this reading is greater of the required value the operator should declare the distributor

as “non-conform” and thus reject it: in reality, the operator doesn’t know if the measured blow-by is coming only from the distributor or if there is a faulty valve on the test bench altering the reading. For example: a typical maximum blow-by flow rate limit is 16 cc/min for 8 seconds (note that this is a very small value for these hydraulic applications); a faulty valve has its own blow-by of 5 cc/min, unknown by the operator. If the operator at step 4 reads a blow-by of 19 cc/min he will reject the distributor, but in reality the distributor is conform because its real blow-by flow rate is actually 19 -5 = 14 < 16 cc/min, which is an acceptable value.

In order to limit this problem, Bucher produced a so-called “master distributor”, i.e. a distributor which blow-by flow rates are known: the master distributor is used to calibrate the test bench by testing it in place of a “production” distributor. By doing this, the operator knows the offset (i.e.: the valve’s 5 cc/min of the previous example) and apply this offset on the reading during the tests. This solution has two main drawbacks: first, the calibration remains reliable only for few tests; second, the block’s valves are always ready to be ruined by the metallic particles flowing with the oil. The valves damaging could also be caused by the natural wearing of their cursor-seat coupling and by the presence of fabrication defects that, in casual manner, evolve and cause a misalignment of the cursor. All of these damaging modes compromise immediately the valve’s sealing, that is: during a test the valve is perfectly working, at the next test the valve is discovered to be unusable.

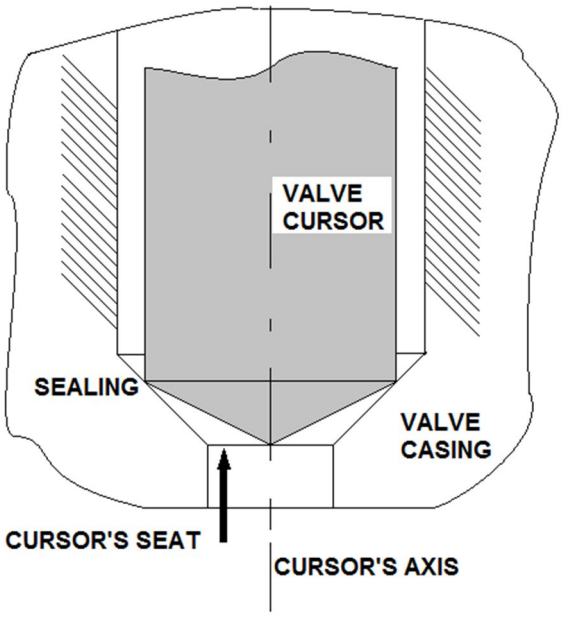

Figure 2.1: general outline of the monitored valve’s sealing.

To complete the description of the problem and to provide an idea of the losses that it causes, the following data should be considered: the testing time of a distributor is 20 - 30 min (this is also the test bench calibration time, i.e. the master distributor

testing time); the time necessary to replace a spoiled valve is 10 – 20 min; the time to identify a spoiled valve is difficult to quantify, but in the *best* case it could be equal to 2 or 3 distributors testing time, i.e.: 40 – 90 min; the price of a distributor vary from tenths to hundreds of euros. A typical scenario is the following: the operator is testing a production lot of distributors, everything runs ok; then he has to reject 2 or 3 distributors consecutively because of exceeding blow-by flow rate; he then suspects that a valve is broken, thus he could decide to test the master distributor (and thus re-calibrate the test bench) or to blindly substitute the valve; then he must re-test the just rejected distributors. Time loss: approximately 110 – 230 min; if we suppose that a distributor of that lot costs 150 euros (they usually cost more), the money loss due to time loss only is 600 – 1350 euros.

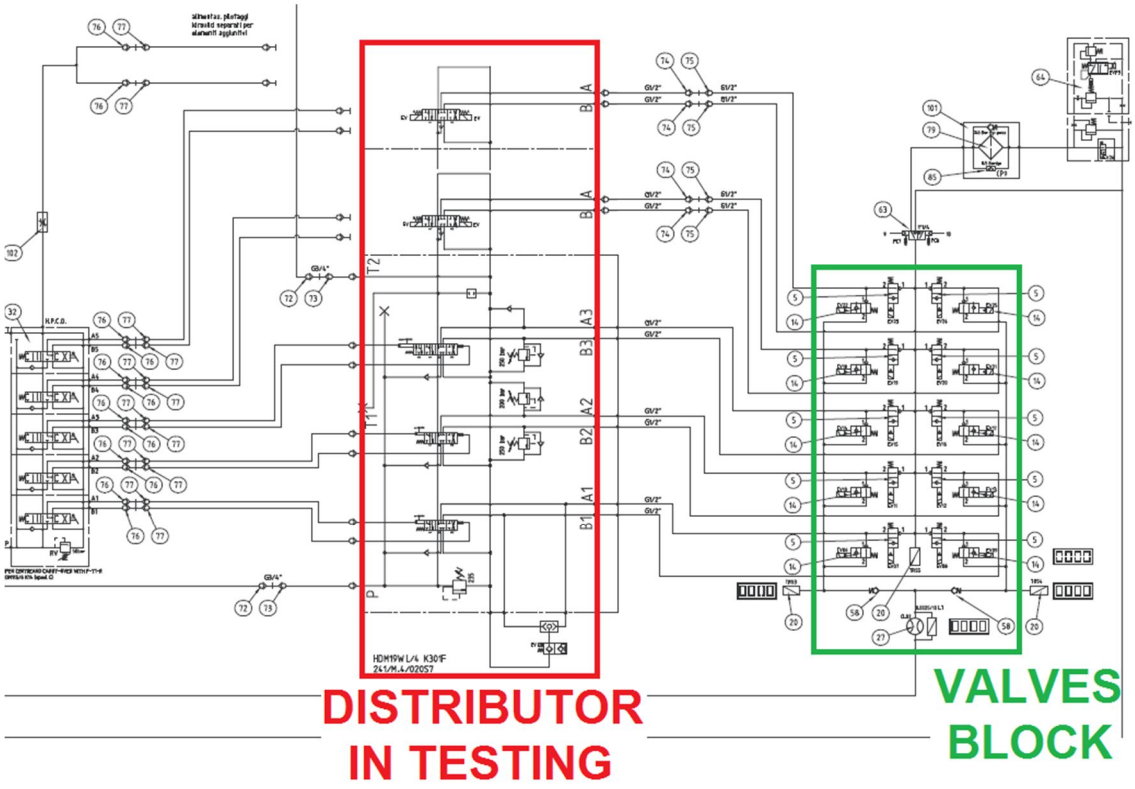

Figure 2.2: extract of the test bench hydraulic scheme.

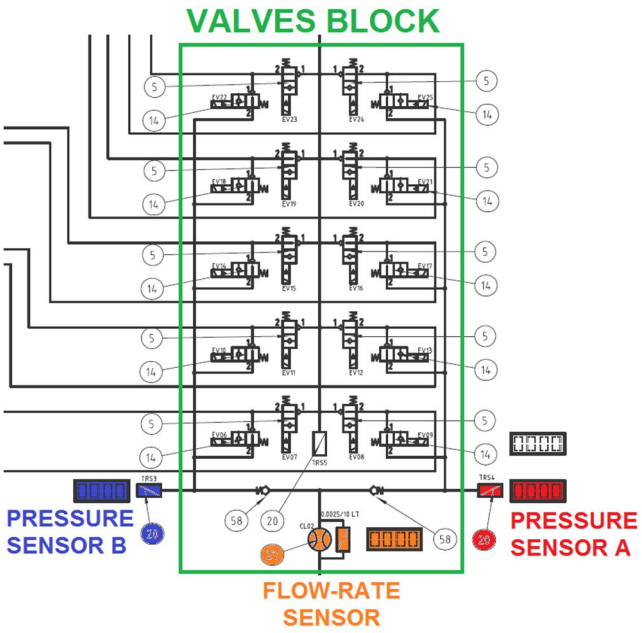

Figure 2.3: detail of the test bench hydraulic scheme. Valves Block and sensors hydraulic placement.

2.2 – Experimental Set-Up

The data acquisition campaign was performed in two steps. It was initially performed on the test bench itself, with the aim to spot a faulty valve during the normal daily test bench operations. It was decided to use a piezoelectric triaxial accelerometer to record the vibrations of the valves' block, besides the recording of the signals coming from the test bench's pressure and flow-rate sensors. The accelerometer was planned to be placed as near as possible to the most utilized pair of valves, the latter named A1 - B1 (fig. 2.4 and 2.5): given the scarcity of space available, it was decided to put the accelerometer almost over the A1 valve. Since every distributor has at least one cursor, this pair is used in every test and for this reason is usually the fastest to be damaged. The distributor may have a maximum of 5 cursors, so the relative pairs of valves are named A1 – B1 to A5 – B5 in the rest of this chapter. The following is a schematic summary of the acquisition hardware and characteristics:

- Sensors
  - Accelerometer: PCB 356A01 (triaxial);
  - Pressure sensors: Wika Micro Tronic M10 (embedded in the test bench);
  - Flow-rate sensor: VSE VS2 (embedded in the test bench);
- Acquisition hardware
  - NI 9234 analog input module: it acquired the 3 vibration channel (X,Y,Z);
  - NI 9229 analog input module: it acquired two pressure sensors (hydraulic channel A and B) plus the flow-rate sensor

    - NI cDAQ 9172: USB carrier for the two acquisition modules
- Acquisition software: National Instrument Signal Express
- Records main characteristics
    - Channels number: 6 (vibration X,Y and Z, pressure A and B, flow-rate)
    - Sampling frequency: 25 kHz
    - Record duration: 90 s (enough to cover the distributor's cursors' internal blow-by test.

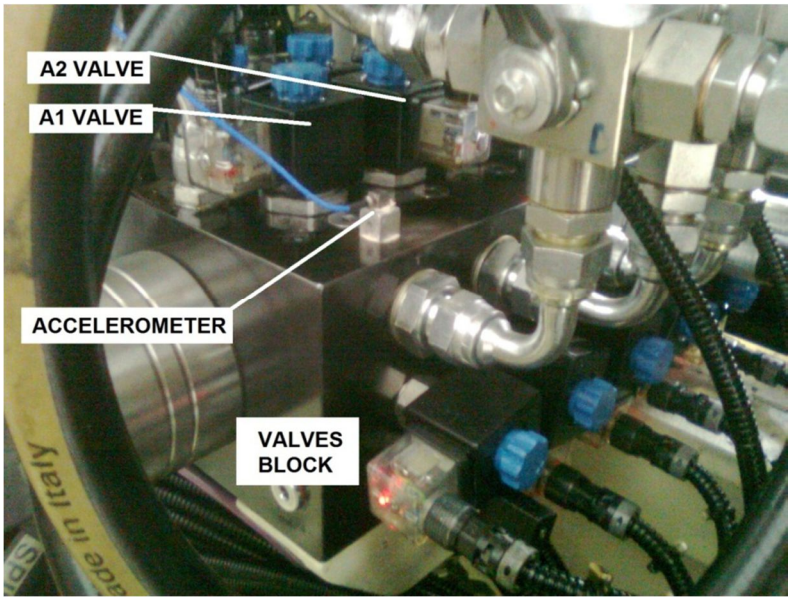

Figure 2.4: the valves block of the test bench.

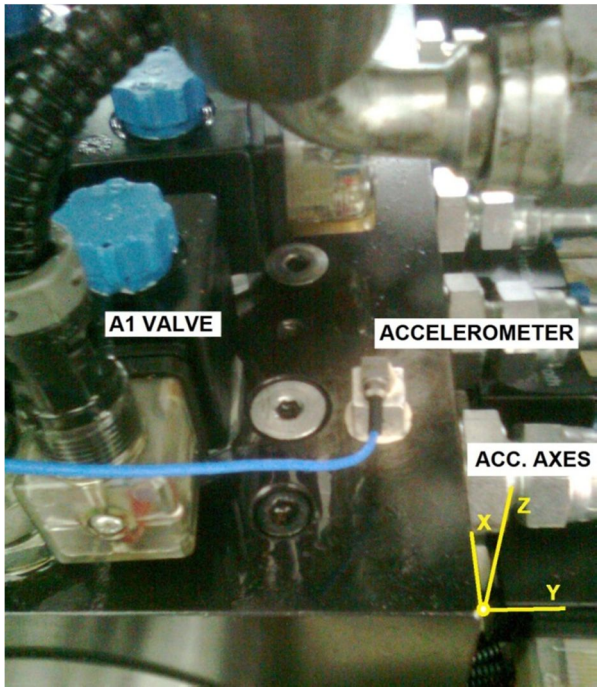

Figure 2.5: detail of the accelerometer positioning and the orientation of its axes.

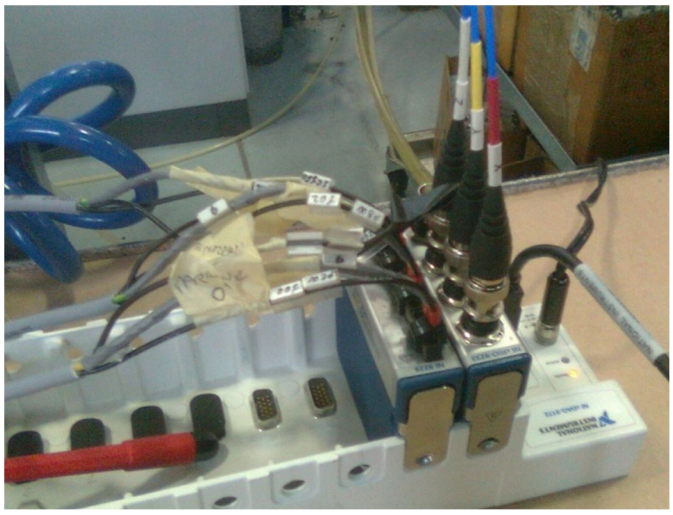

Figure 2.6: the acquisition hardware used for the acquisition campaign.

In figure 2.7 the typical behaviour of the monitored quantities is visible when there is no valve fault. The closure of the valves are evident as peaks of vibrations and they are the event to be monitored in vibrations analysis because of two main reasons: first, the valve has no mobile parts except for its cursor, which moves only when the valve is opening or closing, thus giving a nature of transient to the vibration signals.; second, the impact generated by the closure of the cursor embodies information about the interaction between the cursor and its seat.

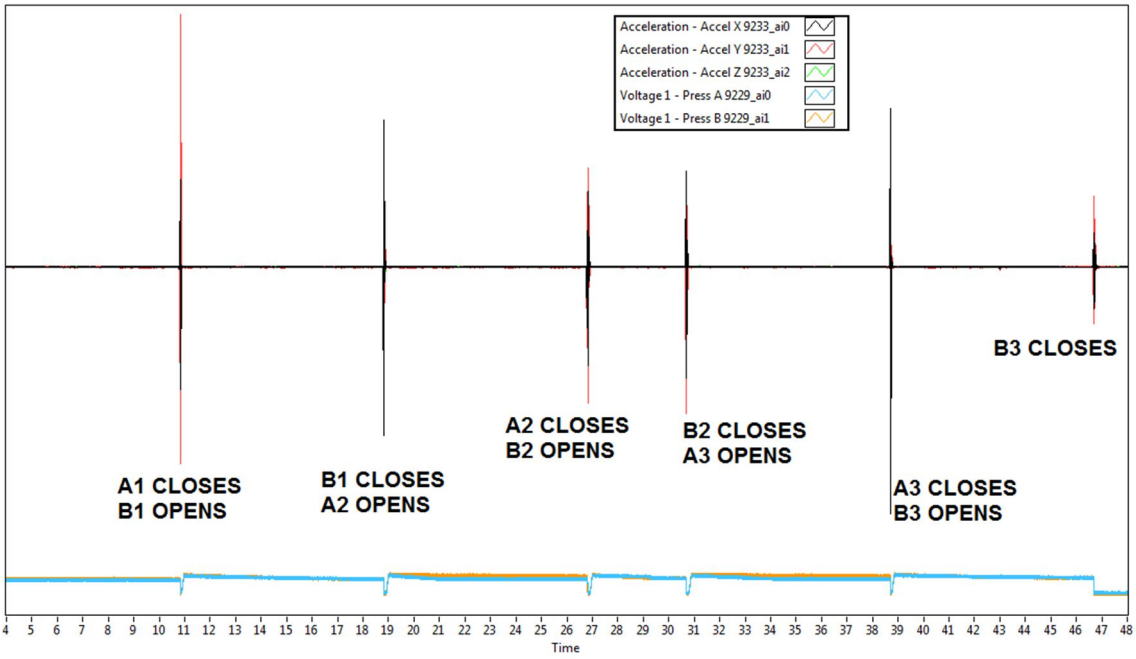

Figure 2.7: signals coming from the blow-by test of a 3 cursors distributor acquired on the test bench.

Unfortunately, during one month of data recording there were only one occasion to record a faulty valve, so it was decided to realize a dedicated test rig in order to

characterize the difference of behaviour of the parameters between a healthy valve and a faulty one. In fig. 2.8 the hydraulic scheme of the test rig is reported: it is a very basic hydraulic circuit that includes a steel block capable of hosting the valve under test; the oil is routed to the valve by a manually controlled valve. A brand-new valve and two faulty valves were tested on this test rig: each trial consist in the recording of openings and closures of the valve when this was under a pressure load in order to simulate the valve's operational behaviour. **It was decided not to record the oil flow-rate because from the analysis of the previous step of the acquisition campaign it was recognized as non-necessary: indeed, the blow-by of a valve can be seen indirectly by means of the pressure, which drops if the blow-by occurs.** The hardware (sensors and input modules) and software used in this series of trials coincided with those previously indicated for the recording performed on the test bench, with the exception of the flow-rate sensor.

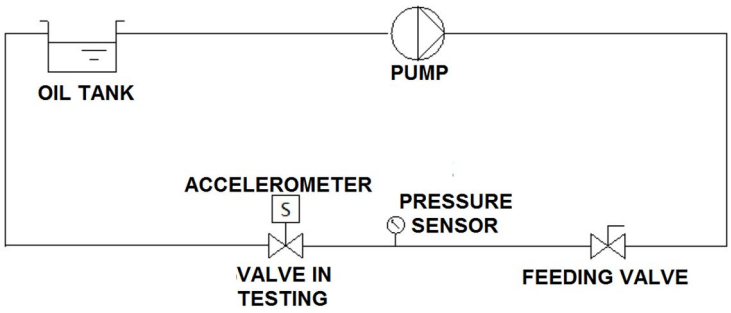

Figure 2.8: the hydraulic scheme of the test rig.

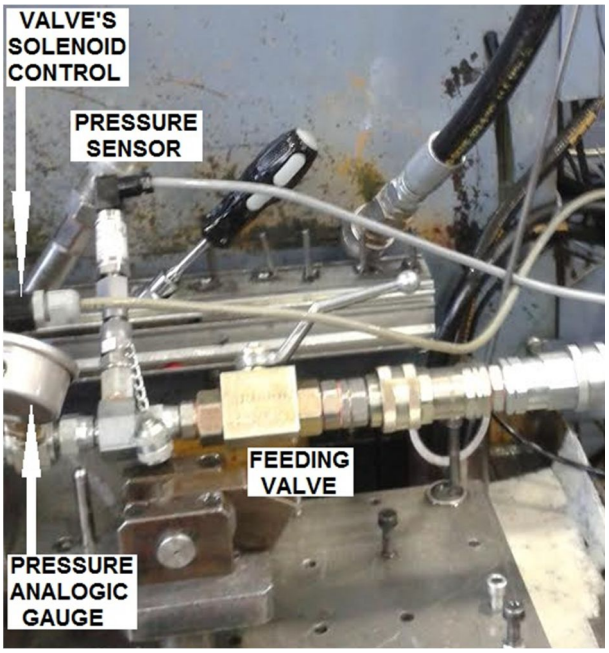

Figure 2.9: particular of the test rig. Pressure sensor and the hydraulic piping directed to the tested valve intake port.

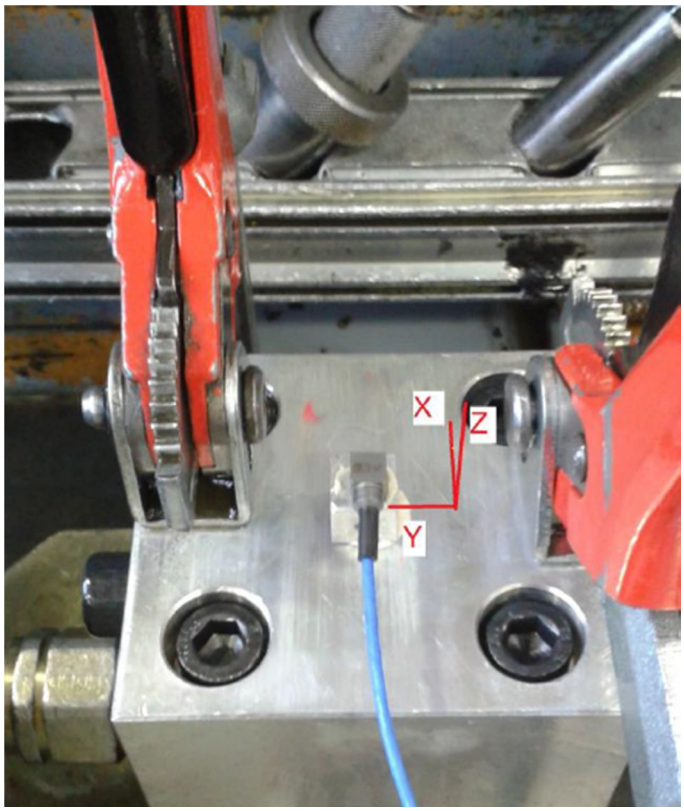

Figure 2.10: particular of the test-rig; the steel block which hosts the valve under testing and the accelerometer with the indication of the orientation of its axes. The y axis is parallel to the valve's cursor axis, and its positive direction is concordant with the movement of the cursor when the latter is closing.

2.3 – Data Analysis

The analysed signals were the vibrations along the three axes joined by the Spatial Acceleration Modulus (SAM): given the transient nature of the recorded events (i.e.: the valve's openings and closures), it was decides to analyse the signals in the time domain. The analysis was focused on the closing of the valves, because it is then that the cursor impacts its seat and for this reason, the valve closing is the event that carries more information on the status of the valve sealing. In figs. 2.11 and 2.12 two complete records taken from the test-rig are reported: fig. 2.11 is relative to the brand-new valve when closing, while fig. 2.12 is relative a faulty valve when closing. From these figures it can be seen immediately the difference in behaviour between the two valve conditions: the healthy valve does not have a blow-by, so its pressure data remains almost constant at 100 bar (which was the pressure set for that trial); instead, the faulty valve clearly shows a pressure drop from 125 bar to less than 25 bar in approximately 3.5 s. Moreover, the peak of the vibration modulus (SAM) generated by the impact of the cursor with its seat is approximately 0.45 g for the healthy valve, while the correspondent peak is 1.25 g for the faulty valve.

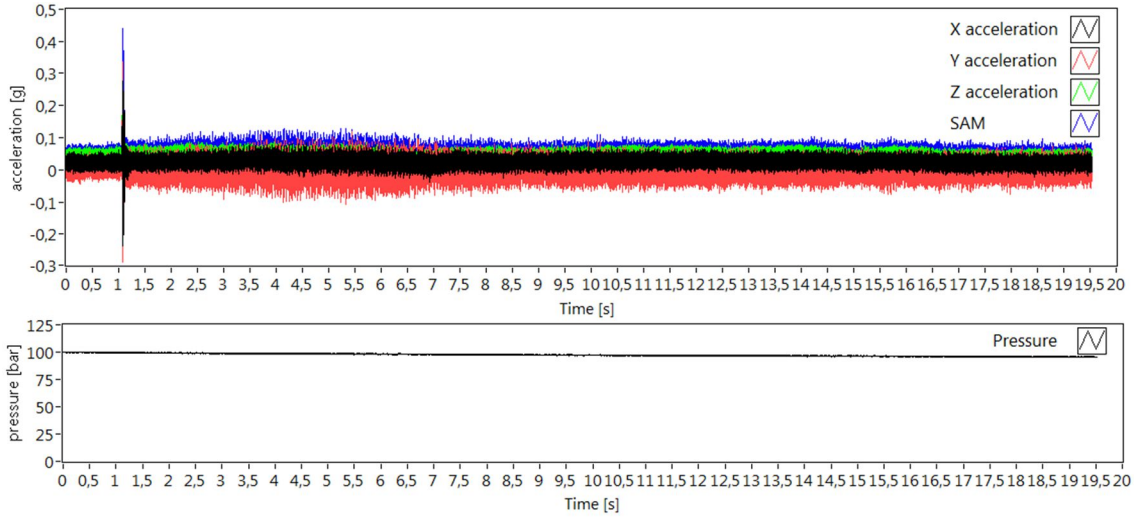

Figure 2.11: raw data acquired on the test rig with a healthy (brand-new) valve in test when closing. The upper graph reports the 3 acceleration axes and the SAM, the lower graph reports the pressure.

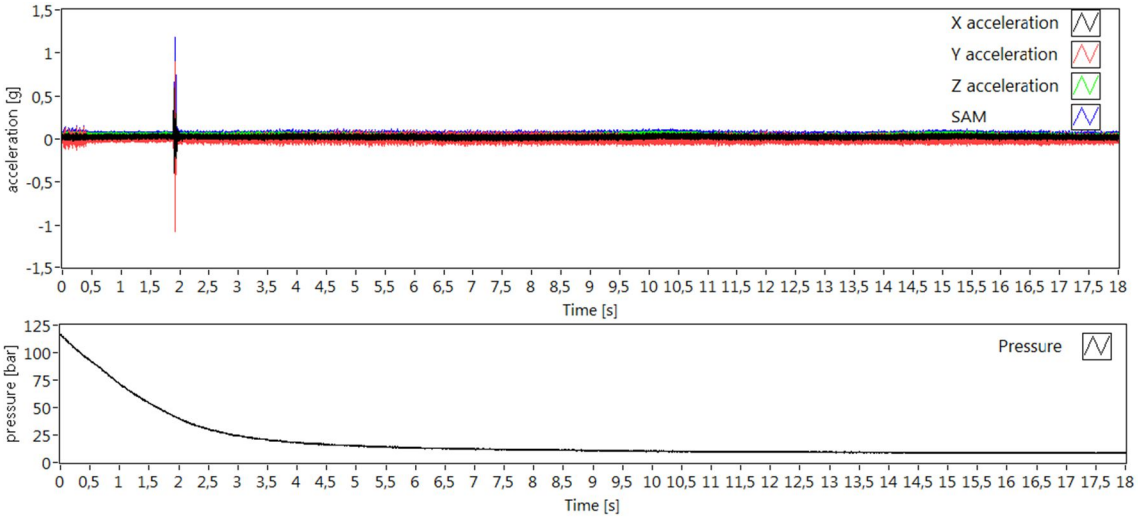

Figure 2.12: raw data acquired on the test rig with a faulty valve in test when closing. The upper graph reports the 3 acceleration axes and the SAM; the lower graph reports the pressure.

It was decided to perform time synchronous averaging (TSA) of the recorded vibrations. As mentioned in §1.2.2.4, TSA is usually performed on signals coming from rotating machinery, and usually it requires a synchronizing signal to be correctly performed. This case is different - there is no rotating machinery nonetheless a synchronizing signal - so it was chosen to synchronize the data via the peak of the SAM, which represent the same event (closing or opening of the valve). As it is visible in fig. 2.11 and 2.12, after the vibratory transient generated by the impact of the cursor with its seat there aren't notable events in the vibration data, so the temporal length of the average was chosen to be 0.3 s. In fig. 2.13, 2.14 and 2.15 are reported

respectively the averages of vibrations of the brand-new valve, the faulty valve and the difference between the two in case of opening of the valves.

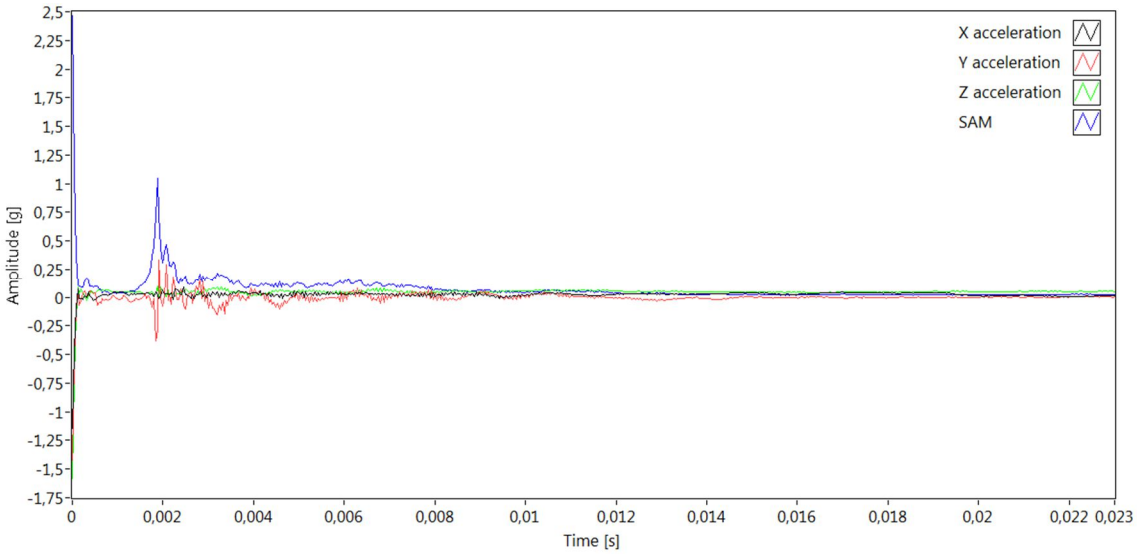

Figure 2.13: time synchronous average of the openings of the brand-new valve.

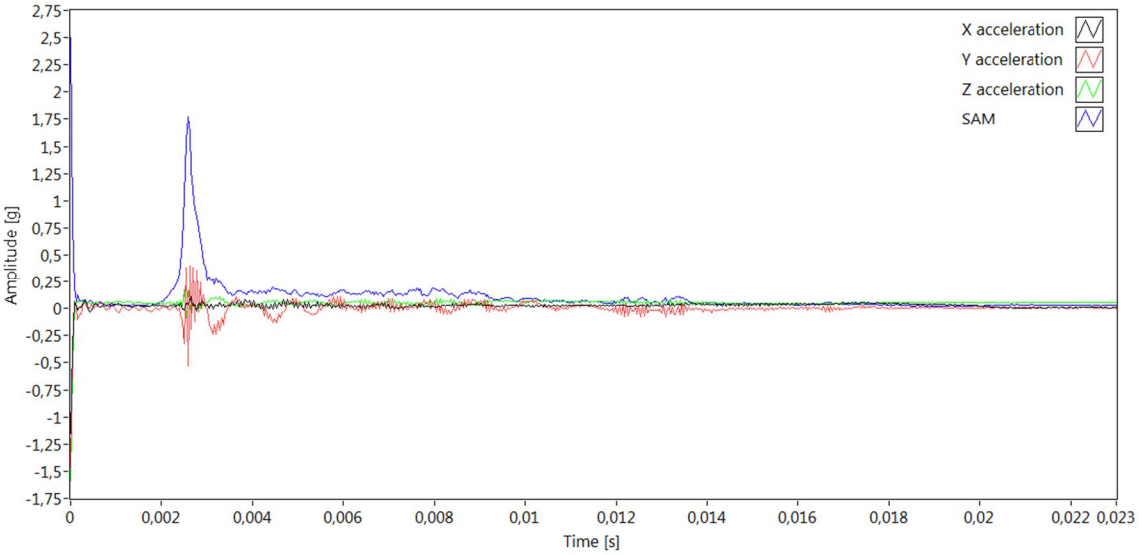

Figure 2.14: time synchronous average of the openings of a faulty valve.

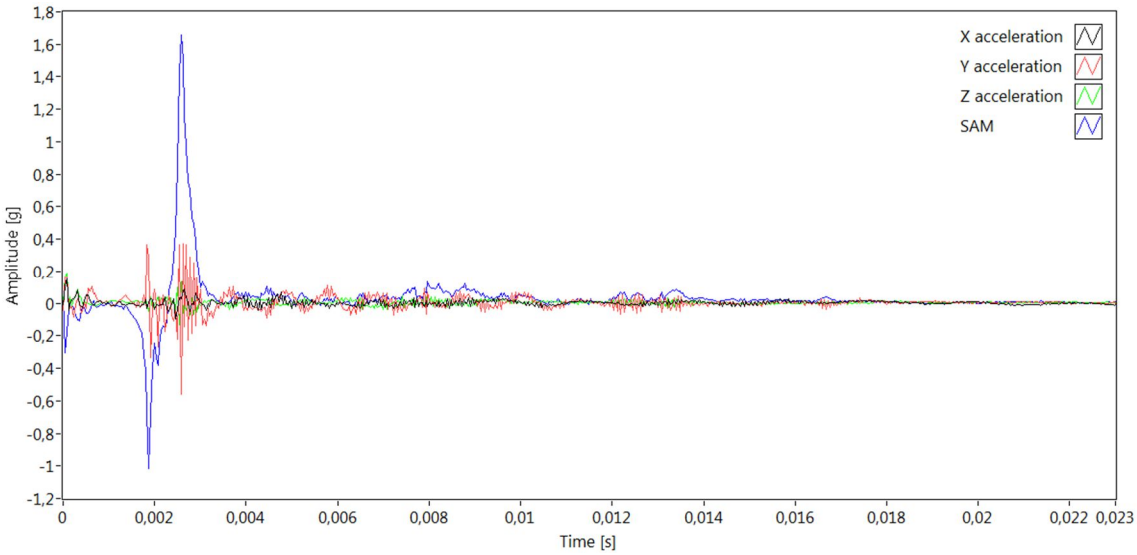

Figure 2.15: difference of vibration between the average of a faulty valve and a brand-new valve when opening.

As mentioned before, when the valve opens the vibration behaviour is very similar when the valve is new or broken: indeed, the initial peak of vibration of the SAM (located at $t = 0\ s$ in fig. 2.12 and 2.13) is 2.5 g in both cases. This peak is followed in both cases by a resonance, especially in the *y* direction: this peak in the SAM signal is almost 1 g for the new valve while it is almost 1.75 g for the faulty valve, and in the latter case the peak occurs slightly later than in the former case (approximately 0.001 s later). This lag could be explained by the following consideration: in hydraulics valves, the verse of closing of the cursor is usually opposite to the verse of the oil flow in order to avoid the cursor sticking to its seat under the pressure of the oil when closed, thus helping the valve opening. In this case, given the better sealing of a new valve, the oil gives a greater thrust to the cursor during its opening because of the higher pressure, and thus the cursor reach the end of its stroke earlier than in case of a broken valve. All these findings are synthetized in fig. 2.15, which report the difference of the averages in fig. 2.13 and 2.14: the difference of the initial peak of vibration is 0 g, while the lag between the second pulses of vibration is clearly visible in the SAM signal. As expected, the opening of the valve does not give many useful information on the valve healthy status, because this lag is very little and so far difficult to be monitored. In figures 2.16, 2.17 and 2.18 are reported respectively the averages of vibrations of the brand-new valve, the faulty valve and the difference between the two in case of closing of the valves.

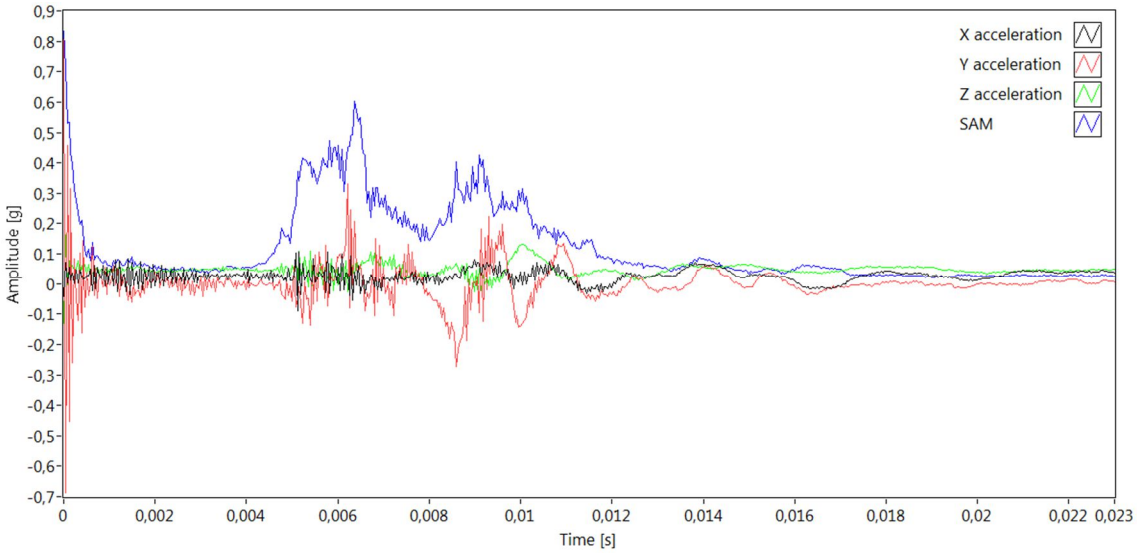

Figure 2.16: time synchronous average of the closings of the brand-new valve.

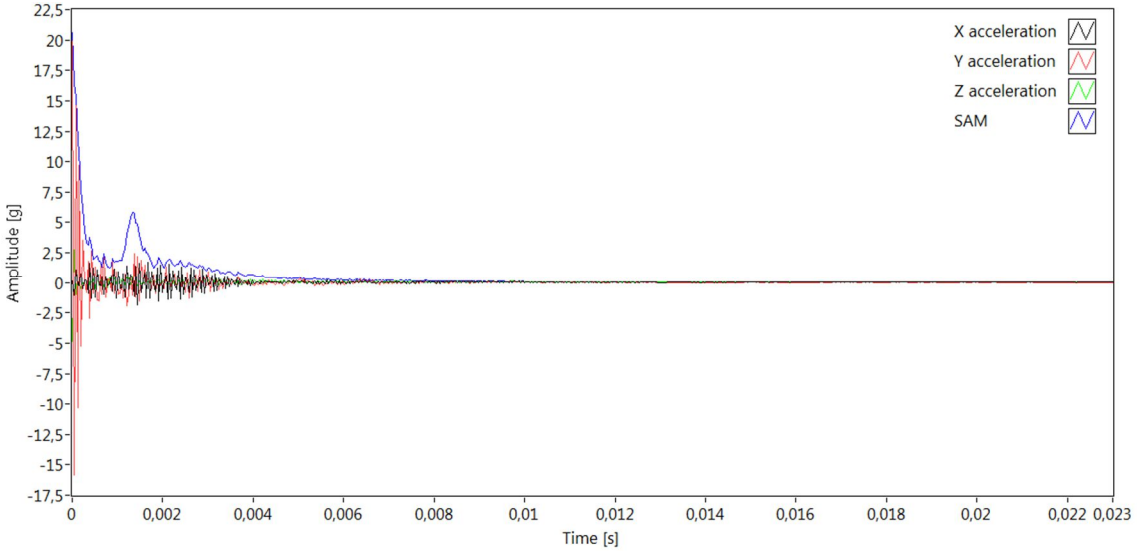

Figure 2.17: time synchronous average of the closing of the faulty valve.

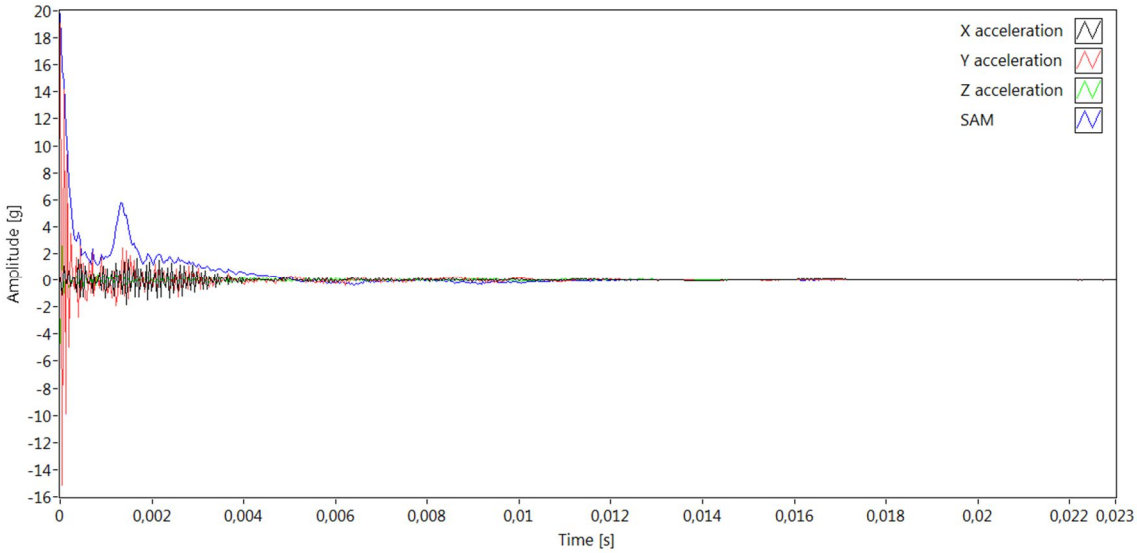

Figure 2.18: difference of vibrations between the average of a faulty valve and a brand-new valve when closing.

In these figures it can be observed that the first peak of vibration in the SAM signal (at t = 0 s in all the aforementioned figures) is 0.9 g for the new valve and more than 20 g for the faulty valve: the vibratory energy resides mainly in the *y* direction of vibration (just like when the valve is opening), and this is expectable because the *y* axis coincides with the direction of movement of the valve cursor. There is a second peak of vibration of 6 g at t = 0.0018 s in case of faulty valve, but in case of a new valve this peak is almost unnoticeable. In the average of a new valve closing (fig. 2.16) there is a longer transient in vibration than in the respective average of a faulty valve (fig. 2.17), and this transient's energy resides mainly in the *y* direction again – although less evidently than in case of the opening of the valve: this transient is present also in case of faulty valve (fig. 2.17), but despite it being stronger (*y* vibrations in fig. 2.17 oscillates approximately between +2.5 g and -2.5 g, while in fig. 2.16 it oscillates approximately between +0.35 g and -0.3 g) it is shorter in time. This probably is caused by the fact that when a brand-new valve closes the column of oil is immediately stopped by the sealing, generating some kind of water hammer and, consequently, a relatively strong vibration which is divided almost equally along the three directions of vibration. In case of a faulty valve, the sealing is not perfect (as it is demonstrated in fig. 2.12), thus the oil isn't completely stopped, and the subsequent water hammer doesn't occur or it's less strong. The vibrations are nonetheless higher than in case of a new valve, but this probably is caused by the stronger initial peak of vibration that is resonating in the metallic block hosting the valve. Indeed, the difference of the two averages (fig. 2.18) is almost equal to the average of the broken valve, because this is approximately 20 times bigger than the average of a new valve, despite the use of the same solenoid to move the cursor in all the trials performed. A possible explanation of this difference is

the following: when the sealing is not perfect, the cursor does not impact its seat at the same moment along the cursor/seat line of contact (fig. 2.1). The sealing may be ruined by some metal particle that indent the surfaces or by a fabrication defect regarding the axis of the cursor, which can be out of centre. In both cases, the impact force is distributed on a smaller surface and it is shifted from the centre axis of movement of the cursor, thus enhancing the resulting vibration.

2.4 – Conclusions

To assess the health status of the valve it is only required checking the intensity of vibration when closing. From §2.3, it can be achieved by means of a tri-axial accelerometer and also by a single axis accelerometer: the latter should be aligned with the direction of movement of the cursor (i.e.: the *y* axis of vibration in chapter 2.3). Further investigations are nonetheless required, because this finding comes from a dedicated test rig where the vibratory effect of other moving parts was strongly reduced: indeed, the valves to be monitored are inside a test bench, so they are embedded in a very noisy and vibrating ambient. Nevertheless, the difference of the peak of vibration is very high (the faulty valve vibrations are 20 times the new valve vibrations) and this is auspicious for the realization and implementation of a condition monitoring system on the test bench.

Unfortunately, in this case the Sensorless approach cannot be used: indeed, the problem studied in this chapter arises from a wrong placement (a posteriori at least) of the flow-rate sensor on the test bench, placement that inhibits a correct reading of the distributor's blow-by flow rate. The sensor needed to read the physical quantity of interest is already present, but with the actual configuration the reading will always be the sum of the blow-by of the distributor and the valve on the test bench.

3 – Diagnostics of Blades for Steel Tubes Cutting

3.1 – Introduction

This chapter deals with the diagnostics of blades used to cut steel tubes. The blades are hosted on the last element (called “Cut-off unit”, fig. 3.1) of long machinery which produces tubes starting from raw steel plate coils. The steel plate coils are scrolled, then they are progressively bended by a series of rollers (each series of roller is dedicated to a specific tube shape and size); at this point the almost formed tube is welded and subsequently cut in rods by the Cut-off unit. From the entering point of the steel coils to the cut-off unit, the tube in forming is basically one very long piece of steel flowing at a specific speed through the machinery while crossing all the processing required. For this reason, the cut-off unit hosts the blade on a carriage, which moves alternatively in order to get synchronous to the tube flow before the actual cut. When the carriage is running synchronously with the tube, and it is at the position required to obtain the final desired tube length, a vice locks the tube and then the blade cut it. Thus there are three main electric motors on the cut-off unit: one motor has the function to make the blade rotating at a specific speed (called “blade motor” in the rest of this chapter); another motor moves the blade in and out of the tube(“translational motor”); the last motor moves the entire carriage (“carriage motor”). Between the blade and the blade motor there is a gearing, which reduce the speed of the motor shaft to obtain the desired blade rotational speed: depending on the type of blade in use, two reduction factors can be selected (8,89/1 or 20,8/1). Indeed, two types of blade can be used depending on the specific cut requirements, these being High Speed Steel (HSS) blades and Tungsten Carbide Tips (TCT) blades (fig. 3.2); during the data acquisition campaign, only TCT blades were used.

Figure 3.1: the Cut-off unit. The yellow part is the carriage which hosts the blade under study.

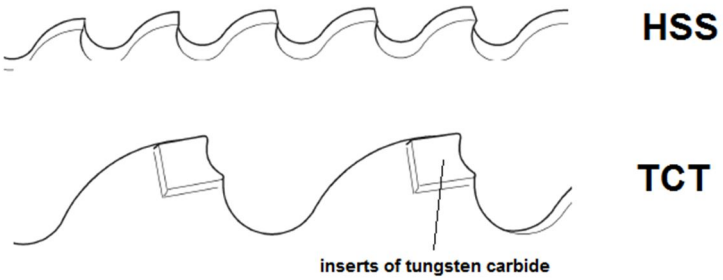

Figure 3.2: difference between HSS and TCT blades teeth.

In this manufacturing sector there is a high interest in knowing when a blade has weared-out, mainly because of the performances of these machinery: indeed, these are capable of very high production rates (during the data acquisition campaign, a material speed of 125 m/min wasn't rare: this means that over 20 steel tubes 6 meters long are produced every minute). Changing a blade is an operation that requires basically the following steps:

- stopping the steel flowing in the machinery: this must be done by progressively slowing the material (while still producing rods), and the time required is a few minutes;
- changing the blade and setting the cut-off unit parameters if the blade is different from the previous one: this operation requires 5-10 minutes;
- restarting the machinery: again, this must be done by progressively accelerating the material flow to the speed required.

Thus, knowing the state of wearing of the blade allow to reduce to the optimum these time losses and, moreover, to fully exploit the life of the blade.

3.2 – Experimental Set-Up

The data acquisition campaign was performed mainly at a customer site, because the cut-off unit can't be in its complete operational status if the rest of the machinery isn't present: this was not possible at OTO headquarters. Nevertheless, an initial study of a few cuts was performed there: the carriage of the cut-off unit was kept still and only the translation a blade motors were used, while only the vibration data were recorded). At the customer's site, a National Instruments compactRio was used to acquire the data: it was programmed to sense the state of the cut-off unit PLC command that closes the vice on the carriage and to use it as the acquisition trigger, so the acquisition is performed only if the vice is closed. The acquired signals were the vibration along the three axes of a tri-axial accelerometer and the three torques of the aforementioned motors: the torques signals come from each motor's drive, and these data are available on the machine control system, thus the Sensorless approach can be performed by using these data. Given the wide amount of data recorded it was chosen to use a NAS to store them. In fig. 3.3 and 3.4 the accelerometer placement is illustrated, while the following is a schematic summary of the acquisition hardware and characteristics:

- Sensors
    - Accelerometer: PCB 356A02 (triaxial);
- Acquisition hardware
    - NI 9234 analog input module: it acquired the 3 vibration channel (X,Y,Z);
    - NI 9229 analog input module: it acquired the "vice state" (trigger) signal and the 3 motor torques
    - NI cRio 9075: compactRio.
- Acquisition software: dedicated cRio program
- Records main characteristics
    - Channels number: 6 (vibration X,Y and Z, carriage motor torque, translation motor torque, blade motor torque)
    - Sampling frequency: 25 kHz
    - Record duration: commanded by the trigger signal.

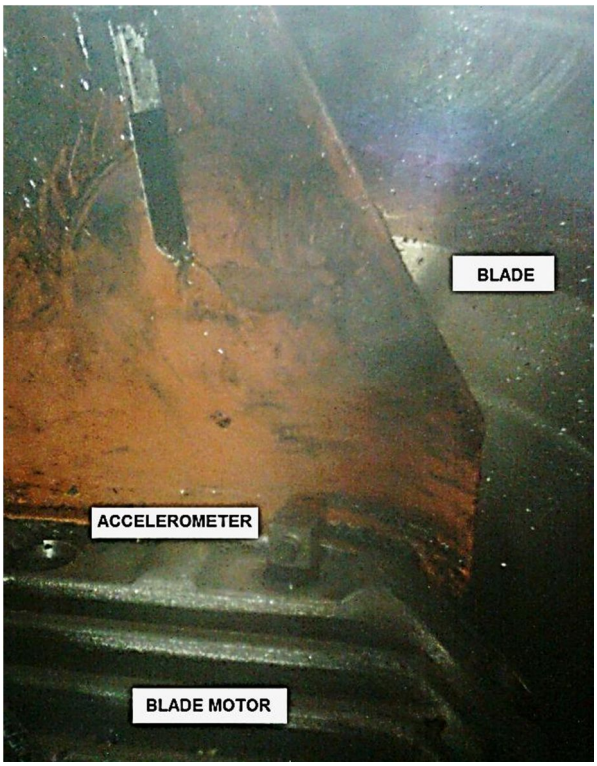

Figure 3.3: accelerometer placement.

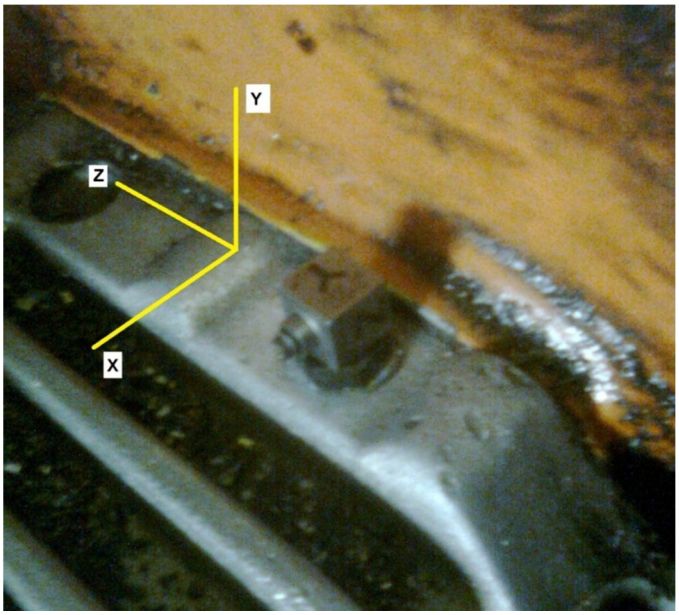

Figure 3.4: detail of the accelerometer placement and its axes. The blade lies parallel to the YZ plane.

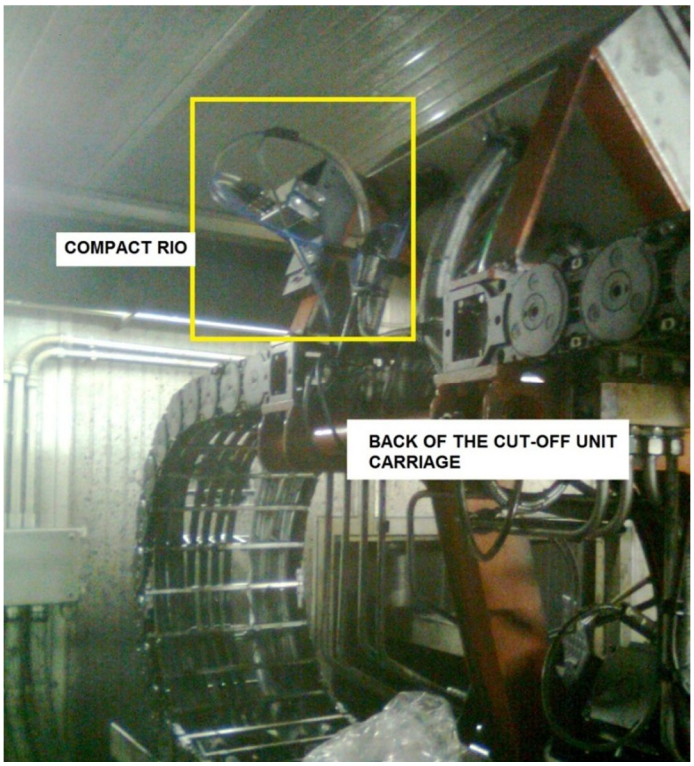

Figure 3.5: placement of the compactRio.

The compactRio was mounted on the back of the cut-off unit carriage (Fig. 3.5), thus was moving with it, and this was mandatory because of the required length of the accelerometer cable: indeed, the nearest alternative placement of the cRio could have been in the cut-off unit's control box (where the NAS was placed), which is about 15m distant, but this distance would have exposed the accelerometer cable to electromagnetic noise. The NAS was reached by means of an Ethernet cable. During the 45 days of acquisition, approximately 200000 cuts were recorded for a total of 300 GB of data.

Besides these data, another set of data was provided by OTO: these data were collected by software that was developed and installed on the machine control system by the OTO itself. This software was directly interfaced with all the control signals of the cut-off unit, thus allowing storing data when some particular conditions occur. The main conditions that trigger the data storing were:

- Machine (production line) in Alarm: it triggers the data storing if a generic alarm occurs (emergency stop and any other event that generates an alarm on the machine control system);
- Cut-off unit door opening: very useful data because the operator must open the door to enter the cut-off unit box and eventually change a blade;
- Calibration of one of the three cut-off unit motors;
- Rotation motor start;
- Translation motor torque over 50% of nominal value;

- Material speed variation: if the operator changes the speed of the material, a trigger is generated only if the absolute difference of speed is over 5 m/min;
- Cut-off unit set-up change: data is stored if the operator effectively changes the configuration file (named “TrajectoryPoint”) of the cut-off unit.

The production line data that were stored are:

- Date/time of the trigger event;
- Trigger event;
- State of the cut-off unit doors (Boolean, TRUE if door open);
- Value of the blade cuts counter (integer number): this counter is reset manually by the operator ideally when a blade is changed;
- Material speed (real number, m/min);
- Translational motor torque (real number, % of nominal torque);
- Line in alarm (Boolean);
- Trajectory file change (Boolean);
- Carriage motor calibration (Boolean);
- Translation motor calibration (Boolean);
- Rotation motor on (Boolean).
- TrajectoryPoint file (stored only when it is changed), containing the complete set of operational parameters of the cut-off unit.

3.3 – Data analysis

3.3.1 – OTO Headquarters’ Data Analysis

The preliminary data acquisition at OTO headquarters resulted in the main finding that the blade vibration spectra are dominated by the frequency equal to the blade rotating frequency times the blade number of teeth, and the harmonics of this frequency (Fig. 3.6). This frequency is named “teeth frequency”, and represent how many teeth per second encounter the tube during the cut. Another finding of this test was that a damaged blade – i.e.: without a tooth – seems to increase the amplitude of its teeth frequency: this is visible in Fig. 3.7 (which is relative to the same blade of Fig. 3.6 but without a tooth) when compared to Fig. 3.6: the amplitude of the teeth frequency rise from 0.88 in Fig. 3.6 to 1.04 in Fig 3.7.

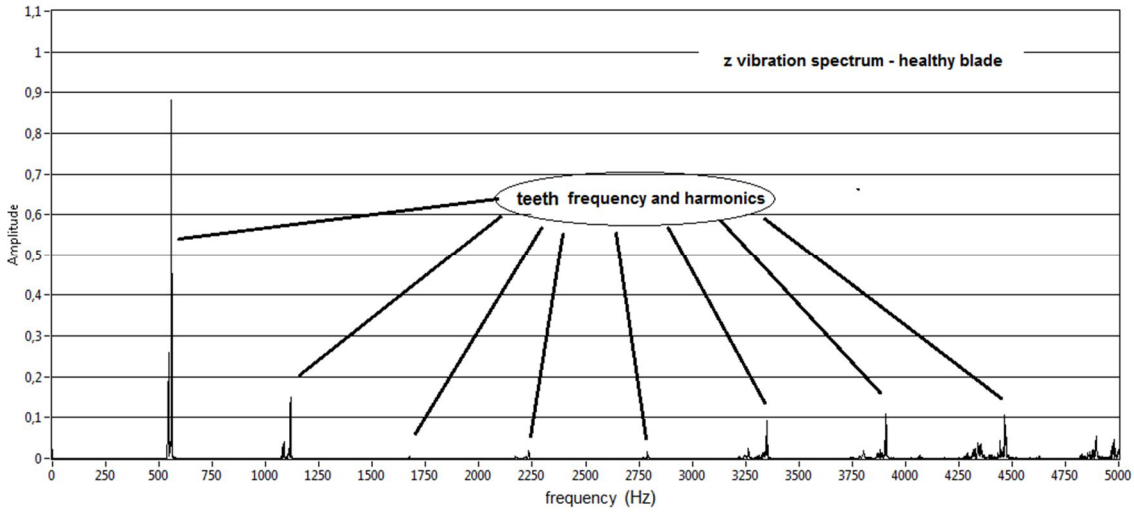

Figure 3.6: spectrum of vibration along the Z direction (lying on the blade plane) in case of a healthy blade. The teeth frequency (amplitude: 0.88) and its harmonics dominate the spectrum.

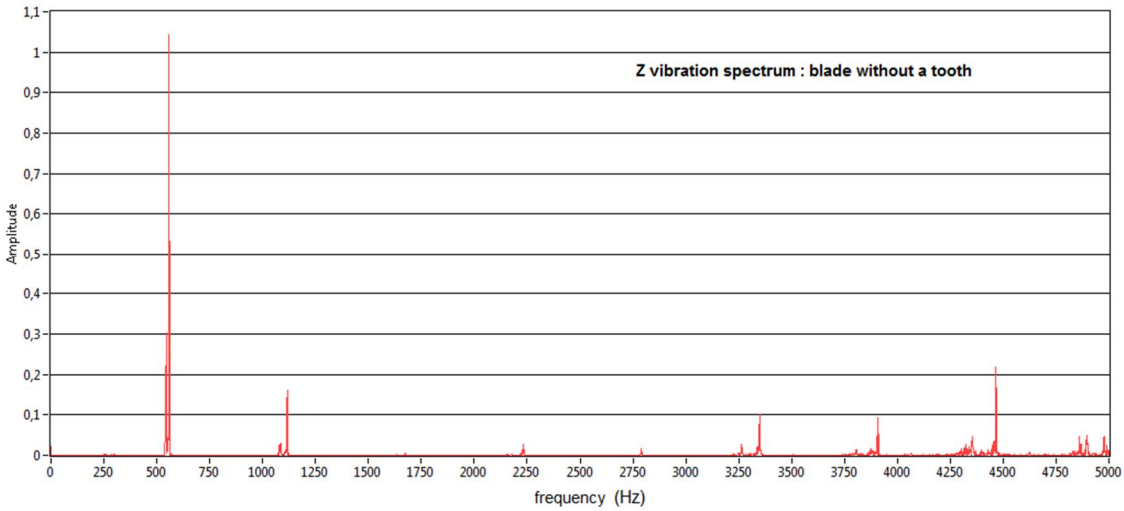

Figure 3.7: spectrum of vibration along the Z direction (lying on the blade plane) in case of the same blade of Fig. 3.6 without a tooth. The teeth frequency amplitude rises to 1.04, and some of its harmonics amplitudes rise too.

3.3.2 – Customer's site data analysis

The data were recorded during the time when the vice was closed: since the cut duration is shorter than this time, the first thing to do is to isolate from the signals only the part relative to the cut. This was done by means of the aforementioned TrajectoryPoint files, wherein all the electric cams of each motor are available (i.e.: the set-point of each motor drive). It was chosen to use the rotation torque as the synchronizing signal: indeed, this torque rises when the blade start to touch the tube and this obviously occurs only when the vice is already closed. Thus, the synchronization of the two set of parallel acquired data (i.e.: the compactRio data and the cut-off control system data) was achieved by means of synchronizing the initial

rising of the rotation torque. In the data synchronization process, the following problems were encountered:

1. The rotation motor set-point is the rotation speed, not the torque: this means that in the TrajectoryPoint file there isn't a "torque set-point" to be used for synchronization. Moreover, the theoretical estimation of the necessary torque for cutting is an open problem in this industrial sector, i.e.: it is hard to find a mathematical relation that yields numerical values which are valid in all the cases given the same cutting parameters;
2. The data recorded by the compactRio embodies some noise and non-idealities, like all data recorded in "the real world", thus increasing the difficulty of the data synchronization.

Problem 1 was overcome by means of equation 3.1, which links the main cut parameters with the theoretical cut torque:

$$T(t) = a\frac{D}{2\tau}\left[z_c(t)\cdot s\cdot p_s\cdot(\omega(t)D)^{-m}\cdot d_z(t)^{1-z}\right] + m_a + J_{app}\dot{\omega}(t)\tau \qquad (3.1)$$

where *a* is a corrective factor, p_s (MPa) is the material specific pressure, *D* (mm) is the blade diameter, *s* (mm) is the blade thickness, ω (Hz) is the blade rotational speed, τ is the transmission ratio between the motor and the blade, $z_c(t)$ is the number of teeth that are currently cutting, $d_z(t)$ (mm) is the amount of material removed by each tooth, m_a is an estimate of the friction moment, J_{app} is the blade's apparent moment of inertia, *m* is the angular speed correction factor, and *z* is the thickness correction factor; *m* and *z* are cutting parameter that are reported in all the milling manuals. The theoretical torque $T(t)$ was used in the analysis as a reference to compare the acquired torque with, in analogy with the "control error" in the control systems field.
Problem 2 was resolved by the following series of signal processing performed on the acquired rotation torque:

1. The acquired torque signal ($A(t)$) appears very different to the theoretical torque ($T(t)$): after a preliminary spectral analysis, it was recognized that there are two frequencies superimposed to a waveform very similar to $T(t)$. These frequencies correspond to the motor rotation speed and its half, so two Moving Average (MA, §1.2.2.6) filters were implemented to cancel out these two frequencies from the $A(t)$ signal in order to obtain the underlying waveform;
2. the moment of the start of the cutting was estimated by analysing the derivative of the acquired torque; when this derivative exceed an appropriate threshold in proximity of the main rise of the torque, the cut is probably starting. Let's name this moment as t_d;
3. A first approximation of the part of signal related to the actual the tube cut was then extracted from the acquired torque signal ($A(t)$); from the TrajectoryPoint

file the duration T_{cut} of the cutting process is known, thus $A(t)$ was limited to the $[t_d - 0.1s\ ,\ t_d + T_{cut} + 0.1s]$ time interval, that is: isolating the cutting signal part with extra 0.1s at the beginning and at the end of it (giving a total duration of $T_{cut} + 0.2s$). Let's name this part of the acquired torque as $A_{est1}(t)$;

4. The theoretical torque signal $T(t)$ was limited (in duration) in the same manner as point 2, i.e.: its duration is T_{cut} plus 0.1s at the beginning and at the end. Let's name this part of the acquired torque $T_{est1}(t)$;
5. The cross-correlation of $A_{est1}(t)$ and $T_{est1}(t)$ was then evaluated; the cross-correlation is the equivalent of the autocorrelation (§1.2.1) wherein the time-shifted copy $x(t+\tau)$ of the signal $x(t)$ is replaced by the time-shifted version $y(t+\tau)$of another signal $y(t)$. In this case, the cross-correlation of $A_{est1}(t)$ and $T_{est1}(t)$ is given by $R_{xy}(\tau) = E[T_{est1}(t)A_{est1}(t+\tau)]$, and it is a measure of the similarity between $T_{est1}(t)$ and $A_{est1}(t)$ shifted of τ seconds;
6. τ_{max} was identified as the time-lag of maximum similarity between the two signals $A_{est1}(t)$ and $T_{est1}(t)$, that is: the τ corresponding to the maximum of $R_{xy}(\tau)$.
7. Finally, the part of $A_{est1}(t)$ relative to the tube cutting only (named $A_{cut}(t)$) was extracted from the time interval $[\tau_{max}\ ,\ \tau_{max} + T_{cut}]$. τ_{max} was subsequently used to extract the part of the other acquired signals relative to the tube cutting only, so that each analysed signal has duration of T_{cut}.

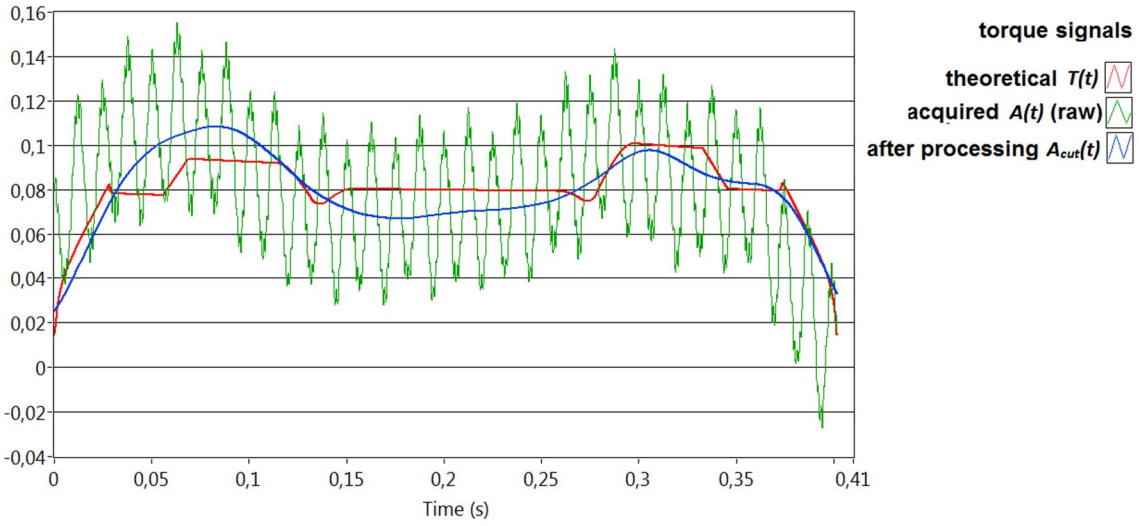

Figure 3.8: example 1 of the result of the pre-processing of the torque signal. The theoretical torque $T(t)$ is the red curve, the raw acquired torque $A(t)$ is the green curve, which after processing (MA filters) and synchronization becomes the blue curve $A_{cut}(t)$.

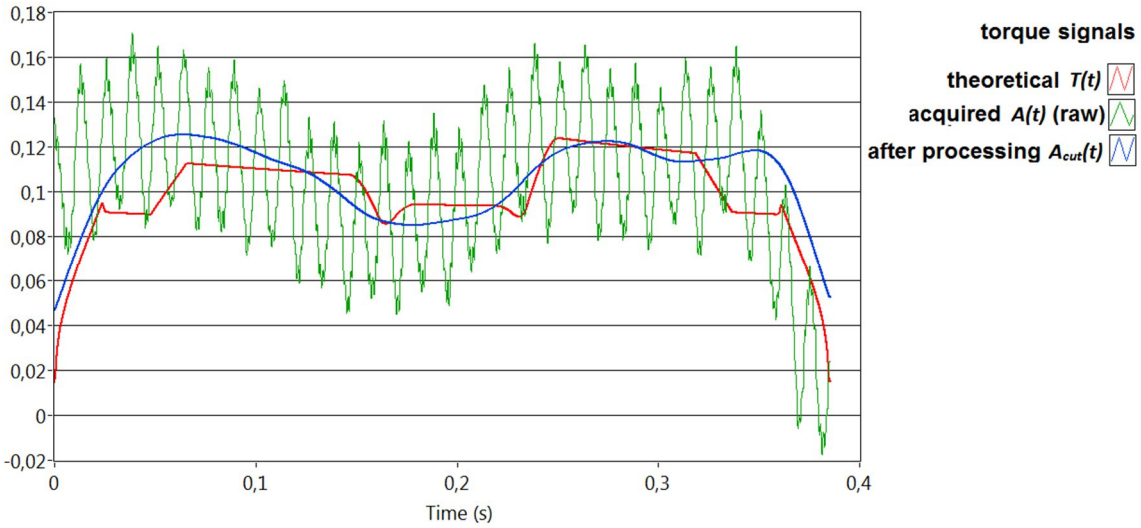

Figure 3.9: example 2 of the result of the pre-processing of the torque signal. The theoretical torque $T(t)$ is the red curve, the raw acquired torque $A(t)$ is the green curve, which after processing (MA filters) and synchronization becomes the blue curve $A_{cut}(t)$.

The synchronization obtained with this procedure was not perfect for all the data available, but the "wrong" cases are a limited amount of the total; *de facto*, this procedure allowed to analyse the big amount of data automatically, and their results are reported in Fig. 3.8 e 3.9 in two different cases.

After this pre-processing, the signals that were chosen for the data analysis are the following:

- vibrations along X, Y and Z. Directions Y and Z identify the plane of the blade;
- SAM and SAM YZ: the former has been defined in §1.2.2.7 and represent the global intensity of vibration, while the latter represent the intensity of vibration in the plane of the blade, that is: $SAM\ YZ(t) = \sqrt{(y(t) - \mu_y)^2 + (z(t) - \mu_z)^2}$;
- rotation motor torque $A_{cut}(t)$ obtained after the aforementioned signal processing (i.e.: with the oscillations at the motor rotating frequency and its half removed by the Moving Averages filters);
- difference between the acquired rotation motor torque and the theoretical torque evaluated by means of equation 3.1, that is: $D(t) = A_{cut}(t) - T(t)$;
- non-filtered rotation motor torque $A_{cut,nf}(t)$, i.e.: same as $A_{cut}(t)$ but without passing through the two moving average filters;
- difference between the non-filtered rotation motor torque and the theoretical torque, that is: $D_{nf}(t) = A_{cut,nf}(t) - T(t)$;
- translation motor torque;
- difference between the acquired translation motor torque and its theoretical counterpart.

Several parameters of two different nature (i.e.: statistical parameters and spectral parameters) were evaluated for each of the aforementioned signals, and they are summarized in the following list:

- Statistical parameters
    - Maximum
    - Minimum
    - Mean
    - Variance
    - Skewness
    - Kurtosis
    - Root Mean Square value (RMS)
    - Entropy
- Spectral parameters
    - Amplitude of the teeth frequency f_t
    - Spectral Energy in the frequency band $[f_t - 0.02f_t\,, f_t + 0.02f_t]$
    - Sum of the amplitude of all the harmonics of the teeth frequency $nf_t, n \in \mathbb{N}$

Indeed, a general aim in condition monitoring is firstly to find a signal parameter which is able to communicate the state of the monitored part. In this case, one should find a parameter correlated with the blade wear: since wear is a progressive phenomenon, the parameter we are searching for should exhibit a trend along a blade life. It was thus chosen to evaluate this wide set of parameters for each signal in order to isolate the best parameter(s) from the best signal(s), and chosen parameters are the following:

- Vibration along the Y direction: Maximum, Variance, RMS, Entropy;
- rotation motor torque $A_{cut}(t)$: Maximum, Mean, Variance, RMS, Entropy;
- difference between the rotation motor torque and the theoretical torque $D(t)$: Maximum, Mean, Variance, RMS, Entropy.

The behaviour of these parameters is shown in Figures 3.10 to 3.33 along four blade lives, the patter named blades A, B, C and D.

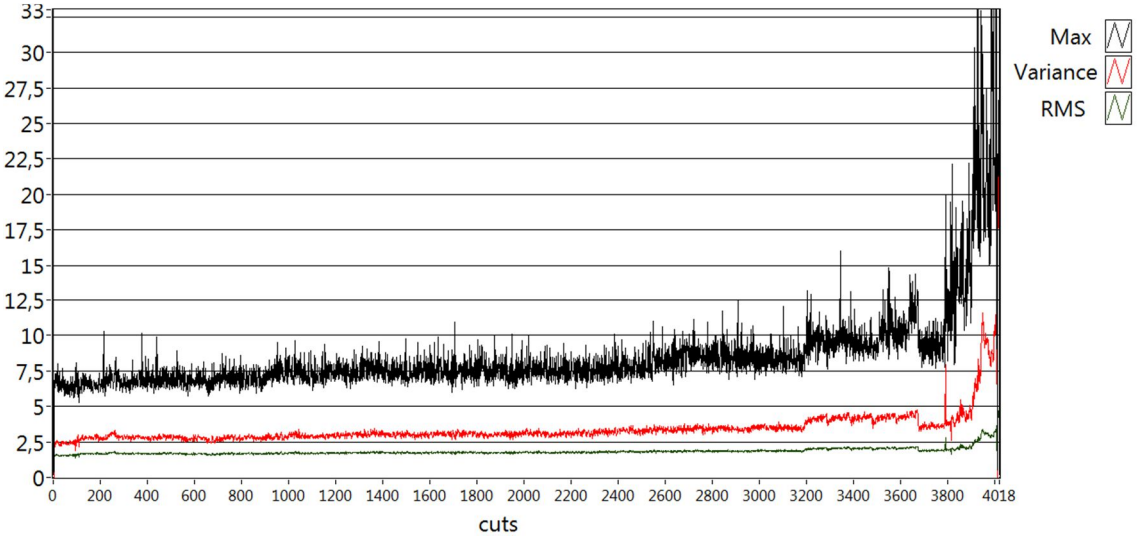

Figure 3.10: maximum, variance and RMS of the Y vibration signal during blade A life.

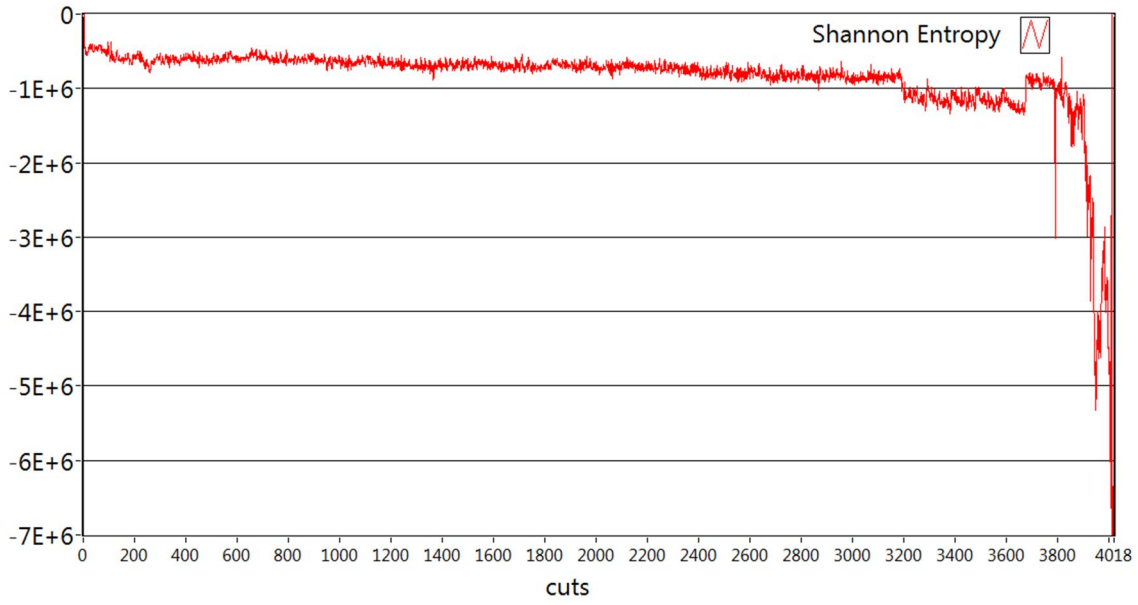

Figure 3.11: entropy of the Y vibration signal during blade A life.

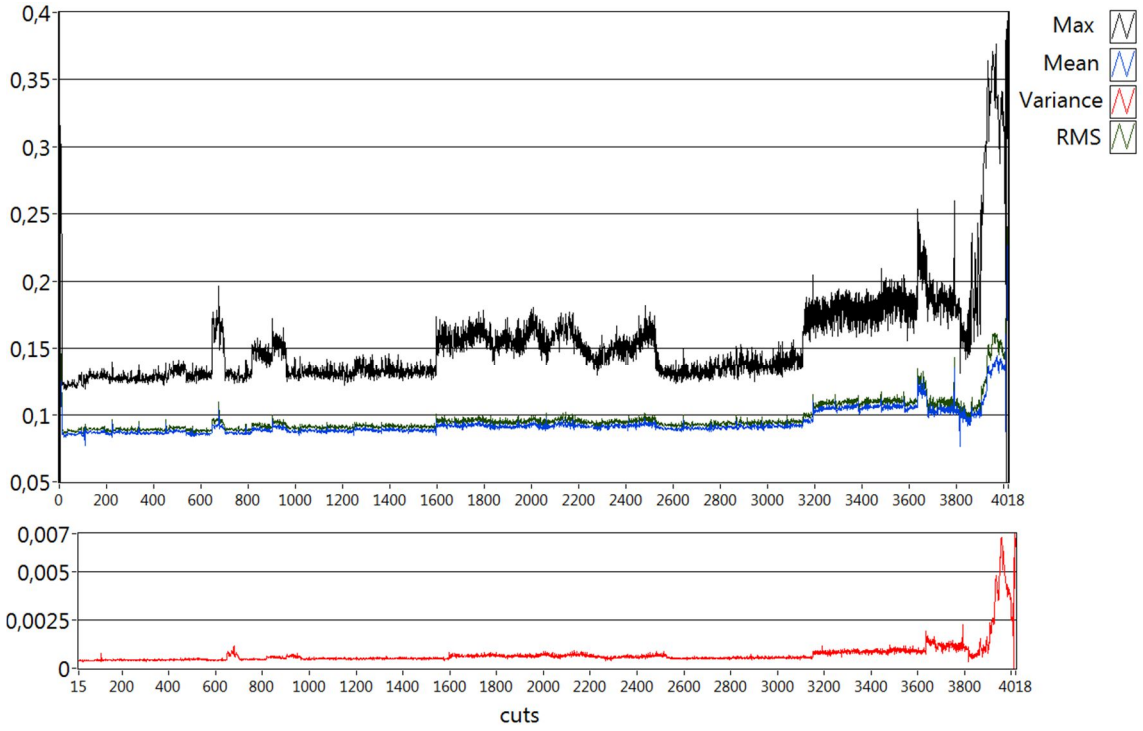

Figure 3.12: maximum, mean, variance and RMS of the $A_{cut}(t)$ signal during blade A life.

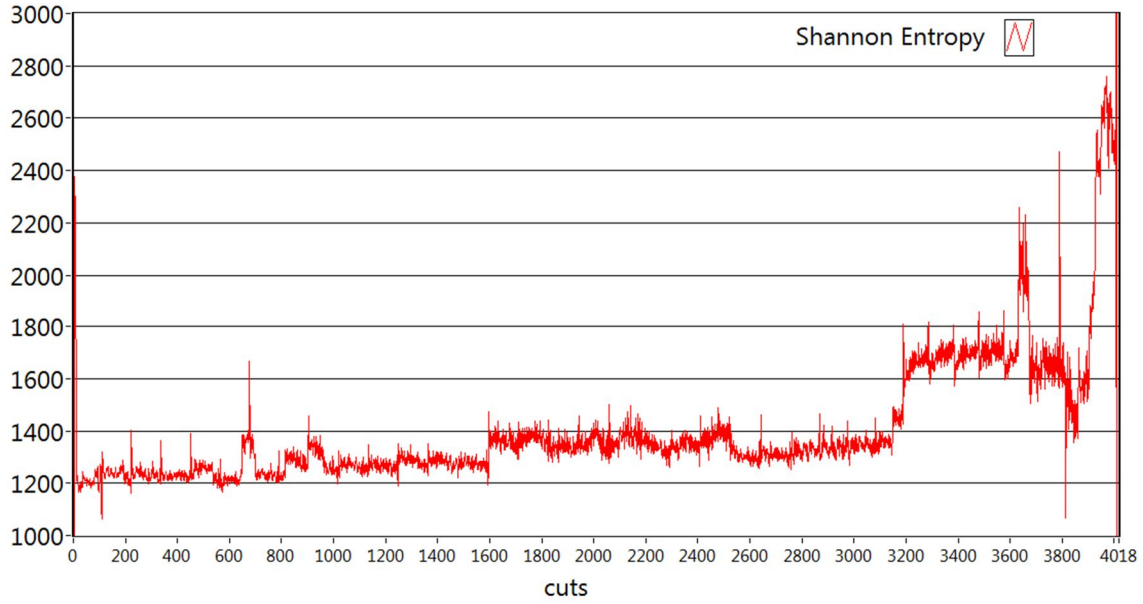

Figure 3.13: entropy of the $A_{cut}(t)$ signal during blade A life.

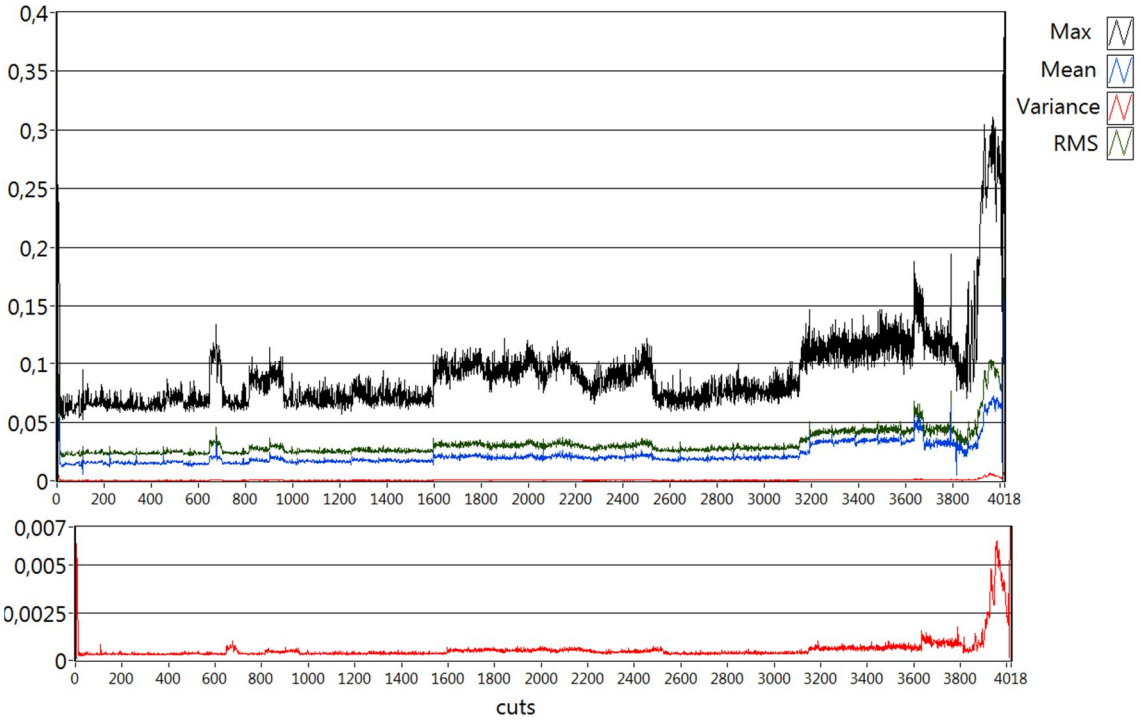

Figure 3.14: maximum, mean, variance and RMS of the $D(t)$ signal during blade A life.

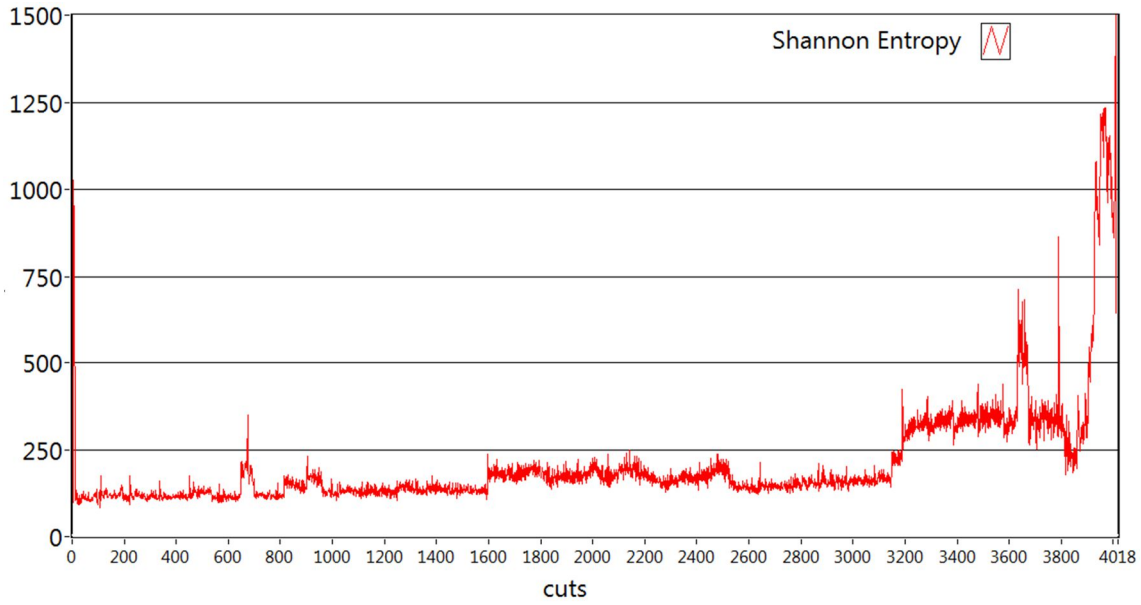

Figure 3.15: entropy of the $D(t)$ signal during blade A life.

In Figures 3.10 to 3.33 one can see a general agreement of the chosen parameters, that is to say that the information that each parameter carries is almost the same of the other parameters in every blade life. Looking at blade A (Figs. 3.10 to 3.15) one can see that every parameter value rises approximately at the cut number 3200 and then rises resolutely at the cut 3900, just 200 cuts before the blade substitution. The behaviour of the parameters along the blade A life is almost the same: there are

temporary oscillations (e.g.: from cut 1600 to cut 2500) that are represented more or less clearly in every parameter.

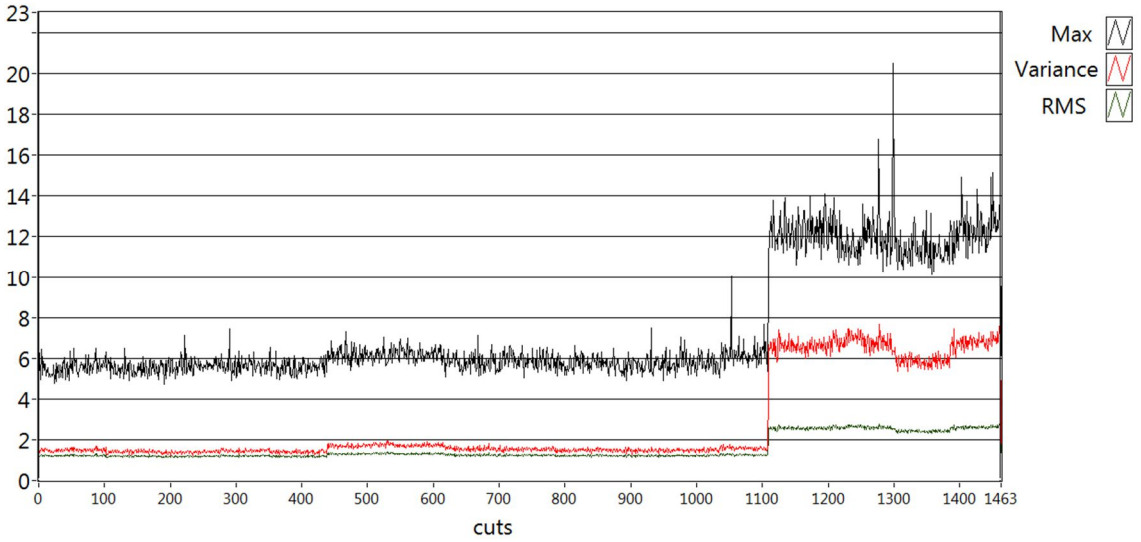

Figure 3.16: maximum, variance and RMS of the Y vibration signal during blade B life.

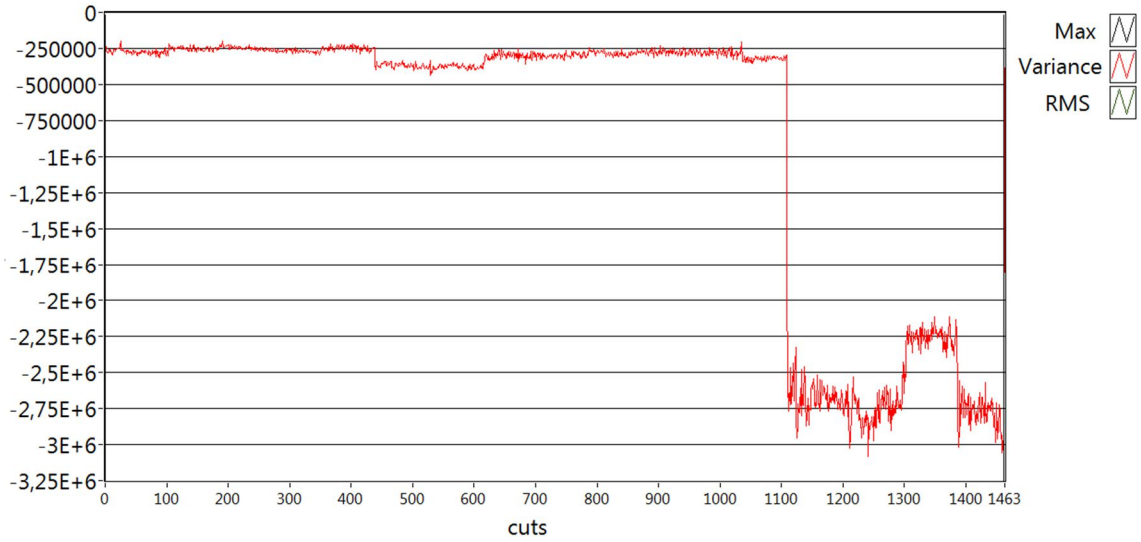

Figure 3.17: entropy of the Y vibration signal during blade B life.

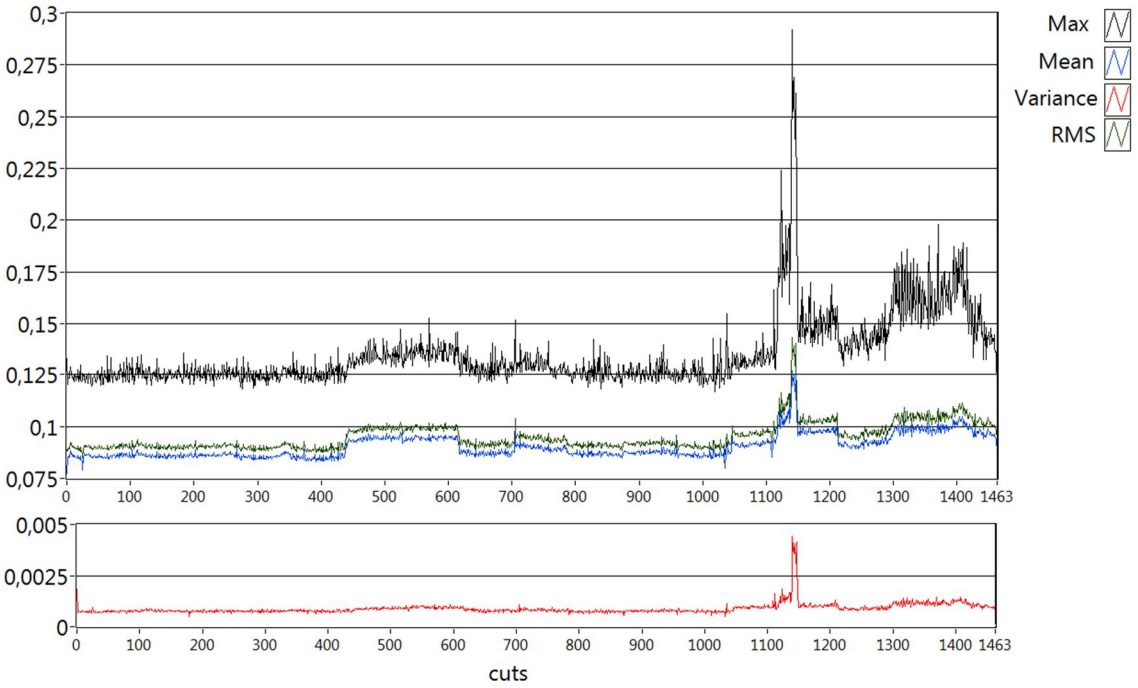

Figure 3.18: maximum, mean, variance, RMS and a zoom of the variance of the $A_{cut}(t)$ signal during blade B life.

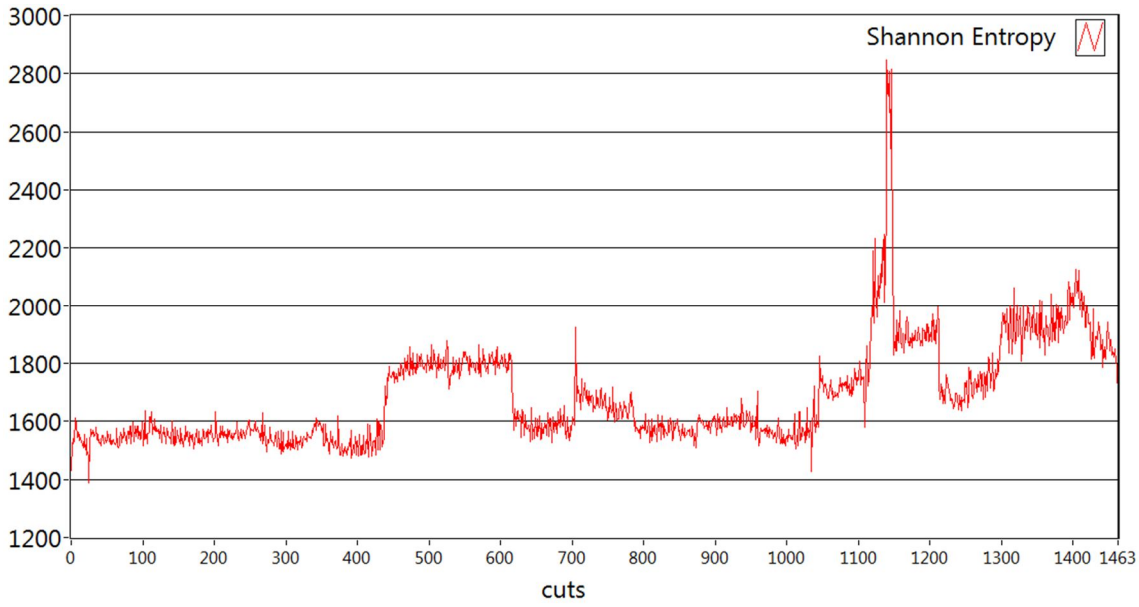

Figure 3.19: entropy of the $A_{cut}(t)$ signal during blade B life.

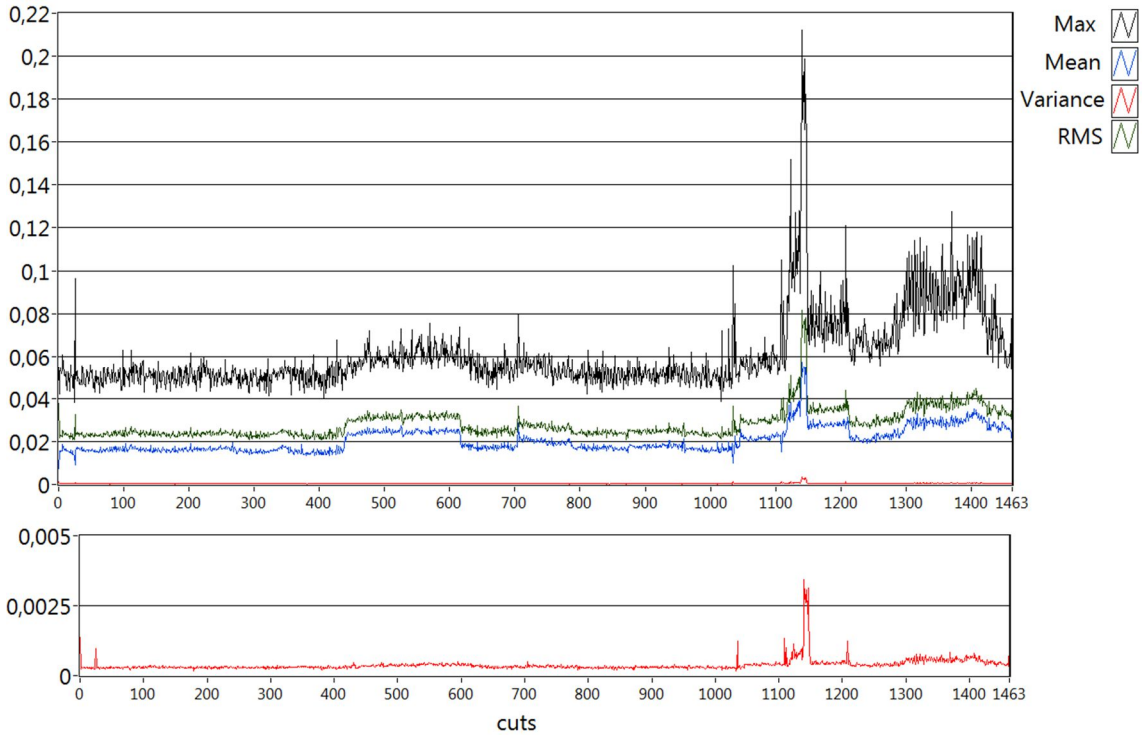

Figure 3.20: maximum, mean, variance, RMS and a zoom of the variance of the $D(t)$ signal during blade B life.

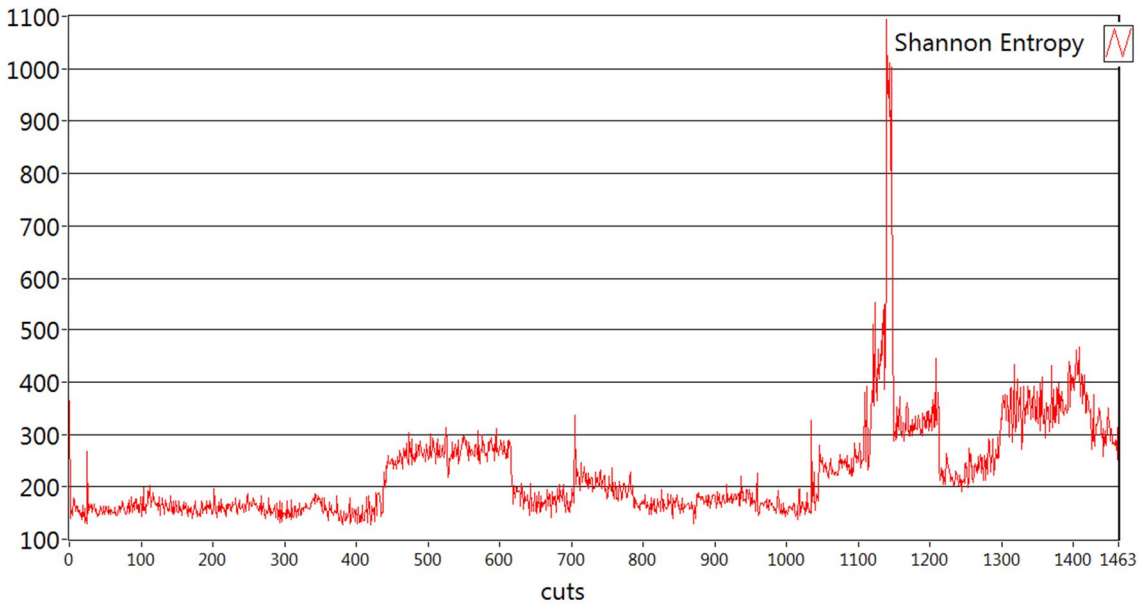

Figure 3.21: entropy of the $D(t)$ signal during blade B life.

Along the blade B life, every parameter informs that something is occurring soon after cut number 1100: the vibrations parameters rise and then stay an almost stable value (Figs. 3.16 and 3.17), while the torque parameters (Figs. 3.18 to 3.21) exhibit a peak slightly later than vibrations (approx.. at cut 1150, Figs. 3.18 to 3.21) and then exhibit lower values, that are in general higher than prior of cut 1100. As for blade A, the

general behaviour of all the parameters is qualitatively the same, for example all parameters rises in the interval between cut 450 and cut 620.

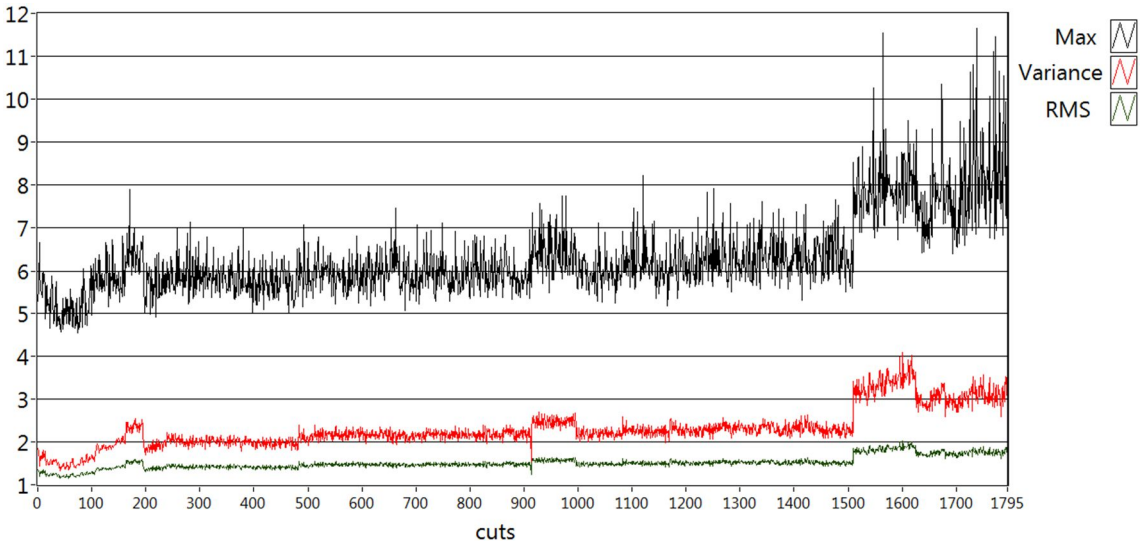

Figure 3.22: maximum, variance and RMS of the Y vibration signal during blade C life.

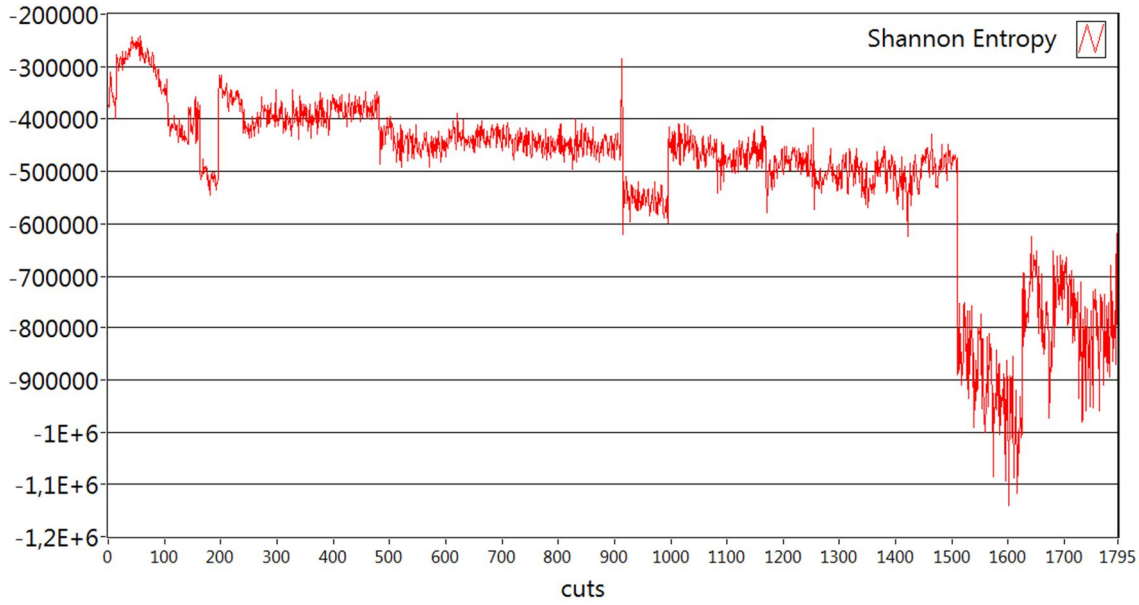

Figure 3.23: entropy of the Y vibration signal during blade C life.

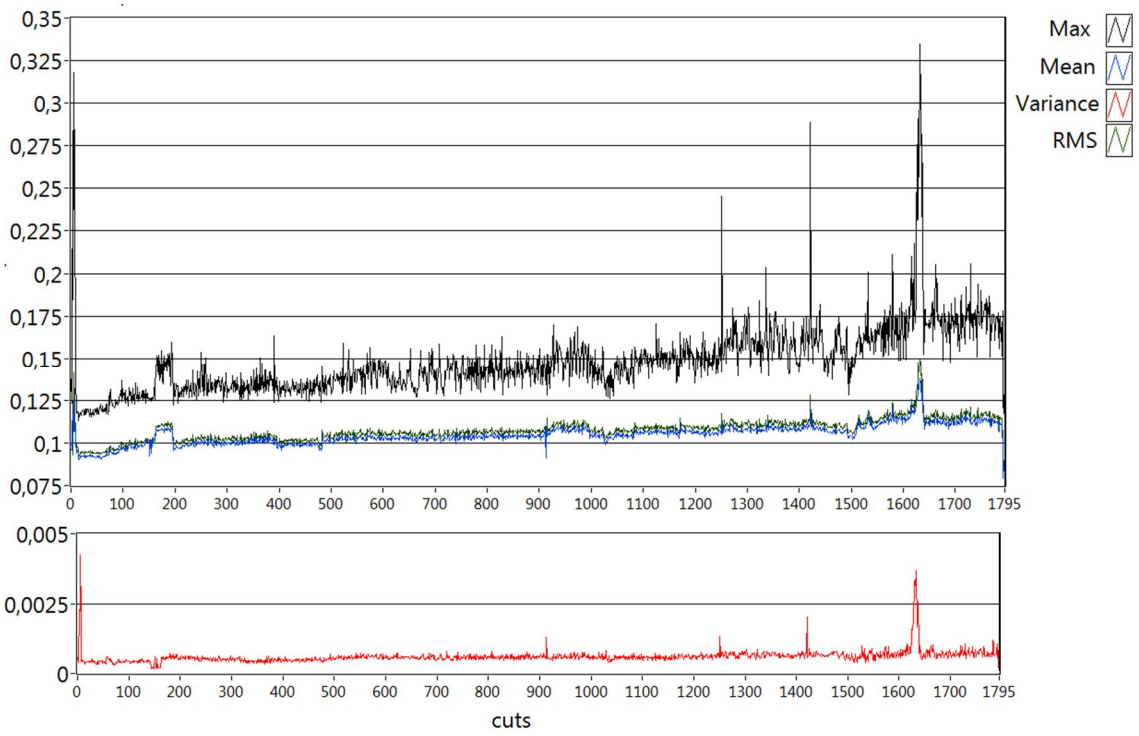

Figure 3.24: maximum, mean, variance, RMS and a zoom of the variance of the $A_{cut}(t)$ signal during blade C life.

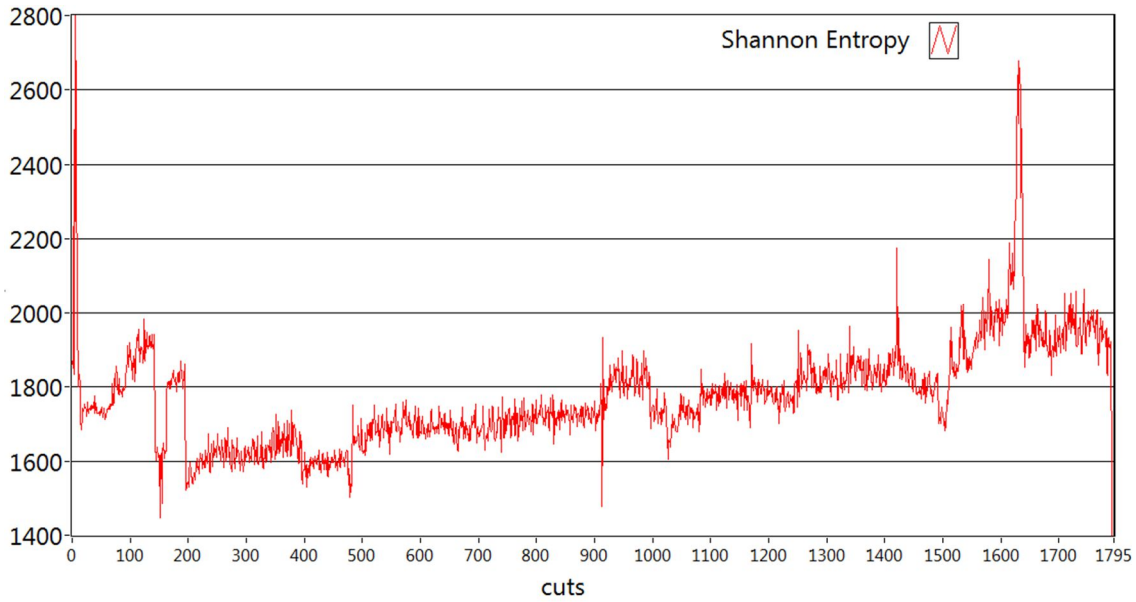

Figure 3.25: entropy of the $A_{cut}(t)$ signal during blade C life.

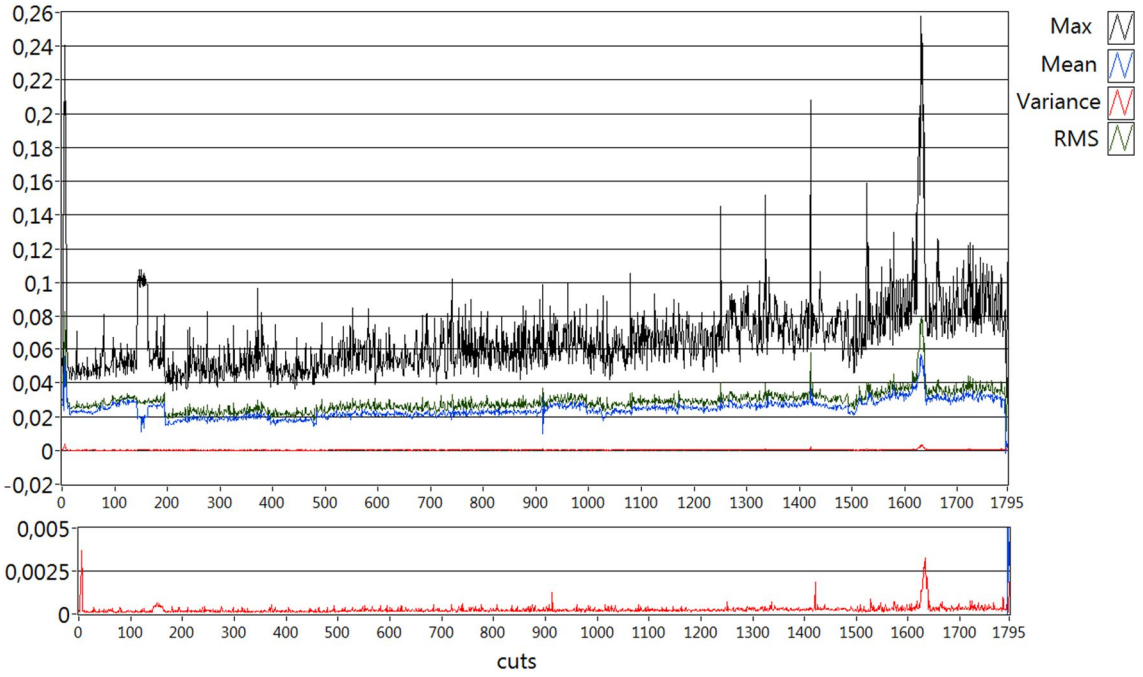

Figure 3.26: maximum, mean, variance, RMS and a zoom of the variance of the $D(t)$ signal during blade C life.

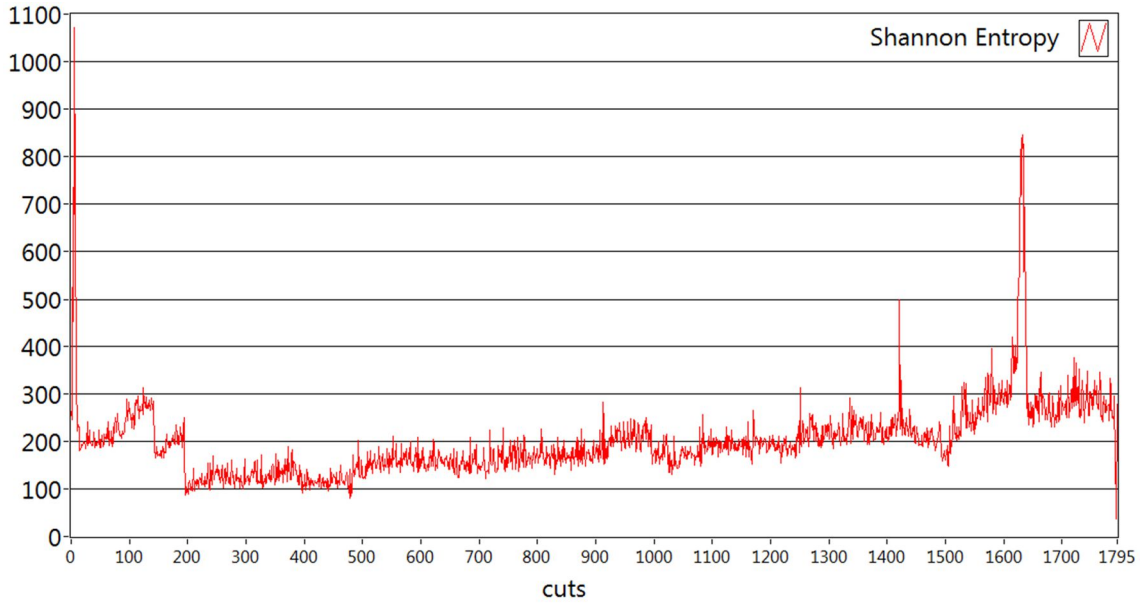

Figure 3.27: entropy of the $D(t)$ signal during blade C life.

What has been said for blades A and B can be said also for blade C, that is: a general agreement of the parameters behaviour. In this case, the major rising in the vibration parameters (Figs. 3.22 and 3.23) occurs soon after cut number 1500, and then they remain almost stable at a higher value than before of the cut number 1500. The torque parameters (Figs. 3.24 to 3.27) seem to respond a few cuts later than vibrations parameters, and again they exhibit a peak and then exhibit lower values, that are in general higher than prior of cut 1500, but they present progressively bigger peaks also

at cuts number (approximately) 910, 1250 and 1420; these peaks aren't explicitly present in vibrations parameter, and they are probably anticipating what happens at cut 1500. These peaks of the torque parameters are the most evident in this particular blade C life, but they are present also in the other blades lives even if they are more hidden and slightly harder to find.

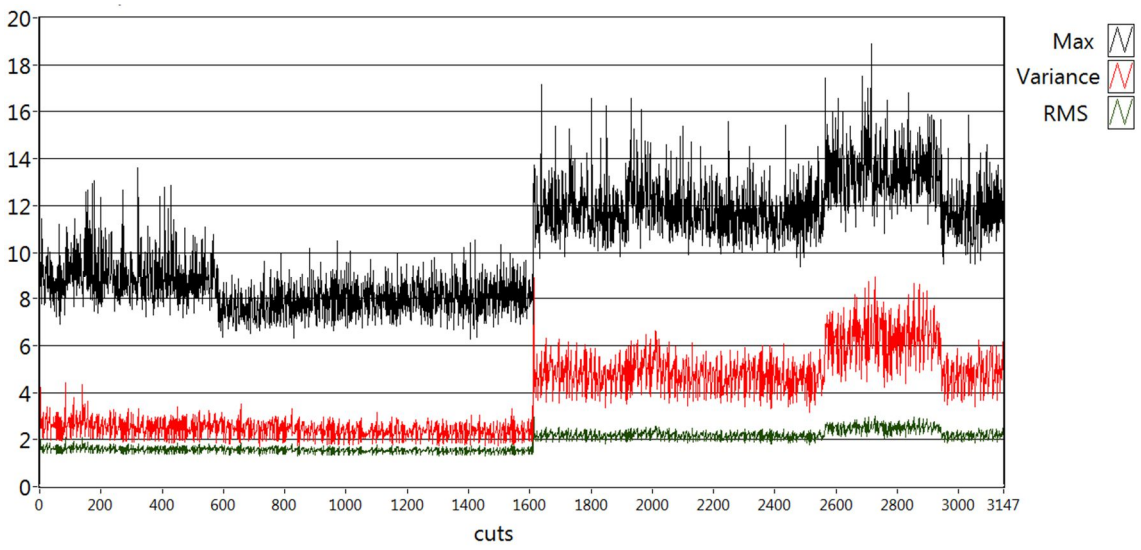

Figure 3.28: maximum, variance and RMS of the Y vibration signal during blade D life.

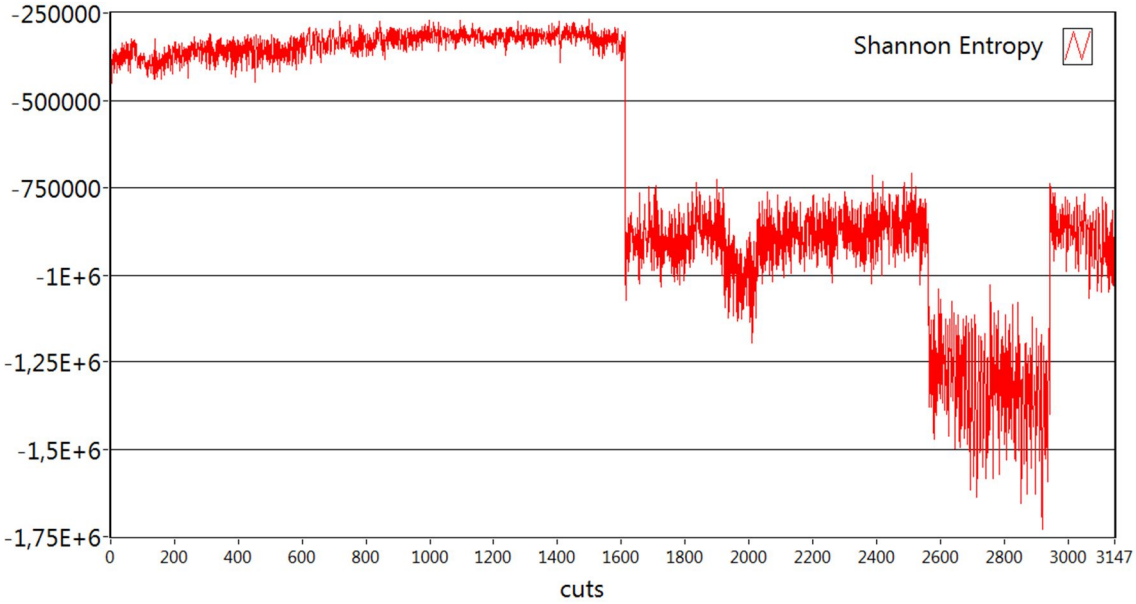

Figure 3.29: entropy of the Y vibration signal during blade D life.

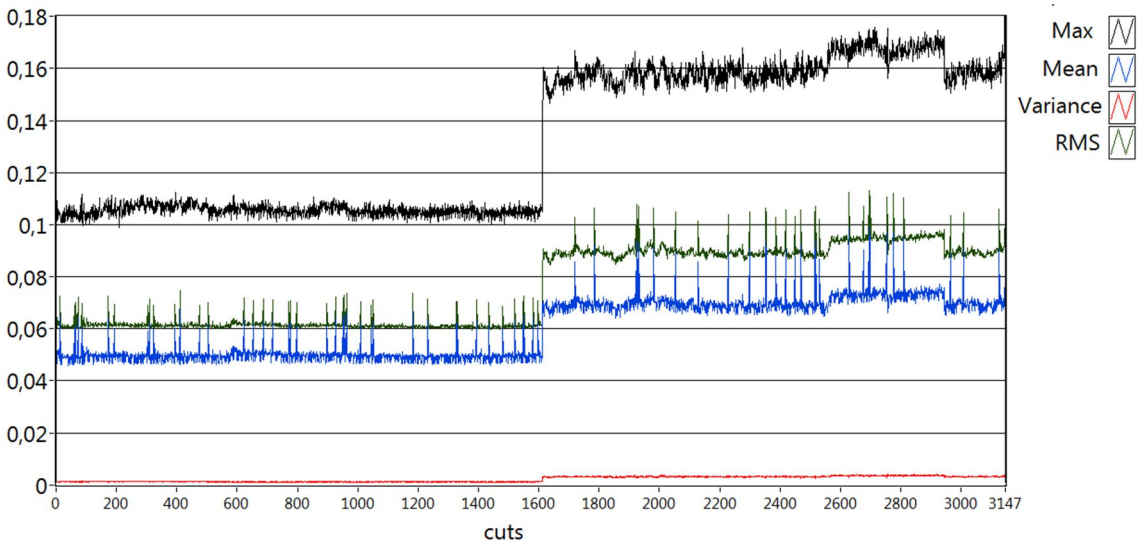

Figure 3.30: maximum, mean, variance and RMS of the $A_{cut}(t)$ signal during blade D life.

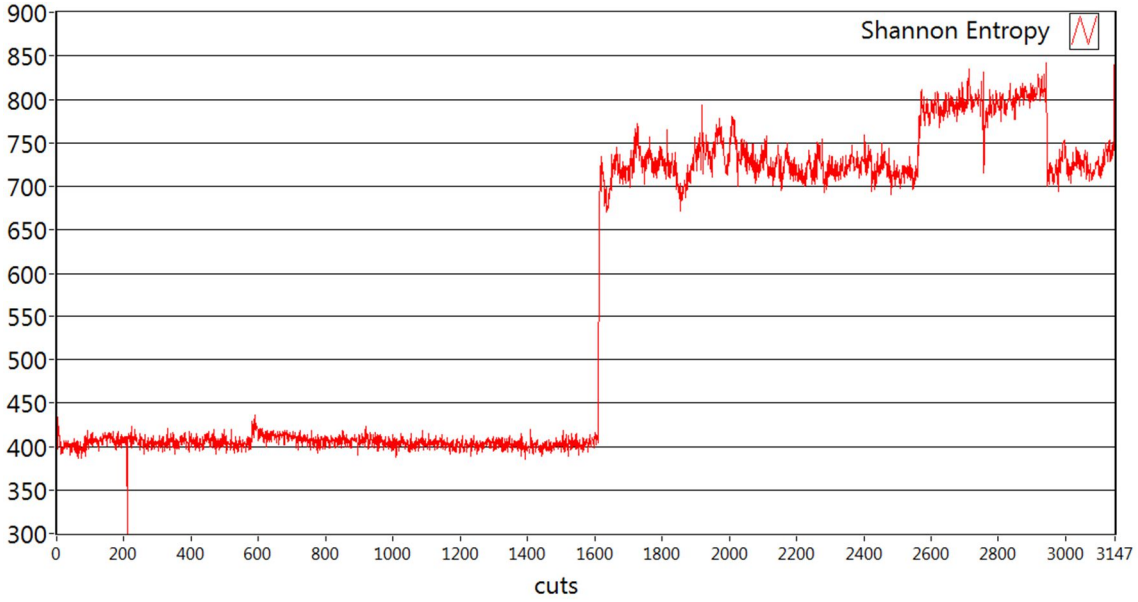

Figure 3.31: entropy of the $A_{cut}(t)$ signal during blade D life.

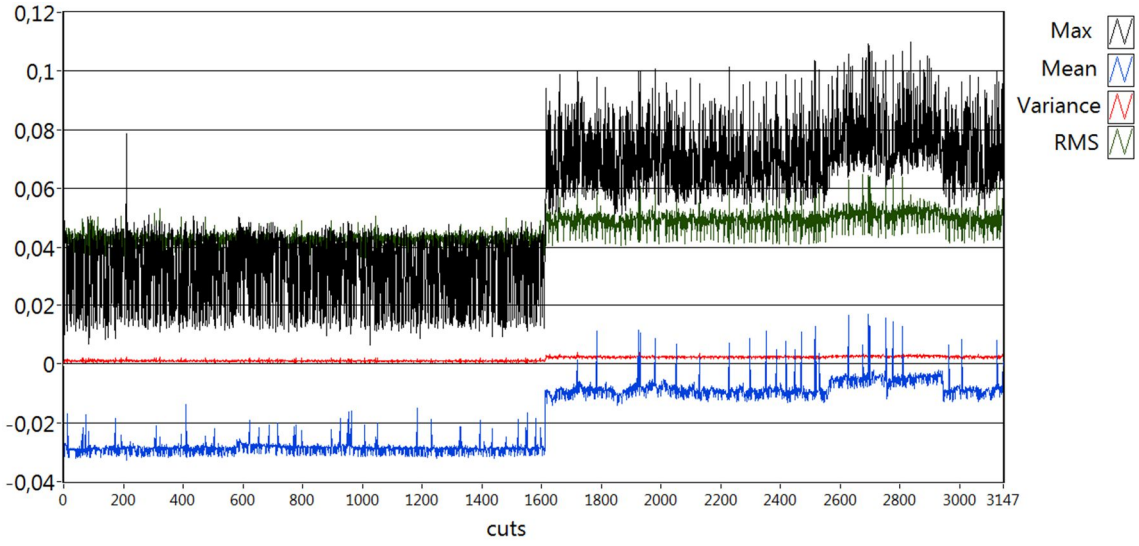

Figure 3.32: maximum, mean, variance and RMS of the $D(t)$ signal during blade D life.

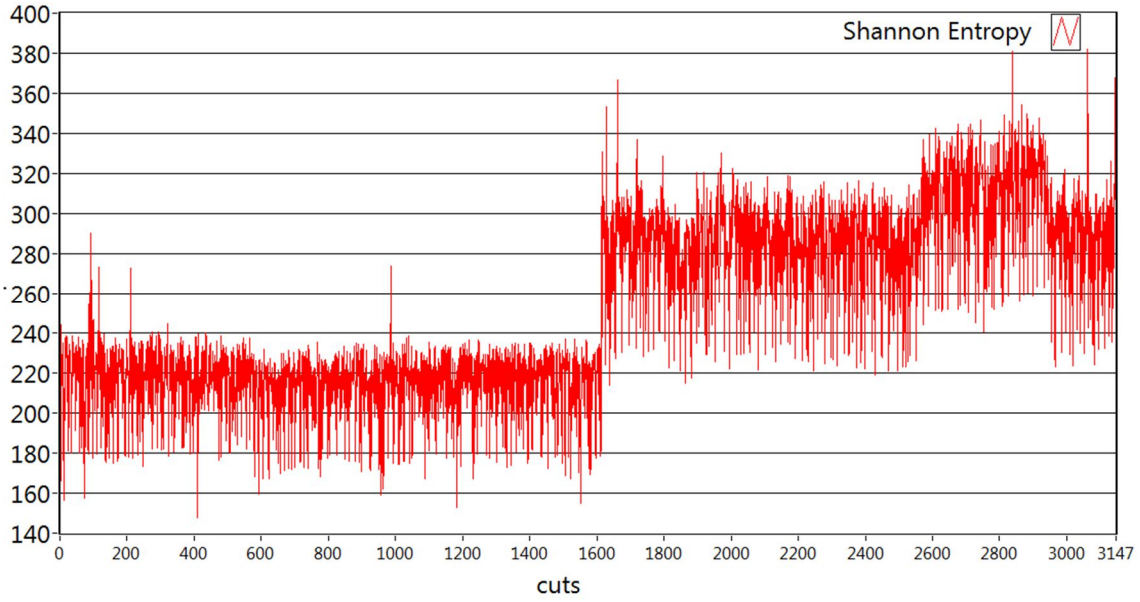

Figure 3.33: entropy of the $D(t)$ signal during blade D life.

Along blade D life (Figs. 3.28 to 3.33) one can observe the same behaviour highlighted in previous blades analysis. in particular, this case is very similar to blade A, that is: the parameters of all the signals rise resolutely briefly after cut number 1600 and then stay almost stable (the slightly rise again between cuts number 2550 and 2950): in this case, the entropy of vibrations (Fig. 3.29) seems more sensible than the other vibrations parameters (Fig. 3.28). The torque parameters exhibits spikes (i.e.: occasional peaks) that are distributed almost uniformly along the blade D life and are almost of the same amplitude: these spikes are an effect of a non-perfect result of the synchronization procedure of the torque signal, so they don't represent something occurring to the blade. A part from this, the torque parameters remain generally in

agreement with vibrations parameters and they are able to provide almost the same information.

3.4 – Conclusions

The aim of this thesis work has been reached: it has been demonstrated that it is possible to perform the condition monitoring of the blade with the Sensorless approach via the analysis of the torque of the motor that rotates the blade. Indeed, the information that the torque provides is the same that vibrations provide, so the same event can be recognized in both these signals. The parameters that seem to be best correlated with the blade wear are a subset of the statistical parameters listed in §3.3.2, namely:

- maximum, variance, RMS and entropy of the vibration signal along the Y axis (which lies in the plane of the blade);
- maximum, mean, variance, RMS and entropy of the $A_{cut}(t)$ signal, which is the acquired torque signal after the pre-processing described in §3.3.2;
- maximum, mean, variance, RMS and entropy of the $D(t)$ signal, which is obtained by subtracting an estimate of the theoretical torque $T(t)$ needed to cut to $A_{cut}(t)$.

Two main considerations have to be made, the first regarding the spectral parameters: these are in general performing worse than the statistical parameters, despite the findings reported in §3.3.1. This can be explained by the fact that the augmentation of the amplitudes of the teeth frequency and its harmonics occurred in case of the removing of one tooth from the blade, i.e.: in case of a local defect of the blade. Wear, on the contrary, is a distributed defect, so this should explain the inefficiency of the spectral parameter in carrying information about the wear of the blade. The second consideration regards the values exhibited by the chosen parameters: indeed, these values don't allow finding an absolute threshold (obviously different for each parameter) that could be used to declare that the blade needs to be changed because it's too weared (e.g.: when the threshold is exceeded by the actual parameter value). In fact, in condition monitoring, the ideal parameter exhibits always the same value when the blade is new and always another value when the blade is weared, and it goes monotonically from the first value to the second. This is not the case, probably because of the varying conditions of the blade operations: along the blade lives, the operators change frequently the working parameters of the cut-off unit in order to maximize its performances, and these changes are felt by the vibrations and torque parameters. Another fact that doesn't allow finding thresholds for the diagnostic

parameters is the following: there is not the certainty on the real state of the blade when the operator changes them, because they may substitute a blade when it is not completely weared out. For example, this can occur when there is a change of the tube format: the operator must usually change the vice in the cut-off unit to use the one that matches the new tube format. When this occurs, the operator frequently changes the blade also, and this is done to prevent the machine to stop again to change the blade soon later ("soon" may be intended as "2 days after" also): notice that, in doing this, he is doing a version of the Preventive Maintenance. For all these reasons, threshold can't be set yet, and third data acquisition campaign is necessary: in this campaign, several blades should be monitored from the "brand new" state until they are completely weared out. Each blade should be monitored with the same cut-off unit operational parameters during all its life, and changing these operational parameters should be done only when changing a blade: these precautions will allow to estimate the influence of the cut-off operational parameters on the diagnostic parameter founded in this thesis, and to provide a consistent data set from which find the thresholds.

One last consideration on the signal processing required to perform the Sensorless condition monitoring in this case: the synchronization problem described in §3.3.2 doesn't exist for OTO, because the cut-off control system knows exactly when the blade is starting to touch the tube, so it can easily trigger the data acquisition start at the right moment. The only signal processing required is thus the Moving Average filtering, in order to clean the acquired torque and made it more easily comparable with the theoretical estimate (which is itself passible of enhancement). In the author's opinion, the best signal to use for condition monitoring purposes is indeed the difference between the acquired torque and the theoretical estimated torque of the rotation motor, because it can provide deepest insight in what is really happening to the blade.

4 – Diagnostics of an Epicyclic Gearbox

4.1 – Introduction

This chapter deals with the diagnostics of an epicyclic gearbox tested by Brevini in an endurance test. Gearboxes are one of the most common parts in mechanics, and for this reason they had been well studied along the decades also from the condition monitoring point of view.

The gearbox that was studied in this thesis work was subject to an endurance test, which has the purpose of verifying the theoretical life of the gearbox which, in this case, is estimated to be 4650 hours. Actually, on the test bench two identical gearboxes were installed, one opposed to the other: the first gearbox increases the speed while the second reduce it, so that the input shaft speed is equal to the overall output shaft speed. Moreover, the test bench hosts a parallel shaft (which rotates at the same speed of the gearbox assembly input shaft) with a limiting torque joint, on which an encoder and a torque sensor are mounted: these sensors are used by the Brevini to monitor the gearbox performance, so they can be used by the Sensorless approach. The shafts are rotated by an asynchronous electric motor directly plugged to the power supply, i.e.: without a drive to control it: consequently, the nominal input shaft speed is always the same, and it is approximately 1480 RPM. The test bench has also a hydraulic cooling system which maintains the gearboxes oil temperature below 70 °C: since endurance test are carried on 24 h / 24 h and 7 days / 7 days, there is not a continuous presence of the operators, thus the test is automatically stopped if the temperature is too high.

Each epicyclic gearbox used in this endurance test is composed of two reduction stages, named E16 and E50: the output of the E16 stage is the input of the E50 stage. The following Table 4.1 reports the main parameters of each stage

Stage	**E16**	**E50**
Number of planet gears	3	4
Number of teeth of the sun gear z_s	27	27
Number of teeth of the planet gears z_p	27	27
Number of teeth of the ring gear z_r	83	83
Transmission (reduction) ratio τ	1 : 0,245455	1 : 0,245455

Table 4.1: main characteristics of the two stages of reduction E16 and E50.

4.2 – Experimental Set-Up

The data were acquired by means of a National Instruments compactRio that was programmed to record 40 s per hour and then store the data on a USB stick. A single axis accelerometer was placed on the external of the E50 reduction stage of the gearbox 2: this choice comes from the fact that Brevini noticed that this stage is the most stressed of the two, and thus the eventual failures are more easily to occur to this stage. The other data recorded come from an extra current sensor used to measure the current flowing inside the driving motor and the encoder, and the torque sensor already in use by Brevini. Typically, encoders provide 3 signals that are usually named “Zero”, “A” and “B”: the “Zero” channel gives one pulse per revolution and was used in this thesis work as a “tacho signal” (§1.2.2.5); “A” and “B” are two square waves with n periods per revolution (in this case, $n = 1024$), with “B” being in quadrature (i.e.: 90 degrees phase difference) with respect to “A”, thus allowing to discriminate the verse of rotation; signal “A” was recorded for future works. The following is a schematic summary of the acquisition hardware and characteristics:

- Sensors
    - Accelerometer: PCB 353B18 (single axis);
    - Torque sensor: HBM MN468 T22
    - Encoder: Heidenhain ERN 120
    - Current sensor: IME TT35A
- Acquisition hardware
    - NI 9233 analog input module: it acquired the vibrations signal;
    - NI 9239 analog input module: it acquired the signals of the torque and current sensors
    - NI 9402 digital input module: it acquired the encoder signals “Zero” and “A”;
    - NI cRio 9076: compactRio.
- Acquisition software: dedicated compactRio program
- Records main characteristics
    - Channels number: 5 (vibration, torque, current, encoder “Zero” and “A”);
    - Sampling frequency: 10 kHz for the analog data (vibrations, torque, current) and 62,5 kHz for the digital data (encoder “Zero” and “A”);
    - Record duration: 40 s;
    - Recording strategy: one record per hour. During the tests with the E50 sun gear with the incision, the records were progressively more frequent.

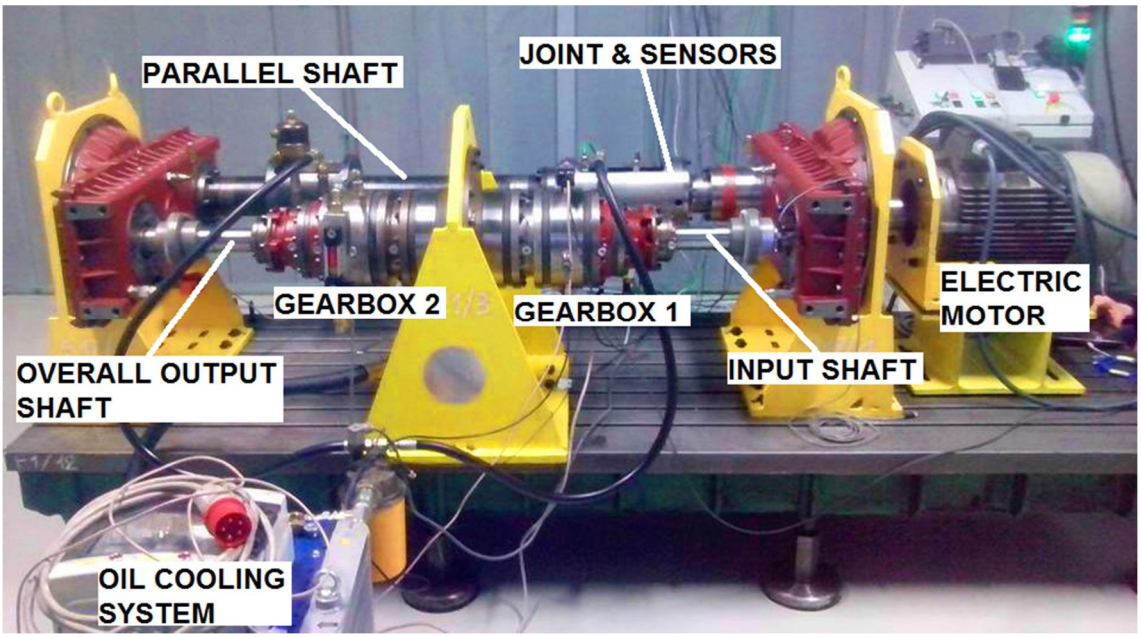

Figure 4.1: the gearbox test bench.

The gearbox endurance test lasted 10 months, and was stopped every 250 hours to investigate the status of each component. Unfortunately, a few problems were encountered during the data acquisition campaign, and these resulted in losing one month of data recording: fortunately, during this "lost month" no particular event happened in the gearbox so that no relevant data was lost. At the end of the endurance test, the ring gear of the E50 stage was found with a missing tooth (Fig. 4.2). Moreover the sun gear of the E50 stage was artificially damaged by making an incision on a tooth side that was progressively deepened and enlarged for a total of 3 increasing depths (Figs. 4.3 to 4.5). After each incision, the test was restarted but for a limited amount of hours due to limited availability of the test bench. In table 4.2 are reported the approximate dimensions of each incision and the relative number of hours of testing and data recording.

Incision number	Depth (mm)	Width (mm)	Hours of testing
1 (Fig. 4.3)	0.1	1	90
2 (Fig. 4.4)	0.3	1	42
3 (Fig. 4.5)	0.5	1.5	11

Table 4.2: main data of the incisions made on the sun gear of the E50 stage.

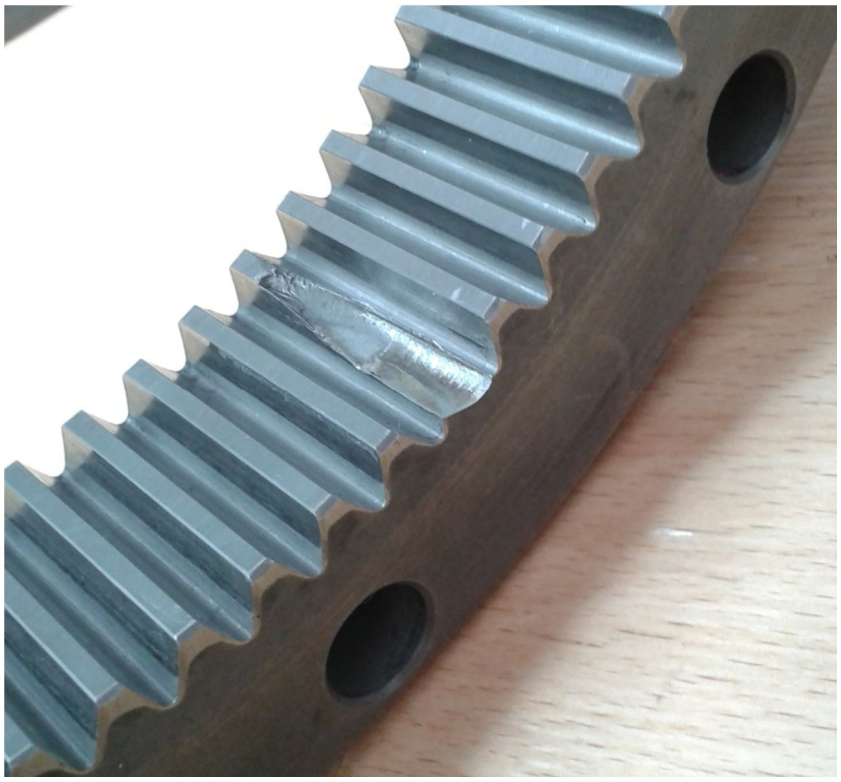

Figure 4.2: the damaged ring gear of the E50 stage.

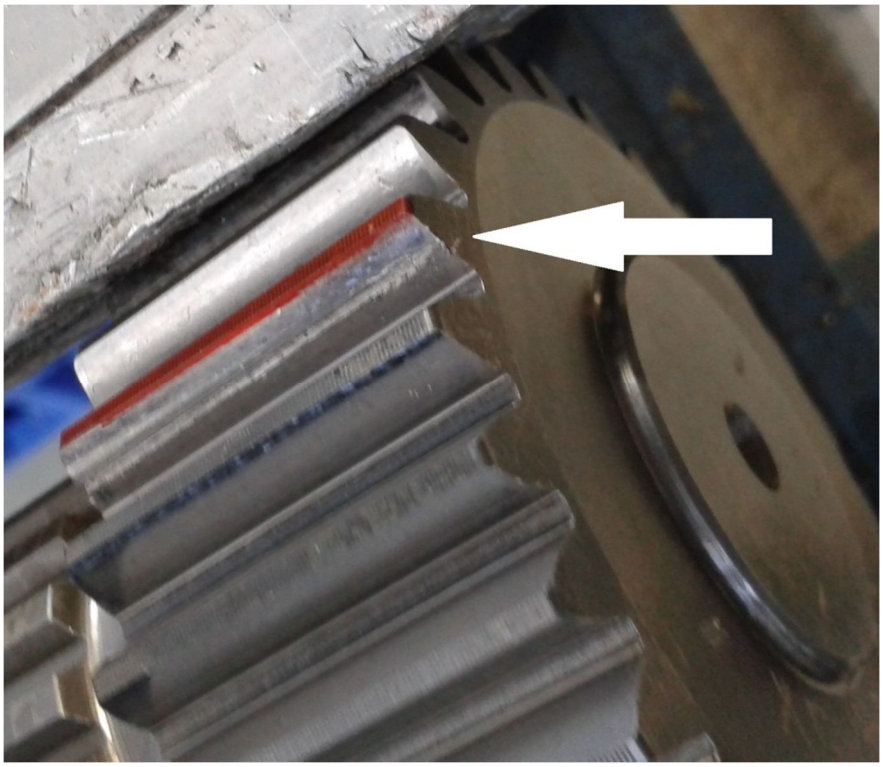

Figure 4.3: the first incision on the sun gear of the E50 stage.

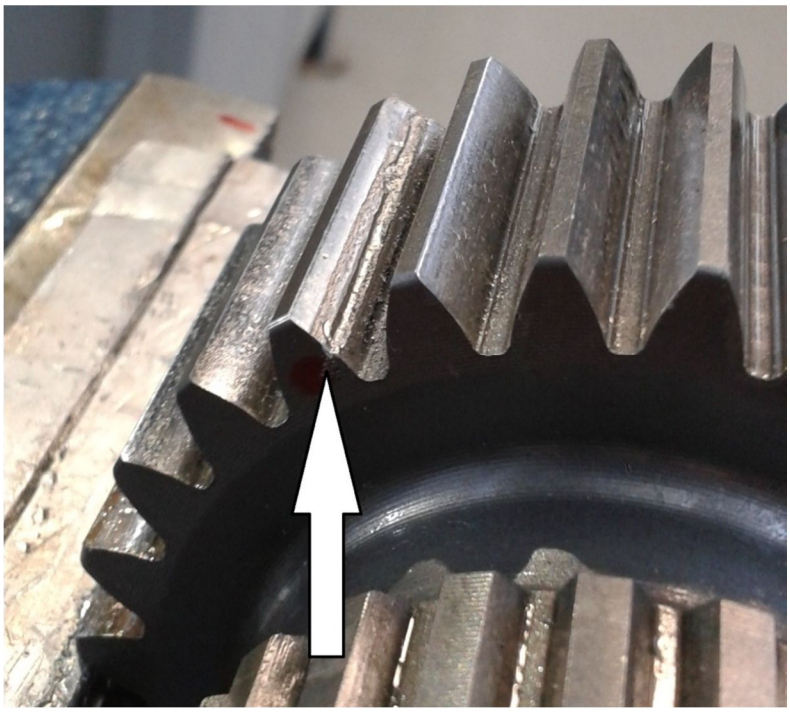

Figure 4.4: the second incision on the sun gear of the E50 stage.

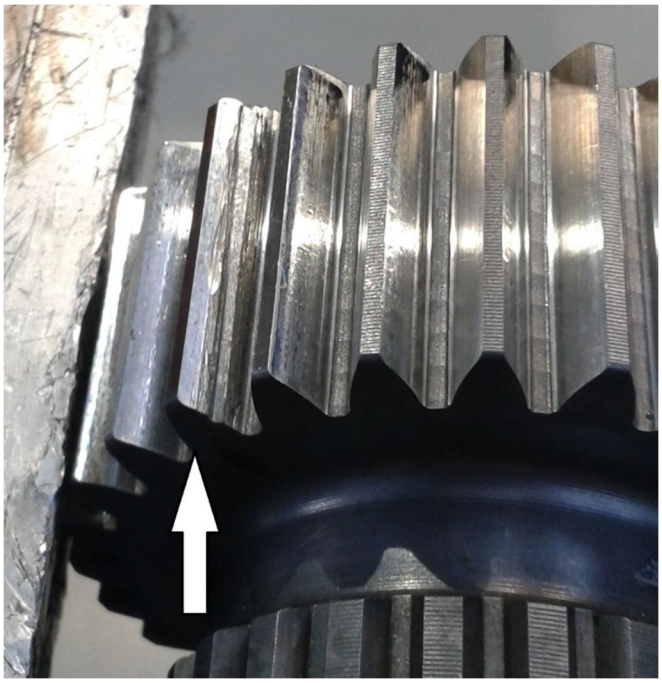

Figure 4.5: the third incision on the sun gear of the E50 stage.

4.3 – Data analysis

4.3.1 – General Theory of Gearbox Condition Monitoring

Gears had been intensively studied along the decades and several indicators of the presence of a fault had been developed. The first steps in the developing of the theory that underlies these indicators may be found in the investigations of Stewart made in the 70's: Stewart [10] analyzed the spectra of the vibrations of gears with respect to the different kind of faults that gear can experience, and noticed that the spectrum is composed of "regular" components, like the Mesh Frequency (GMF) and its harmonics, superimposed on noise (which usually is Gaussian – or White – noise). Moreover, he noticed the presence of sidebands around the GMF and its harmonics at a distance equal to the frequency of rotation of the shaft: these sidebands indicate the presence of modulation phenomena (§1.2.2.3). From these observations, McFadden [11-12] proposed a mathematical model of the ideal vibration signal of a gearbox, that is:

$$x_{ideal}(t) = \sum_{n=0}^{\infty} P_n \cos(n\omega_1 + \phi_n) + w(t) \quad (4.1)$$

where P_n is the amplitude of the n^{th} harmonic of the shaft rotation frequency ω_1, ϕ_n is its phase and $w(t)$ is the superimposed Gaussian noise. Moreover, McFadden [12] noticed that the amplitude and phase modulating functions (named respectively $a_n(t)$ and $b_n(t)$) are periodic functions of period $\omega_1(t)$ and can be expressed as a sum of its harmonics, that is:

$$a_n(t) = \sum_{m=0}^{\infty} A_{nm} \cos(\mathrm{m}\omega_1 + \alpha_{nm}) \quad (4.2a)$$

$$b_n(t) = \sum_{m=0}^{\infty} B_{nm} \cos(\mathrm{m}\omega_1 + \beta_{nm}) \quad (4.2b)$$

By inserting equations 4.2 in equation 4.1, a more accurate model of the vibration signal of a gear is obtained:

$$x_{ideal}(t) = \sum_{n=0}^{\infty} P_n [1 + a_n(t)] \cos(n\omega_1 + b_n(t) + \phi_n) + w(t) \quad (4.3)$$

In order to estimate the changes in amplitude of the modulating functions, Stewart proposed the "difference signal" $d(t)$, described by the following equation:

$$d(t) = x_{TSA}(t) - y_d(t) \quad (4.4)$$

where $x_{TSA}(t)$ is the Time Synchronous Average of the signal $x(t)$ and $y_d(t)$ is a signal containing only the regular meshing components, these being the Gear Mesh Frequency (GMF), the harmonics of the GMF and the first order sidebands that are around the GMF and its harmonics. Thus, according to McFadden's model, $d(t)$ is composed by all the non-regular meshing components, these being the sidebands of order higher than 1 and the Gaussian noise. Later, it was proposed not to remove the

first order sidebands from $x_{TSA}(t)$ by creating the "residual signal" $r(t)$ which is defined as:

$$r(t) = x_{TSA}(t) - y_r(t) \tag{4.5}$$

where $y_r(t)$ contains only the GMF and its harmonics. These considerations had allowed formulating a series of indicators of the state of the gears, the main of which are very well summarized in [13] and [14].

4.3.2 – Indicators and Calculations Details

The following is a resume of the indicators used in this thesis work: in equations 4.6 to 4.12, x denotes the sampled signal, i is the sample index, N is the signal's total samples number.

$$CF = \frac{x_{peak}}{RMS_x} \tag{4.6}$$

The Crest Factor (CF, eq. 4.6) is defined as the maximum positive peak of the signal divided by the RMS of the signal. In eq. 4.6, *peak* is the sample index at which the maximum occurs. The Crest factor is a normalized measurement of the amplitude of the signal, and should increase when the signal exhibit a small number of high-amplitude peaks such as those generated in gearboxes vibration signals by some kinds of local tooth damage.

$$EO = kurt[x_i^2 - (x_{i-1}x_{i+1})] \tag{4.7}$$

The Energy Operator (EO) expressed in eq. 4.7 is the Kurtosis value of the discrete version of the Energy Operator $\varphi(g(t)) = \left(\frac{dg(t)}{dt}\right)^2 - g(t)\frac{d^2g(t)}{dt^2}$; in [15] it is shown that EO could perform amplitude and frequency demodulation, and had been used as global indicator of the state of a gearbox.

$$ER = \frac{RMS_d}{RMS_{y_d}} \tag{4.8}$$

Energy Ratio (ER; eq. 4.8) is defined as the ratio of the RMS of the difference signal (eq. 4.4) and the RMS of the signal $y_d(t)$ containing only the regular meshing components: ER is expected to increase in case of heavy uniform wear because in this case RMS_d should increase while RMS_{y_d} should decrease.

$$FM0 = \frac{Peak\ to\ Peak}{\sum A_k} \tag{4.9}$$

FM0 (eq. 4.9) is an indicator defined as the ratio of the peak-to-peak (PP) value of the signal and the sum of all the amplitudes A_k of the mesh frequency and its harmonics. It is an indicator of major faults in the gearbox because major changes occurring in the

meshing patterns can be detected by comparing the PP value to the sum of the mesh harmonics.

$$FM4 = \frac{\frac{1}{N}\sum_{i=1}^{N}(d_i-\bar{d})^4}{\left[\frac{1}{N}\sum_{i=1}^{N}(d_i-\bar{d})^2\right]^2} \quad (4.10a)$$

$$N6A = \frac{\frac{1}{N}\sum_{i=1}^{N}(d_i-\bar{d})^6}{\left[\frac{1}{N}\sum_{i=1}^{N}(d_i-\bar{d})^2\right]^3} \quad (4.10b)$$

$$N8A = \frac{\frac{1}{N}\sum_{i=1}^{N}(d_i-\bar{d})^8}{\left[\frac{1}{N}\sum_{i=1}^{N}(d_i-\bar{d})^2\right]^4} \quad (4.10c)$$

FM4 (eq. 4.10a) was developed by Stewart in 1977 and was designed to complement FM0 by detecting faults isolated to a limited number of teeth. It is obtained simply as the Kurtosis (or fourth order moment) of the difference signal $d(t)$ (eq. 4.4) and it is thus non-dimensional. The Kurtosis of a signal (§1.2.1) has a value of 3 if the signal is purely Gaussian: considering the signal model proposed by McFadden (eq. 4.3), FM4 should thus have a value of 3 if the gearbox is in good state since $d(t)$ should contain only the Gaussian noise $w(t)$, and then deviate from this value when a fault occurs. Proposed by Martin in 1989 [16], N6A (eq. 4.10b, sometimes named M6A) and N8A (eq. 4.10c, sometimes named M8A) are grouped here along FM4 because they are simply the sixth order moment (N6A) and the eight order moment (N8A) of the difference signal $d(t)$: indeed, by doing this the goal is to enhance the sensibility of FM4.

$$NA4 = \frac{\frac{1}{N}\sum_{i=1}^{N}(r_i-\bar{r})^4}{\left[\frac{1}{M}\sum_{m=1}^{M}\frac{1}{N}\sum_{i=1}^{N}(r_{i,m}-\bar{r}_m)^2\right]^2} \quad (4.11)$$

NA4 (eq. 4.11) was developed by Zakrajsek in 1989 [17] as a general gearbox fault indicator: it is designed not only to react at the onset of damage (like FM0, FM4, N6A, N8A) but also to the growth of the fault by taking into account the history of the gearbox. Indeed, NA4 is the Kurtosis of the residua signal $r(t)$ (eq. 4.5) with a modified denominator: in eq. 4.11, $\bar{r}$ is the mean of the residual signal, M is the number of records made until the present moment, m is the index of records. NA4 is thus obtained by dividing the fourth moment of $r(t)$ by the square of its run-time averaged variance: being a Kurtosis, its value is 3 if $r(t)$ is purely Gaussian noise.

$$NB4 = \frac{\frac{1}{N}\sum_{i=1}^{N}(s_i-\bar{s})^4}{\left[\frac{1}{M}\sum_{m=1}^{M}\frac{1}{N}\sum_{i=1}^{N}(s_{i,m}-\bar{s}_m)^2\right]^2} \quad (4.12)$$

NB4 (eq. 4.12) was proposed by Zakrajsek et al [18] in 1994, and it is calculated as NA4 but with the only difference that instead of using $r(t)$ it makes use of the s(t) signal, which is the envelope (§1.2.2.3) of the original signal $x(t)$ band-pass filtered around the mesh frequency. Indeed, the theory behind NB4 is that faults on a limited number

of teeth cause load fluctuations that are different from those generated by a healthy gearbox, and this can be seen by the envelope.

In addition to the aforementioned indicators, RMS and Kurtosis were also calculated. To obtain all these indicators, the following calculus steps were performed:

1. Order Tracking (§1.2.2.5) of the input signal $x(t)$ is performed, with the encoder signal "Zero" used as Tacho signal; after this stage, the signal has a constant number of samples per revolution of the gearbox input shaft: let's name the latter $x_{OT}(t)$.
2. RMS, Kurtosis, CF and EO are evaluated from $x_{OT}(t)$, thus these are global indicators of the gearbox health status.
3. $x_{OT}(t)$ is filtered around the meshing frequency of the E16 reduction stage in order to obtain the $s_{E16}(t)$ signal: then, $NB4_{E16}$ is calculated. The same is done to obtain $NB4_{E50}$ after filtering $x_{OT}(t)$ around the mesh frequency of the E50 stage. $NB4_{E16}$ and $NB4_{E50}$ are global indicators of the health status of respectively the E16 and the E50 stage.
4. Six Time Synchronous Averages (TSA) of $x_{OT}(t)$ are calculated for each gear of the gearbox, these being the sun, planet and ring gear of both E16 and E50 stages. TSAs are obtained by averaging together chunks of the $x_{OT}(t)$ signal: the length (in samples) of the chunks considered for gear *i* is given by the length (in samples) of one revolution of the input shaft divided by the order of gear *i*.
5. ER, FM0, FM4, N6A, N8A and NA4 indicators are calculated for each of the six TSAs obtained in the previous step. These indicators are thereby specialized on each gear and thus will provide information only on the health status of that gear.

This procedure was performed both on the vibration signal and the torque signal, thus providing 18 indicators for each signal for a total of 36. The motor current signal was not used in this thesis work and because it was decided to use it in future analyses (just like the encoder "A" signal).

4.3.3 – Analysis Results

In this section the focus will be on the E50 stage parameters, because this stage was the subject of almost every event occurred along the endurance test: indeed, this is in accord with the forecast of Brevini. In all the figures shown in this chapter the vertical lines mark the periodic dismounting of the gearbox for inspection, that occurred approximately every 250 hours of testing; moreover, the x-axis is the number of record (i.e.: approximately hours) because of the recording problems mentioned in §4.2. The following table 4.3 reports the main events occurred along the endurance test.

Record Index	Event
517	-E50 Sun Gear with some scratches upon some teeth's edges and some slight indentations -A bearing of an E50 planet gear exhibits wear
1694	-Substitution of the bearing found weared at hour 517
1944	-Two bearing of E50 planet gears with scratches on the race -E50 Ring gear with scratches
2189	-Substitution of the two bearing found with scratches at hour 1944 -Ring gears found with evident scratches
3539	-E50 ring gear founded with tooth missing and substituted -Start of the test with first incision on E50 sun gear
3784	-Start of the test with second incision on E50 sun gear
3924	-Start of the test with third incision on E50 sun gear

Table 4.3: main events regarding the E50 stage along the endurance test.

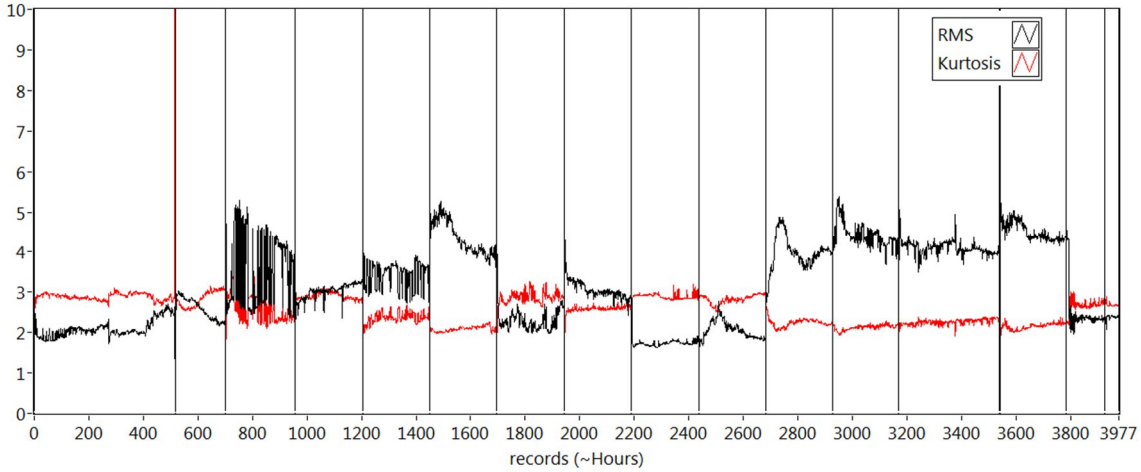

Figure 4.6: RMS and Kurtosis of the vibration signal.

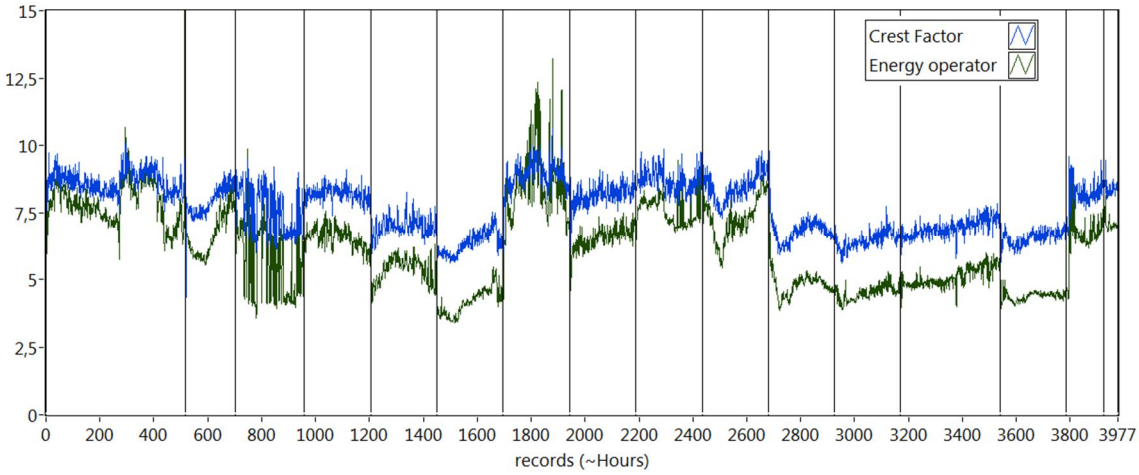

Figure 4.7: Crest Factor (CF) and Energy Operator (EO) of the vibration signal.

In Fig. 4.6 and 4.7 the RMS, Kurtosis, CF, and EO are reported when calculated from the vibration signal; it can be seen that there is not a well-established trend along the whole gearbox test, although trends can be observed between two consecutive dismounting of the gearbox (in particular for CF and EO, Fig. 4.7). The influence of the dismounting process on the indicators is recognizable: indeed, Brevini operators guaranteed that generally nothing was changed in the gearbox parts (except for the events listed in table 4.3), even the oil used before a dismounting was re-utilized. The disassembly, however, seems to change the stiffness of the system (which could explain the variation of the RMS occurring before and after a disassembly) probably because of differences in tightening of the screws and, in general, differences in mounting in the assembly process. Thus, the general behaviour of these global indicators in this specific endurance test doesn't show the regularity required to use them as diagnostic parameters, despite some indications of anomaly that they supply.

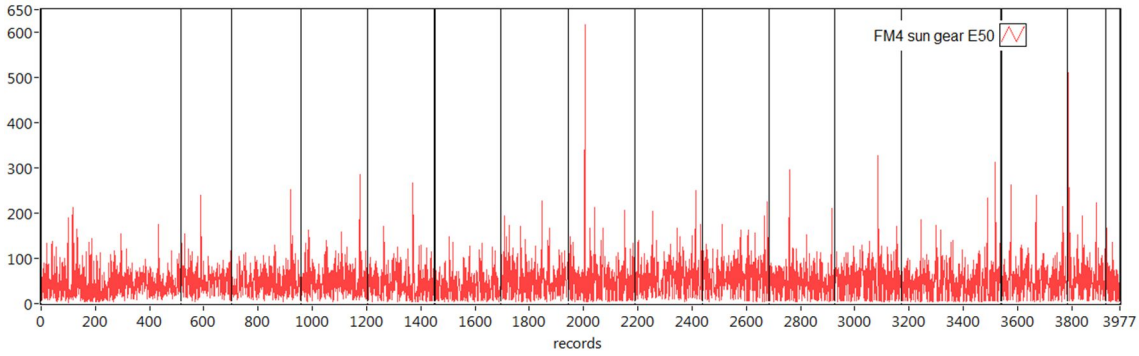

Figure 4.8: FM4 evaluated for the E50 sun gear from the vibration signal.

In Figure 4.8 the FM4 of the vibrations of the sun gear of the E50 stage is shown. FM4 is used here as an example of what happens in general for FM0, FM4, N6A, N8A and NA4, when calculated both from the vibration and the torque signal: these parameters don't exhibit the behaviour that one expects, i.e.: their value is different from the

theoretical (which is 3 for a healthy gearbox) and they don't react explicitly when damage is present. This could be explained by the fact that the spectrum of both vibrations and torque contains a wide number of discrete frequencies that aren't related to the gearbox, and therefore they aren't removed because they are not meshing regular components: thus, $d(t)$ and $r(t)$ signals described in the previous section don't contain only Gaussian noise. Indeed, this makes these indicators not usable because the theory that underlies them is not verified in this specific case (indeed, a similar fact occurred also in [14]).

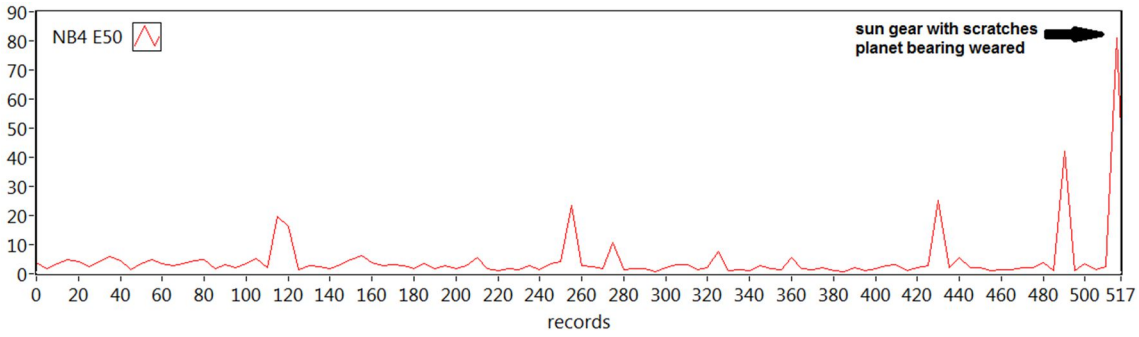

Figure 4.9: NB4 of the E50 stage vibrations during the first 517 records of the endurance test.

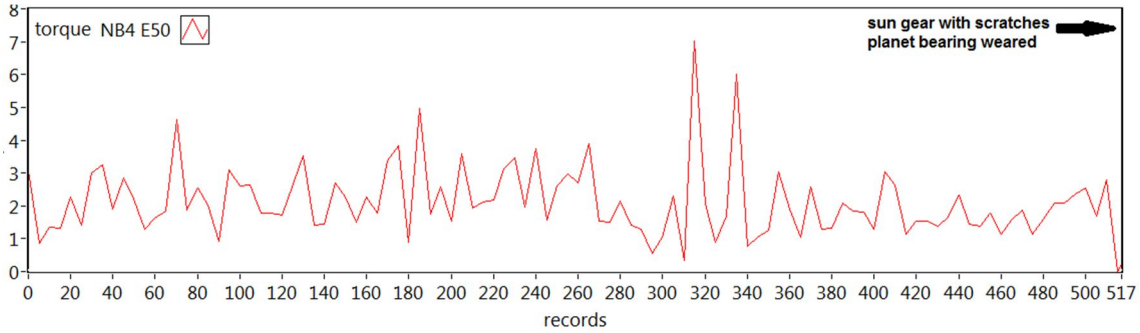

Figure 4.10: NB4 of the E50 stage torque during the first 517 records of the endurance test.

Indeed, the most effective parameter was found to be NB4: this parameter is obtained after bandpass filtering the signal around the mesh frequency of each stage, and this filtering remove the major part of the other discrete frequencies unrelated to the gearbox, thus giving an indicator that can be used in this specific case. In figure 4.9 the NB4 for the E50 stage vibrations is reported form the start of the recordings until the first stop for disassembly, where the E50 stage was found with some scratches on the teeth edges of the sun gear and with a planet bearing exhibiting wear. The NB4 deviate from the nominal value of 3 in the final stages after exhibiting occasional peaks oh high

amplitude from almost 400 hours before the inspection onwards: these peaks are probably related to the events that provoked the scratches on the sun gear. In this case, NB4 of vibrations provide unconfutable diagnostic information. In contrast, NB4 for the torque signal (Fig. 4.10) doesn't provide explicit diagnostics indications except for two small peaks 200 hours before the inspection.

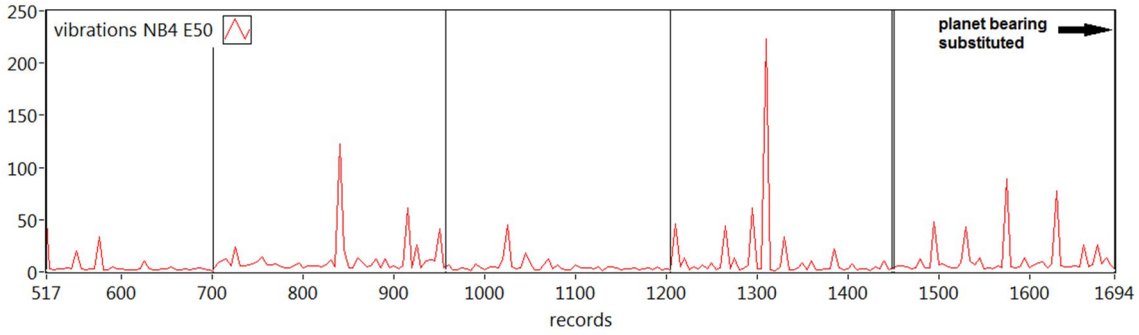

Figure 4.11: NB4 of the E50 stage vibrations from record 517 to record 1694.

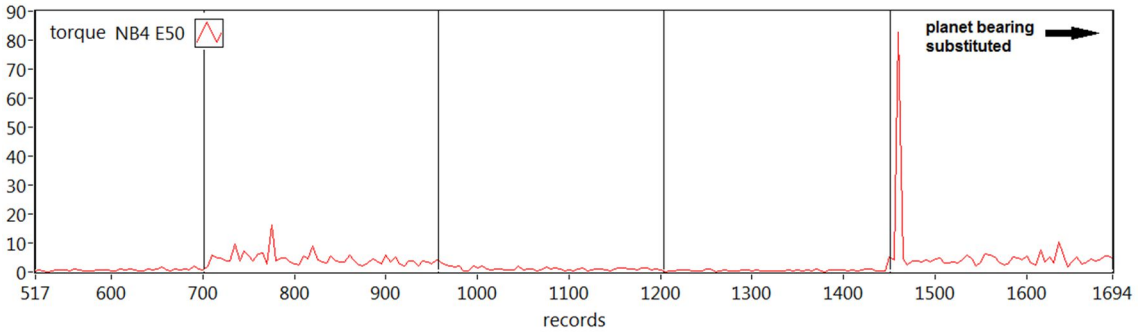

Figure 4.12: NB4 of the E50 stage torque from record 517 to record 1694.

At record index 1694 the planet bearing found weared was substituted: the wearing of this bearing is well pointed out by both NB4 from vibrations (Fig. 4.11) and torque (Fig. 4.12) in a different manner. NB4 from vibrations exhibit very high peaks that occur progressively more frequently, and its value between these peaks is slightly higher than nominal (i.e.: 3): a strong indication of general damage to the E50 stage is provided around record index 1300, which correspond to almost 400 hours before the bearing replacement. In contrast, NB4 from torque deviate from nominal value after the disassembly at record index 700, return to almost nominal value after disassembly at record index 960, then a high amplitude peak occurs approximately 250 hour before the bearing replacement. The fact that NB4 return to its nominal value after deviating from it could be explained by considering the denominator in its definition (eq. 4.12): this denominator is in fact a running average, meaning that extended deviation from nominal value are progressively embodied in the denominator, thus causing the NB4 value to progressively return to nominal (this is a well-known behavior of this

parameter). Nevertheless, NB4 from torque is able to inform that there is something happening in the E50 stage, and shows it dramatically by the aforementioned peak at record index 1460.

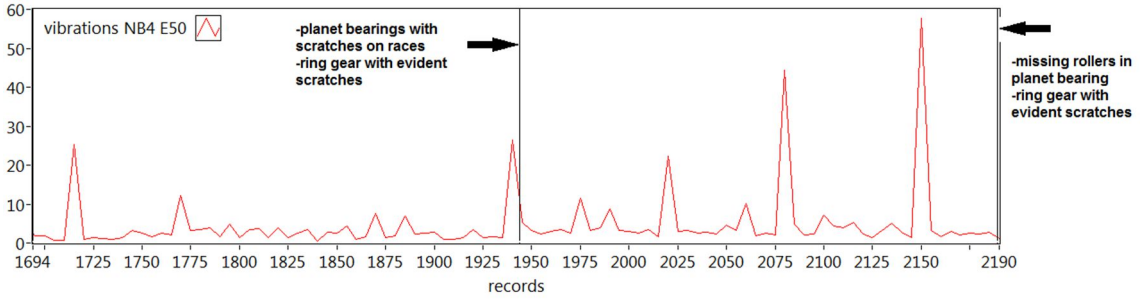

Figure 4.13: NB4 of the E50 stage vibrations from record 1694 to record 2190.

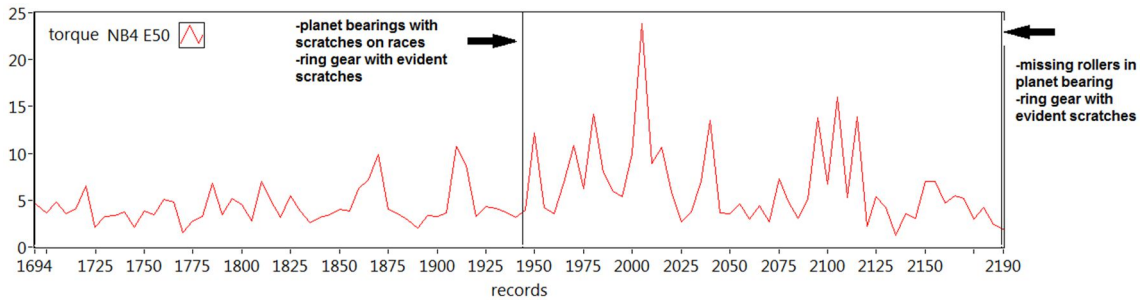

Figure 4.14: NB4 of the E50 stage torque from record 1694 to record 2190.

At disassembly and inspection occurred at record index 1944, the ring gear was found with scratches and planet bearings were founded with scratches on their races; at the subsequent inspection and disassembly, at record index 2189, two rollers were missing in a planet bearing. These events are communicated by vibrations' NB4 (Fig. 4.13) but less evidently than before, with a series of growing amplitude peaks, in particular from record indexes 2020 to 2150; preliminary advises may be found at indexes 1700 and 1940. Instead, the torque's NB4 (Fig. 4.14) exhibit a slight increasing trend, with a significant peak between record indexes 2000 and 2020 (which is in accord with vibrations' NB4). In this case the information is less evident from both NB4s, probably because of the aforementioned "averaging effect", but both provide a strong indication approximately 200 hours before the inspection.

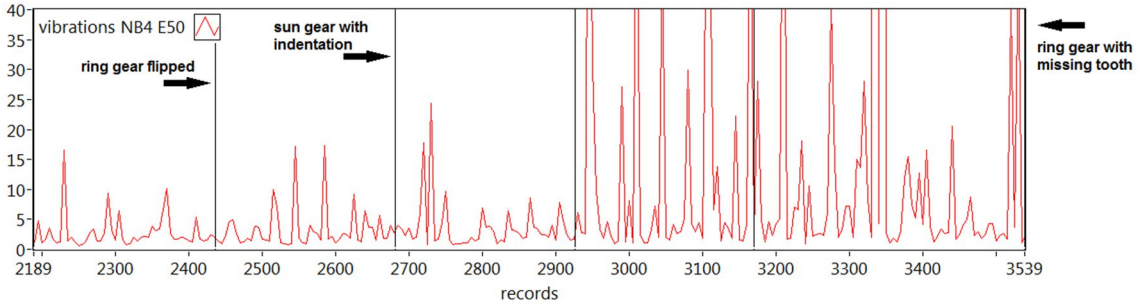

Figure 4.15: NB4 of the E50 stage vibrations from record 2189 to the end of the endurance test.

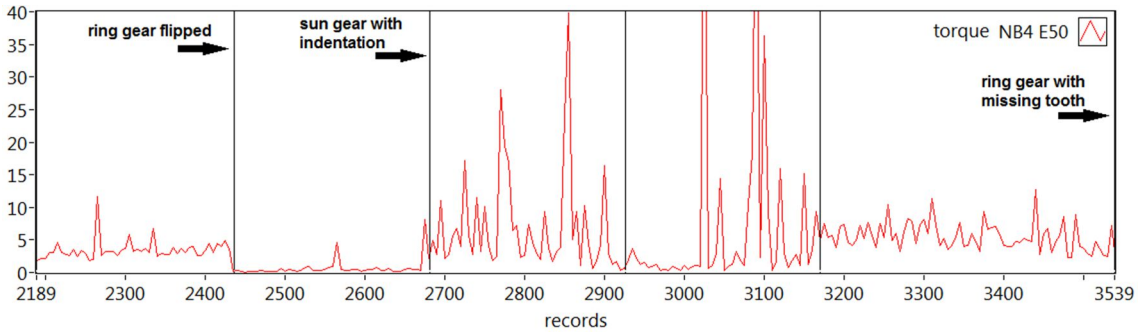

Figure 4.16: NB4 of the E50 stage torque from record 2189 to the end of the endurance test.

Figures 4.15 and 4.16 show the NB4 respectively for vibrations and torque from inspection and disassembly at record index 2189 to the end of the Brevini endurance test. At the inspection at index 2437, the ring gear was flipped in order to use the side that was less weared. This can be recognized in particular in the torque's NB4, which drops from values slightly beyond the nominal to almost zero: indeed, the flipping of the ring gear can be seen as a return of the E50 stage to a relatively "brand-new" state. Torque's NB4 goes almost to zero because its denominator had increased along the history of the test, by means of the aforementioned averaging effect: the numerator reacts immediately to this "brand-new" state but the denominator needs some time to do the same. Nevertheless, this is an indication of the good quality of the information provided by torque's NB4. Vibrations' NB4 (Fig. 4.15), in contrast, doesn't react to this event: indeed it remains at values around the nominal except for some peaks. At the subsequent inspection (record index 2682) the sun gear was found with an indentation: it is possible that the vibrations' NB4 peaks are communicating this fact, because this behavior continues after this inspection and disassembly since the sun gear was not substituted. Torque's NB4 exhibit only a small peak just before this inspection. Both NB4s are advising that a major problem is developing from record index 2682 onwards, even if with different reaction times: in this period, they both exhibit strong peaks well beyond nominal value. Indeed, at the end of the test a tooth was missing from the ring gear: nothing new was noticed in the two inspections and

disassembles at indexes 2926 and 3170, but the ring gear exhibited scratches from long before. Both NB4's are probably advising about the developing of these scratches into a crack or an inception of a new crack. Torque's NB4 seems to spot this crack before vibration's NB4, and this can be explained by considering that the crack causes fluctuations in the transmitted torque when a planet gear encounters the cracked tooth, and the torque signal is naturally more sensitive to torque fluctuations than vibrations, also because the latter are more contaminated by environmental noise coming from other sources of vibrations. Indeed, vibrations NB4 advises about this crack later, when this crack is developed enough to be recognized by vibration's NB4 and continue to exhibit peaks until the end of the test: torque's NB4, in contrast, descend to a value still higher than nominal but lower than the one exhibited in the first stage of the crack developing: this is probably caused by the averaging effect.

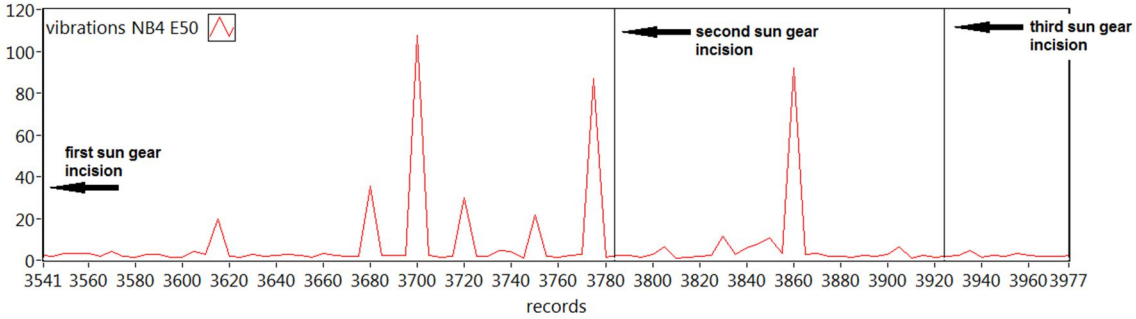

Figure 4.16: NB4 of the E50 stage vibrations during the test with incised sun gear.

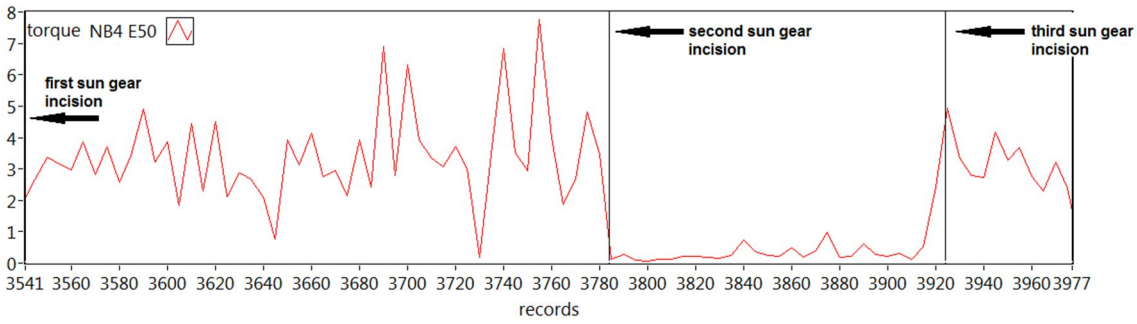

Figure 4.17: NB4 of the E50 stage torque during the test with incised sun gear.

In figures 4.16 and 4.17 the NB4 from respectively vibrations and torque are shown when incisions were made on the E50 sun gear. Both NB4 don't react immediately to the presence of the incision, but start to communicate the presence of damage around record index 3700, i.e.: after about 24 hours of testing: vibrations' NB4 exhibit very high peaks while torque's NB4 value is around 7, more than double of the nominal. After the second incision, torque's NB4 fall to zero and vibrations' NB4 stay at nominal value, except for a peak at record index 3860. After the third incision, torque's NB4 rise again to the nominal, while vibrations' NB4 remains to the nominal. This behavior was

not expected, and could be explained by the averaging effect in the denominator: at record index 3541, this denominator (which is used as a reference) is relative to an E50 stage with strong damage (a missing ring gear tooth), thus, in this condition, the nominal value of NB4 refers to the damaged condition rather than “no damage” condition of the gearbox. Unfortunately, due to limited availability of the test bench, it was not possible to start the test with a brand new gearbox, and this was necessary at least to allow a correct evaluation of NB4. Restarting the averaging from record 3541 yields the same results for the same reasons.

4.4 – Conclusions

NB4 evaluated from vibrations signal ad torque signal is the best diagnostic parameter in the set used for this endurance test, but it doesn’t behave like an ideal diagnostic parameter: nevertheless, NB4 can provide useful information, on the basis of which the endurance test could be automatically stopped: this was one of the goals of Brevini. Some points remain to be investigated: firstly the influence of the disassembly of the gearbox on the state of the gearbox itself: this influence is clear by the examination of the global indicators that indeed change in correspondence of each disassembly even if nothing was changed in the gearbox. It should be stressed that another kind of test is required to assess the real effectiveness of the set of metrics evaluated in this thesis work: despite stopping the test and completely disassemble the gearbox at regular intervals, one should let it run continuously unless the metrics communicate that something is occurring. This thesis work demonstrates that at least NB4 could provide this information, both if it is calculated on the vibration signal or on the torque signal. NB4 behave slightly differently from vibrations to torque: in case of vibrations, it appears generally more reactive than in case of torque. Torque’s NB4 seems to advise that something is occurring when there are relatively high induced fluctuations in the torque signal. Sensorless diagnostic could be performed in this case by monitoring the torque signal, because it seems to provide almost the same information than vibrations.

5 – Final Comments

The two main aim of this thesis work were reached: first, valid diagnostic indicators were obtained in the "classical" manner, which is via adding sensors (an accelerometer) to the monitored machine. Second, the Sensorless approach was then used in two cases on a total of three, and the results show that it can provide the same information obtained by the classical approach to condition monitoring. Specifically, in the case of the condition monitoring of blades the Sensorless approach (analysis of torque) gave equal or better results than the classical approach (analysis of vibrations), while in the case of the gearbox condition monitoring the two approaches were comparable. In general, this work shows that a data acquisition campaign oriented to condition monitoring provides for sure the best diagnostics information, but it shows also that it is possible to join the requirements of daily activities of a factory with the requirements of condition monitoring (CM) in the same data acquisition campaign: the results obtained in the latter case (which coincides with the kind of data acquisition campaigns performed in this work) seems to reflect the trade-off between the two set of requirements, trade-off that was made when the data acquisition campaign was set. This gives to a factory interested in CM the possibility to further reduce the initial costs of condition monitoring by embodying or placing side-by-side the daily activities requirements with CM requirements, that is: reducing the CM costs that come from the data acquisition campaign by embodying it into the daily activities.

Technological transfer is the background of this thesis, and from this point of view this work has the main result of demonstrating that condition monitoring can be performed and implemented on various types of products, and with reduced costs by the use of the Sensorless approach. Subsequently, methods of testing and analysis were transferred to the productive sector, mainly to the factories involved in this thesis work but not exclusively to them.

6 – References

[1] Randall R., “Vibration-based Condition Monitoring”, Wiley (2011), ISBN: 978-0-470-74785-8.

[2] Antoni J., “Cyclostationarity by examples”, Mechanical Systems and Signal Processing 23 (2009), 987–1036.

[3] Lawrence Marple Jr. S., “Computing the discrete-time analytic signal via FFT”, IEEE Transactions on Signal Processing, 47 (9) (1999), 2600-2603.

[4] McFadden, P.D. and Toozhy, M.M., ”Application of synchronous averaging to vibration monitoring of rolling element bearings,” Mechanical Systems and Signal Processing 14 (6) (2000), 891-906.

[5] McFadden P. D., “A technique for calculating the time domain averages of the vibration of the individual planet gears and the sun gear in an epicyclic gearbox”, Journal of Sound and Vibration 144 (l) (1991), 163-172.

[6] Gade, S., et al. "Order tracking analysis, technical review no. 2." Naerum: Bruel & Kjaer (1995).

[7] Cotogno M., Cocconcelli M., Rubini R., “Spatial acceleration modulus for rolling elements bearing diagnostics”, Advances in Condition Monitoring of Machinery in Non-Stationary Operations (2014), 587-595, ISBN 978-3-642-39348-8, DOI 10.1007/978-3-642-39348-8_51.

[8] Cotogno M., Cocconcelli M., Rubini R., “Effectiveness of the Spatial Acceleration Modulus for rolling elements bearing fault detection” Diagnostyka 14(4) (2013), 27-34

[9] Immovilli F., Bianchini C., Cocconcelli M., Bellini A., Rubini R., “Bearing fault model for induction motor with externally induced vibration” IEEE Transactions on Industrial Electronics 60 (2013), 3408-3418

[10] Stewart R. M., “Some useful data analysis techniques for gearbox diagnostics”, Institute of Sound and Vibration Research, Paper MHM/R/10/77 (1977)

[11] McFadden P.D., Smith J.D., “An explanation for the asymmetry of the modulation

sidebands about the tooth meshing frequency in epicyclic gear vibration", Proceedings of the Institute of Mechanical Engineers 199 (1985), 65-70

[12] McFadden P.D., “Examination of a technique for the early detection of failure in gears by signal processing of the time domain average of the meshing vibration”, Mechanical systems and signal processing 1(2) (1987), 173-183

[13] Samuel P.D., Pines D. J., “A review of vibration-based techniques for helicopter transmission diagnostics”, Journal of Sound and Vibration, 282(1) (2005), 475-508

[14] Mosher M., Pryor A. H. and. Huff E. M., “Evaluation of standard gear metrics in helicopter flight operation”, NASA Ames Research Center (2001)

[15] Liang M., Bozchalooi I. S., “An energy operator approach to joint application of amplitude and frequency-demodulations for bearing fault detection”, Mechanical systems and signal processing 24(5) (2010), 1473-1494

[16] Martin H.R., “Statistical moment analysis as a means of surface damage detection”, Proceedings of the Seventh International Modal Analysis Conference, Society for Experimental Mechanics, Schenectady, NY (1989), 1016–1021

[17] Zakrajsek J. J., “ An investigation of Gear Mesh Failure Prediction Techniques”, NASA, Technical Memorandum (1989), Cleveland, Ohio

[18] Zakrajsek J. J., Decker H.J., Townsend D.P., “An analysis of Gear Fault Detection Methods as Applied to Pitting Fatigue Failure Data”, NASA Technical Memorandum, Lewis Research Center (1993), Cleveland, Ohio

Acknowledgements

ॐ 道

which also means: "thanks to"
la mia Famiglia, i miei Amici

and it also means
"specially for the technical side support: thanks to"
Prof. Riccardo Rubini, Ing. Marco Cocconcelli
Ing. Francesco Lolli, Ing. Matteo Cigarini, Ing. Antonio Armento,
Ing. Domenico Reca
Dott. Alessandro Scarabelli, Dott. Simone Micheletti

and it also means
"specially for this opportunity that I was given: thanks to"
Unindustria Reggio Emilia
Bucher Hydraulics, OTO Mills, Brevini Power Transmission
Prof. Cesare Fantuzzi, Prof. Leonardo Orazi

and it also means
"specially for nothing in particular: thanks to"
all the people that have supported me in all the possible ways
all the people that haven't supported me in any way

and it also means: "thanks to"
tutto/i e niente/nessuno

but it properly means:
" "